

INSTITUTE OF EXPERIMENTAL PHYSICS
DEPARTMENT OF PHYSICS
WARSAW UNIVERSITY



Neural dynamics underlying brain
thalamic oscillations investigated with
computational models

by

Piotr Suffczyński

Advisor

Prof. dr hab. Katarzyna J. Blinowska

A DISSERTATION SUBMITTED IN PARTIAL FULFILLMENT
OF THE REQUIREMENTS FOR THE DEGREE OF
DOCTOR OF PHYSICS

OCTOBER 2000

Acknowledgments

Many people from more than two laboratories have contributed to this work. First, I would like to thank my advisor, prof. Katarzyna Blinowska, for support of my work in every possible way and introducing me to brain research group in Amsterdam, without which my thesis could not have been developed into the present form.

In the Netherlands I was accepted not with typical Dutch hospitality. My supervisor, prof. Fernando Lopes da Silva, from the beginning kept me on the right track and was always ready to answer my questions. I thank him for his time devoted to this project, a readiness to share his knowledge and contagious will to understand the brain.

Working, discussing and sailing on a living boat with dr. Jan Pieter Pijn was a great pleasure. I benefited greatly from his creative insight and stimulating enthusiasm. Dr. Jan Pieter Pijn passed away and to the memory of him this thesis is dedicated.

I am also very grateful to dr. Stiliyan Kalitzin, whose suggestions and ideas influenced greatly the last part of this thesis and to Wouter Blanes, dr. Dimitri Velis and dr. Jaime Parra from the Institute of Epilepsy in Heemstede who provided friendly advice and help in overcoming difficulties ranging from computers to health.

Finally, I would like to express gratitude to my colleagues and secretary from the Laboratory of Medical Physics who took care of my things (and student courses) when I was abroad and who create excellent atmosphere at my workplace.

Abstract

This thesis is concerned with normal and pathological oscillations generated in thalamocortical neuronal network. By means of anatomically and physiologically based computational models we attempt to provide insight into phenomena such as event-related dynamics of alpha band rhythms and spontaneous generation of absence seizures. We present novel hypothesis regarding the neurophysiological substrates and functional significance of antagonistic behavior of alpha band rhythms in neighboring cortical areas during performance of attentional tasks. We also identify cellular and network properties that may condition epileptic oscillations and the transition from normal to pathological state. Furthermore we demonstrate annihilation of pathological rhythm by external stimulation, which may contribute to development of seizures suppression.

Contents

1	Introduction	1
1.1	Why study nervous system?	1
1.2	Brain at different scales	1
1.3	EEG and brain oscillations	2
1.4	The aim and scope of this work	6
1.5	The plan of this work	6
2	Experimental motivation	9
2.1	Event-related dynamics of alpha band rhythms	9
2.2	Absence seizures	12
3	Methods	15
3.1	Why modeling?	15
3.2	Modeling approach	16
4	Physiology	19
4.1	Thalamocortical network	19
4.2	Cellular mechanisms	21
4.3	Generation of thalamocortical rhythms	22
5	Alpha rhythm model	25
5.1	Distributed network vs. lumped circuit	25
5.2	Model description	25
5.3	Linear system analysis	27
5.4	Nonlinear behavior	30
5.5	Blurring of the bifurcation point due to dynamic noise	30
6	Two modules - nonlinear feedback model of ERD/ERS	33
6.1	Formulation of the model	33
6.2	Mathematical description of the model	35
6.3	Results	37
6.3.1	Two modules model	37
6.3.2	Quantitative analysis	41
6.3.3	More modules	41
6.4	Discussion	43

7	Model of normal and pathological brain thalamic oscillations	45
7.1	Integrating neuronal and network properties	45
7.2	Model description	45
7.3	Results	52
7.3.1	Simulation of burst firing	52
7.3.2	Activities in a single module	52
7.3.3	Desynchronized activity and 10 Hz oscillations	52
7.3.4	Transition from 10 to 3 Hz oscillations induced by cortical input	53
7.3.5	Spontaneous transitions.	56
7.3.6	Analysis of the seizure threshold.	56
7.3.7	Periodic sensory stimulation.	59
7.3.8	Counter-stimulation.	60
7.3.9	Role of the cortex.	61
7.3.10	Antagonistic behavior of two modules.	62
7.3.11	Paroxysmal activity in two modules model.	62
7.4	Discussion	62
8	General discussion and conclusions	69
8.1	Discussion	69
8.1.1	Questions for modeler	69
8.1.2	Answers	69
8.1.3	Future directions	72
8.2	Conclusions	72
	Appendix	75
	Bibliography	80
	List of author's papers	88

Chapter 1

Introduction

1.1 Why study nervous system?

There are many reasons to study nervous system. One reason may be to satisfy our own curiosity; Since we learn that all animal and human behavior depends on the nervous system, we may become anxious to understand how it works. Additionally, the central nervous system - the brain - is considered to be the most complex system in nature. Therefore, understanding its mechanisms offers the greatest challenge in all of biological and physical sciences. On the other hand, the efforts to reveal brain's secrets are rarely motivated only by pure scientific interest. Through increasing knowledge of the nervous system, neuroscience aims to improve diagnosis and therapy of many nervous diseases such as epilepsy, or Parkinson disease or mental disorders such as depression, or schizophrenia. Understanding the neurobiological basis of human behavior may give us insight into the nature of being human. The questions like "What makes people hate or love each other?" or "Is there a neurophysiological basis of being a criminal or a talented musician?" are also the subjects of neuroscientific research. Finally, there is a hope that understanding the brain may help to develop new technologies that reproduce brain-like logical operations, an example being artificial neural networks.

1.2 Brain at different scales

What is the brain? The answer that the (human) brain is "a collection of 10^{11} nerve cells (neurons), strongly interconnected and surrounded by 10 to 50 times more numerous glial cells" is correct but is also too simplistic. It does not address the critical issue of the organization of nerve cells into functional circuits that process information and mediate behavior. A concept, which underlies the neurobiological way of thinking about the brain is that of functional units (Shepherd, 1994 [86]). These elementary units are formed at different levels of neural organization, which are shown in Fig. 1.1A. On the other hand, a scientific theory must make direct connections to experiments. Various experimental techniques applied to study the human brain operate on different spatial and temporal scales. Therefore, in parallel to hierarchical levels depicted in Fig. 1.1A, a more quantitative description of neural levels of organization may be

useful. An example of spatial and temporal scales of experimental brain studies is offered by Churchland and Sejnowski (1988) [12] and is shown in Fig. 1.1B. The question of scale is especially relevant in electrophysiology, where the ex-

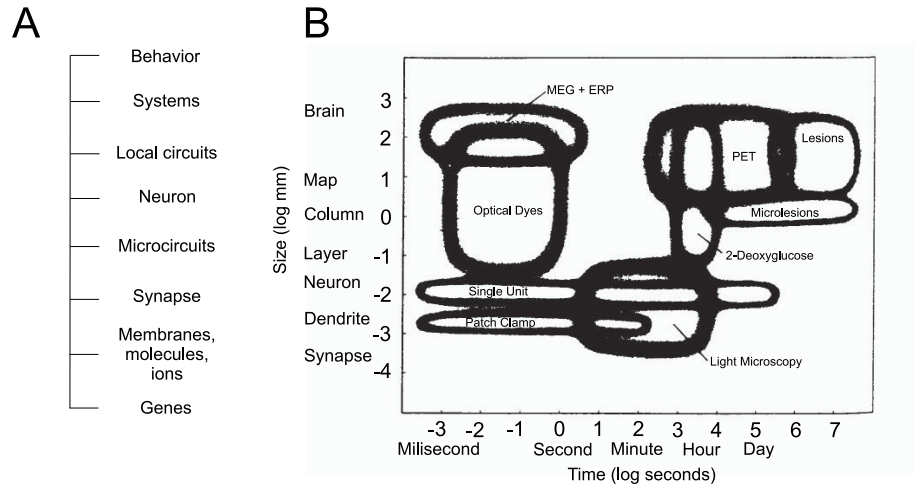


Figure 1.1: Levels of neural organization; (A) Hierarchical scale. Based on Shepherd (1994) [86]. (B) Spatial and temporal scales at which brain is investigated using several experimental techniques. From Churchland and Sejnowski (1988) [12].

perimental results depend critically on the size and location of the electrodes and on the period over which signals are averaged. Throughout this work we will often refer to brain electrical activity at various scales. Therefore we should first answer the question; What are the sources of electric and magnetic fields in the brain?

1.3 EEG and brain oscillations

An electric potential difference exist within a system whenever positive and negative charges are separated. This is a case in every neuron where charge separation is provided by different ion concentrations of two electrolyte solutions across a permeability selective barrier, such as a cell membrane. This potential difference is called membrane potential (MP) and, when the cell is at rest it is called resting membrane potential (RMP). By convention, the potential outside the cell is defined as zero. According to this convention the resting membrane potential in most neurons ranges from about -60 mV to -70 mV. The inputs that a neuron receives from other neurons may change its membrane potential. These synaptic inputs are of two types: those which produce excitatory postsynaptic potentials (EPSPs) and depolarize the membrane of the output neuron and those which produce inhibitory postsynaptic potentials (IPSPs) and act on the membrane in the opposite manner. These phenomena are illustrated in Fig. 1.2A. In the example shown in this figure, the two EPSPs in a short succession trigger an impulse, i.e., action potential (AP) in the postsynaptic neuron. All voltage traces in Fig. 1.2A correspond to intracellular recordings,

i.e., to the voltage across the membrane due to transmembrane ionic currents. These currents generate secondary ionic currents along the cell membranes in the intra- and extracellular space as shown in Fig. 1.2B. The portion of these

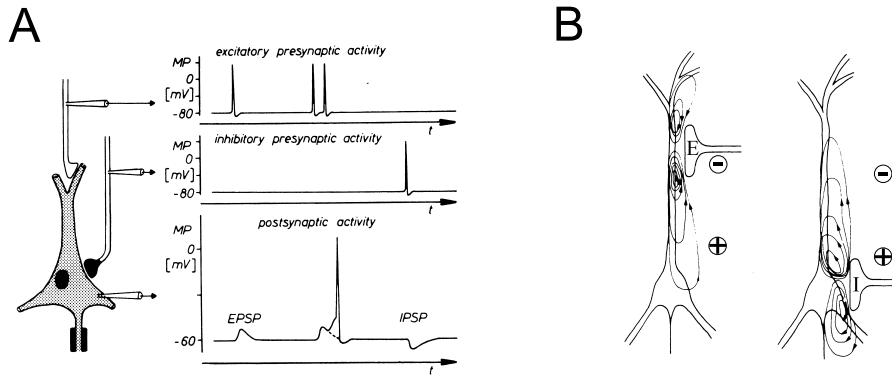


Figure 1.2: Generation of brain electrical activity. (A) Neuronal activity recorded intracellularly; The schematic location of intracellular microelectrodes is shown at left. In three graphs, from top to bottom, time courses of membrane potentials of the presynaptic excitatory and inhibitory neurons and of the postsynaptic neuron are shown. Action potentials generated by excitatory and inhibitory presynaptic neurons lead to EPSP and IPSP, respectively, in the postsynaptic neuron. Two EPSPs in short succession sum up to a suprathreshold potential, triggering an action potential in the postsynaptic neuron. (B) Current flow due to excitatory (E) and inhibitory (I) synaptic activation. At some distance from the cell the distribution of sources \oplus and sinks \ominus is that of current dipole. Note that an inhibition at the soma generates similar extracellular current flow as an excitation at the dendrites. Modified from Niedermeyer and Lopes da Silva, 1999 [68].

currents that flows through the extracellular space is responsible for the generation of field potentials (FP) that can be measured at a distance from the source. At locations not too close to the neuron, current distribution due to single synaptic action appears to be dipolar and the potential behaves as if it was produced by current flow between two poles (in Fig. 1.2B currents sources and sinks are marked by \oplus and \ominus , respectively). The synaptic activity of many parallel and synchronously active neurons produces the extracellular current flow that gives rise to the electric potential recorded from the scalp and termed the electroencephalogram (EEG) and to magnetic field, recording of which is called the magnetoencephalogram (MEG). The voltmeter of the EEG recording circuit is shown in Fig. 1.3

One of the salient features of the EEG signals is that they exhibit oscillations of various frequencies. The frequency bands within which EEG rhythms can occur have been named after Greek letters: Delta: below 3.5 Hz, Theta: 4 - 7.5 Hz, Alpha: 8 - 13 Hz, Beta: above: 13 Hz or more recently 14 - 30 Hz, Gamma: above 30 Hz. Apart from these rhythms that can be recorded in healthy adult subjects, there are also many abnormal EEG patterns often associated with brain dysfunction. Electroencephalography is a valuable clinical tool in, e.g., diagnosis of epileptic seizure disorders. Example of pathological rhythm - the

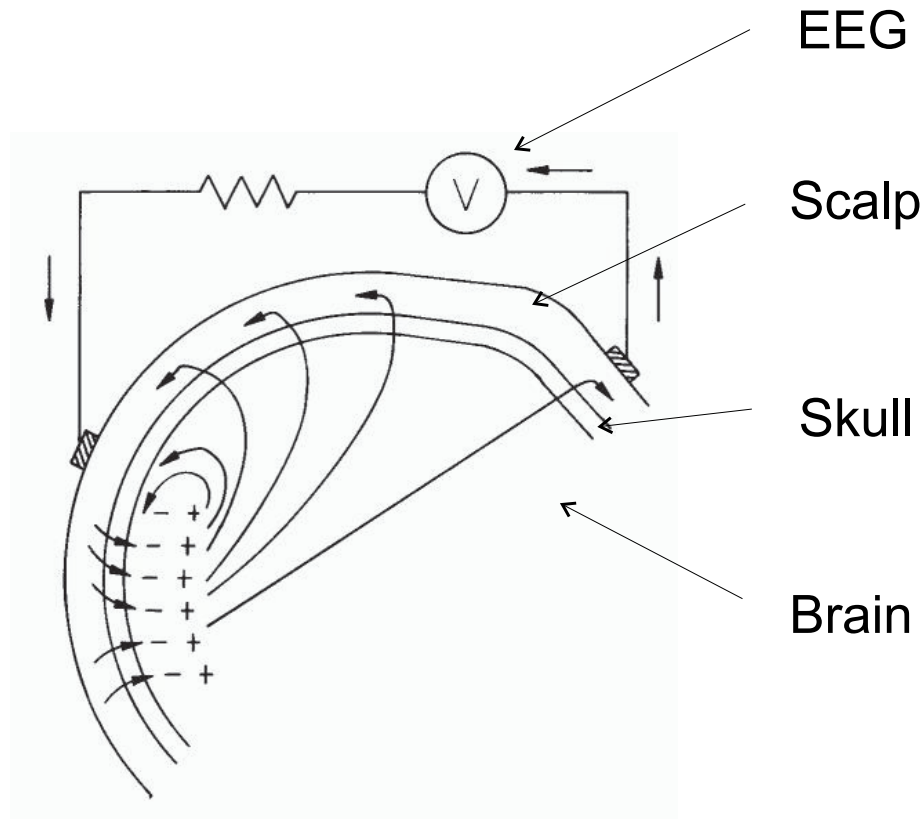


Figure 1.3: Origin of scalp potentials; Current in the EEG measuring circuit depends on the nature and location of the current sources, on the electrical properties of the brain, skull and scalp and on location of both electrodes. Modified from Nunez (1981)[69].

3 Hz spike and wave (SW) pattern that supports the diagnosis of absence type of epilepsy in 16 year old boy is shown, together with normal EEG rhythms, in Fig. 1.4.

Nature loves to oscillate (Bullock and Achimowicz, 1994 [9]) and apparently the brain does too. Brain oscillations may trigger different kinds of questions; Where and how are they generated? What are the main factors that condition different rhythms, often generated in the same neuronal system? What types of dynamics underlie these oscillations, i.e., do they correspond to linear Gaussian process, nonlinear limit cycle, low-dimensional chaotic process, transients or other process? Finally, do brain oscillations have a functional meaning in the nervous system or are they epiphenomena (i.e., by-products) of neuronal processes? (The correlation between particular stimuli and rhythmicity is not enough to conclude that the oscillation observed is relevant to neural information processing (Stryker, 1989) [92].) The work presented here attempts to answer some of the questions mentioned above.

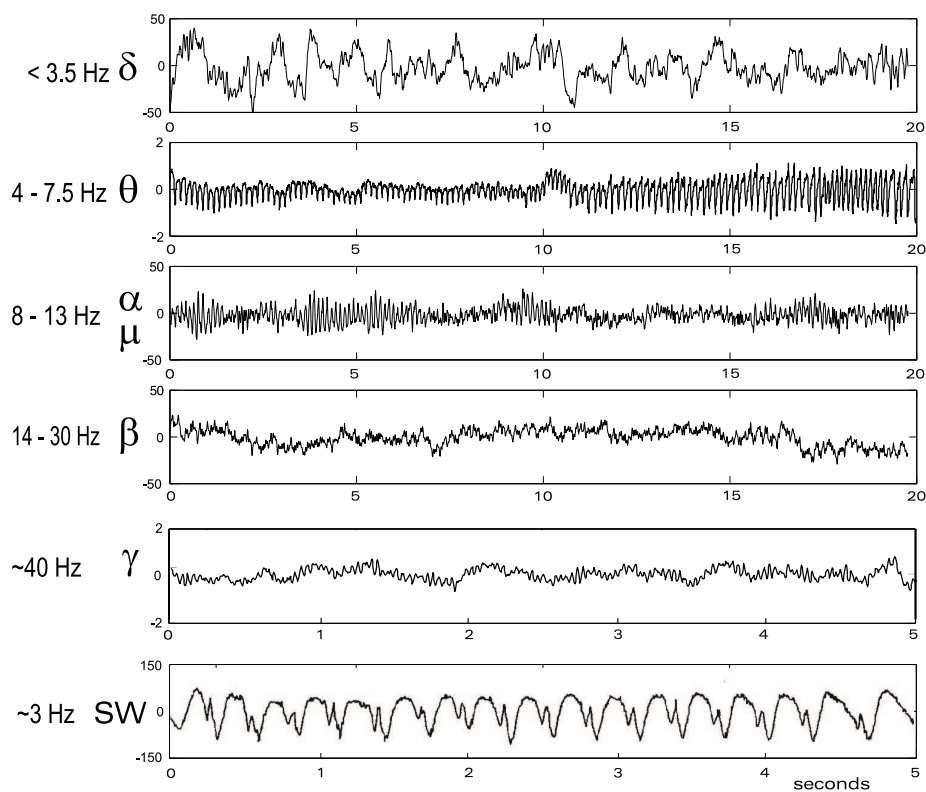


Figure 1.4: Example of various EEG rhythms described in the text; The delta, alpha, beta and SW waves were recorded by scalp EEG electrodes. The theta and gamma oscillations were recorded by depth electrodes implanted into human hippocampus. X - axis: seconds; Y - axis: μV (delta, alpha, beta, SW), mV (theta, gamma); Note that the time scale of gamma and SW rhythms is different than that of other rhythms shown.

1.4 The aim and scope of this work

This work is an attempt to provide insight into brain oscillations that emerge in the networks of neurons that build up thalamocortical neuronal network. More specifically, we were interested in two phenomena. First was related to the experimental observations that some mental (e.g., focusing attention) or motor (e.g., voluntary finger movement) actions may cause EEG rhythm variations over various locations on the scalp. Interestingly, EEG rhythmicity changes in the alpha band were observed not only at brain locations related to an event but they were also present in neighboring areas that did not correspond to the action performed. E.g., a hand movement influenced neuronal activity of the cortical foot area and vice versa. Second phenomenon of interest was related to the abnormal brain functioning, namely to the spontaneous generation of absence epileptic seizures that consist of a sudden lapse of consciousness with impairment of mental functions. Such short cessations of activity may even pass unnoticed by the subject but they are clearly represented in the EEG as the 3 Hz spike and wave (SW) pattern. The detailed neurophysiological basis of both phenomena mentioned above is not well established although many relevant experimental data are available. Therefore, we constructed anatomically and physiologically based computational models that were able to reproduce experimentally observed behavior.

Models are presented with increasing degree of complexity. First model presented is a 'classic' lumped alpha rhythm model developed by Lopes da Silva and colleagues [59] to elucidate the origin of rhythmic activity in neuronal populations. We considered this model, based on essential features of thalamic network, as a basic thalamic module responsible for rhythmic activity in alpha frequency range. In the next step, we implemented its extended version consisting of a chain of such modules mutually inhibitory connected by experimentally identified connections. It allowed to simulate spatial inhomogeneity of power in alpha band activity in neighboring thalamic modules. We hypothesized that the mechanism of mutual inhibition at the thalamic level may be responsible for antagonistic behavior of alpha band rhythms observed in the EEG at the cortical level. Finally, we extended the alpha rhythm model further, to account for abnormal oscillations at frequency 3 Hz associated with absence epileptic seizures. We show how complex interactions in thalamocortical network may be responsible for SW oscillation, which transiently emerges from the normal background. We also suggest that insight into dynamics of pathological rhythm may have therapeutic implications.

Models presented in this thesis allowed to test hypotheses regarding the neurophysiological substrates and dynamical properties of the normal and pathological oscillations mentioned above and finally led to the conclusions concerning the mechanisms by which attentional processes and spontaneous absence seizures may be organized.

1.5 The plan of this work

This work is organized as follows. After this introductory chapter, which contains basic information about the brain and its electric activity, follows Chapter 2, which describes in more detail two experimentally observed phenomena

that inspired the present modeling work. Chapter 3 begins with the general discussion on the computational modeling as a tool to investigate brain functions. Next, different neural modeling approaches are described and the choice of modeling method made in the present study is justified. Chapter 4 contains physiological and anatomical data that were used to build computer models of the brain structures, which mediate behavior of interest here. Next three chapters contain computer models of increasing complexity. We start with a classical alpha rhythm model (Chapter 5) developed about 25 years ago. In Chapter 6 we show how this alpha rhythm model may be extended to simulate the antagonistic behavior of the alpha band rhythms in neighboring cortical locations. In Chapter 7 we present a model which may reproduce both experimentally observed phenomena and we identify neuronal and network mechanisms responsible for their generation. The functional aspects of modeled mechanisms and relevance of presented studies are discussed in Chapter 8. The discussion is concluded by suggestions for future extensions of presented models.

Chapter 2

Experimental motivation

2.1 Event-related dynamics of alpha band rhythms

Since the first human scalp recordings done by Berger (1929) [6] it has been known that conscious experience may influence the EEG characteristics. For example the human alpha rhythm at frequency between 8–13 Hz is generated during relaxed awake state when the eyes are closed and its amplitude decreases when the eyes open. In some people, mental calculations may cause decrease of alpha rhythmic activity. In electroencephalography this decrease is called alpha blocking or 'desynchronization'. An example of such phenomenon was described by Penfield and Jasper (1954) [71] with Albert Einstein as a subject:

Einstein was found to show a fairly continuous alpha rhythm while carrying out rather intricate mathematical operations, which, however, were fairly automatic for him. Suddenly his alpha waves dropped out and he appeared restless. When asked if there was anything wrong, he replied that he had found a mistake in the calculations he had made the day before. He asked to telephone Princeton immediately. This illustrates how concentration of attention is just a special case of arousal, a local or focused waking response, employing similar neuronal mechanisms.

Except cognitive processing, voluntary movement may also cause desynchronization of the rhythms within the alpha frequency range, localized over somatosensory and motor areas (the so-called mu rhythms). With respect to these phenomena Pfurtscheller and Aranibar (1979) [75] introduced the term Event-related Desynchronization (ERD) for the EEG power changes induced by some event (e.g., finger movement). These authors also suggested the methods for ERD quantification (revived in [80]). To reduce an error in the estimate of event-related power changes, a number of event-triggered trials are necessary. Computing an event-related desynchronization (ERD) and an event-related synchronization (ERS) consists of the following steps, indicated schematically in Fig. 2.1. First, each trial is band pass filtered. The power within a band is computed by squaring amplitudes of filtered trails. Next, average is taken over all trials. Average power signals (A) are smoothed by averaging M consecutive power values. A reference power (R) is computed as a mean power in the reference period (some seconds before an event). A power change, in percentage, with respect to reference power is computed according to the formula:

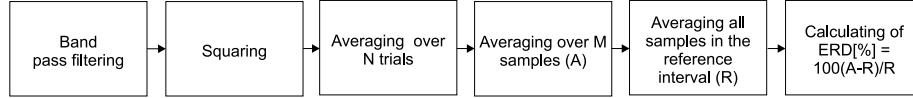


Figure 2.1: Scheme for computing ERD; Raw EEG data are first band pass filtered. Then each sample is squared and averaged over all trials. To reduce the variance the power signals are averaged over M consecutive samples. A reference power is computed using all samples in the reference period. Finally, relative power is computed.

$100(A - R)/R$. A power decrease corresponds to an ERD, a power increase to an ERS. The ERD/ERS can also be quantified in space by selecting a time point and computing ERD/ERS from multichannel data. In Fig. 2.2 the spatial distribution of event-related changes in power of the mu rhythm during voluntary movement of hand and foot is shown. On the right part of the picture we can see how the human body is schematically represented on the somatosensory cortex. During hand movement ERD (red colour) occurs over hand areas, and during foot movement ERD is present over foot areas what one would expect. At the same time, in certain areas the mu power increases (blue colour). During hand movement synchronization of mu appears over foot area. Similarly, ERD of foot area is surrounded by ERS of hand areas. In both cases there is a focal desynchronization/surround synchronization pattern. This finding was surprising because one would not expect that hand movement would influence the neuronal activity of the cortical area of the foot and vice versa. Interestingly, such a pattern appears not only during movement but is already present during movement planning, that is, during focusing attention on certain motor modality.

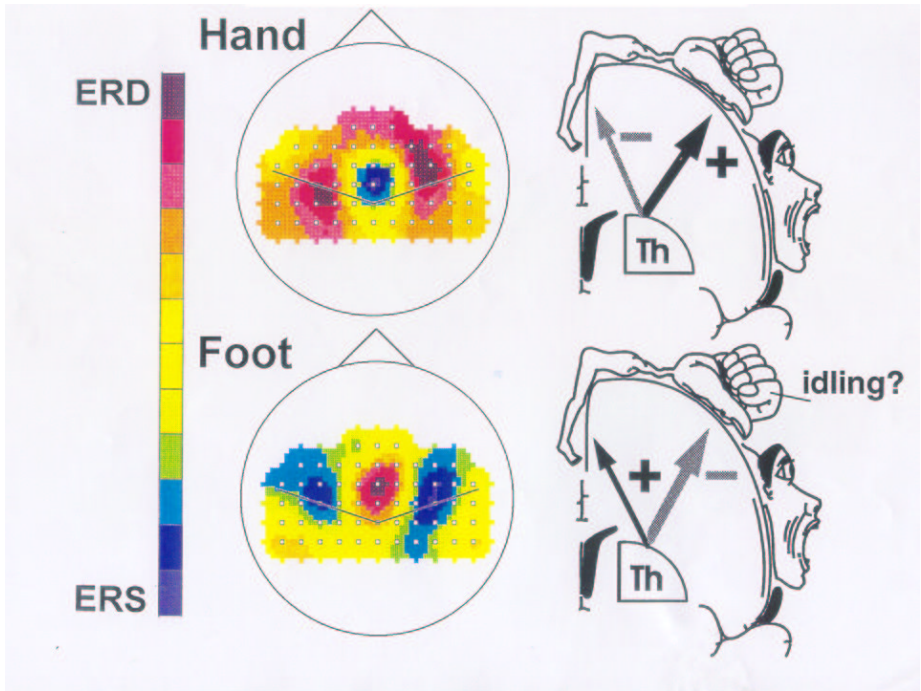


Figure 2.2: (Left): average ERD maps displaying synchronization and desynchronization of the alpha frequency components during voluntary movement (top: hand movement, bottom: foot movement). The colour code is shown in the bar at left: "red" indicates areas with power decrease (ERD) and "blue" with power increase (ERS). Positions of the electrodes used are marked by white squares. (Right): schematic representation of the human body in the somatic sensory cortex: foot areas are located medially (top of the head) and face areas are located laterally (side of the head). Hands are represented in relatively large cortical areas between those of foot and face. Modified from Pfurtscheller and Neuper (1994) [76].

2.2 Absence seizures

There are several classes of epileptic seizures. The most common type of epileptic seizure is the tonic-clonic seizure, which consists of rhythmic muscle shocks of the entire body and is accompanied by loss of consciousness. The kind of epilepsy of interest here is absence epilepsy, or petit mal. Perhaps the first, but accurate, description of absence seizure was made by Poupart in a report to the Académie Royale de Sciences in 1705:

At the approach of an attack the patient would sit down in a chair, her eyes open, and would remain there immobile and would not afterward remember falling into this state. If she had begun to talk and the attack interrupted her, she took it up again at precisely the point at which she stopped and she believed she had talked continuously.

Following Loiseau (1992) [55] absence seizures are characterized by short duration (5 to 10 s in most cases), an abrupt start and termination, an impairment of consciousness, a high frequency throughout the day. Absence seizures are associated with rhythmic spike and wave (SW) complexes recorded on the EEG in both hemispheres. The frequency of SW complexes is 3 Hz at the beginning of the discharges and may slow to 2.5 - 2 Hz towards the end. An example of electroencephalographic recording of an absence seizure is shown in Fig. 2.3.

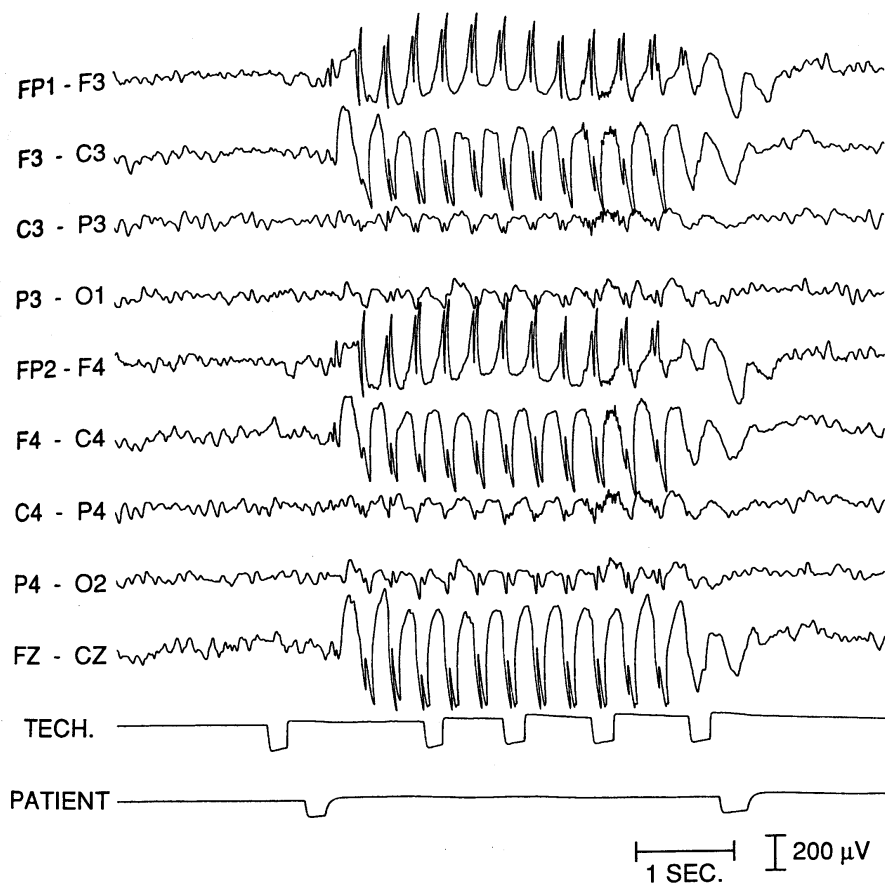


Figure 2.3: 3 Hz spike and wave complexes in the EEG recording of 15 year old girl with absence seizures. Note the patient's unresponsiveness during occurrence of the paroxysmal rhythm; The girl (PATIENT) fails to respond to auditory stimuli from a clicker (TECH.)

Chapter 3

Methods

3.1 Why modeling?

The amount of experimental data concerning physiology and anatomy of the nervous system grows rapidly. Theories based on these data are developed and predictions from these theories are made. Subsequently, experiments designed specifically to test the theory have to be performed. It has been recognized that building computational models of neural structures may significantly improve efficiency of this iterative process. Interactions between theory, experiment and model are shown in Fig. 3.1 and are described below.

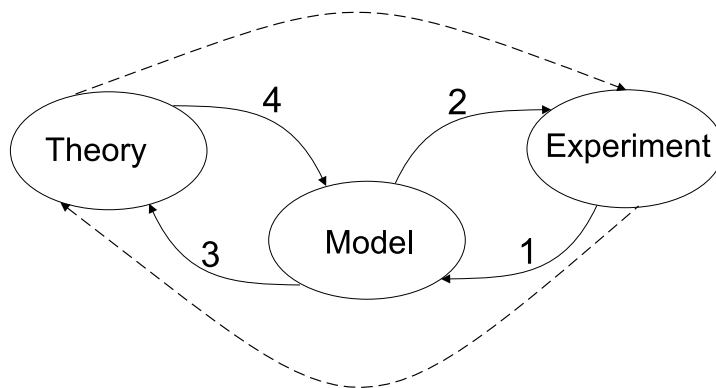


Figure 3.1: Schematic diagram of interactions between modeling, theoretical and experimental studies directed to reveal brain functions. The numbers labeling solid arrows correspond to the points listed below the figure. Dotted arrows represent 'traditional' interaction between theory and experiment.

1. Experiments allow for anatomically and physiologically realistic simulations.
2. Model may generate experimentally testable predictions and may provide interpretation for experimental data.

3. Models may show that a certain well-defined set of mechanisms/rules is sufficient to account for the experimental observations. Furthermore models may generate new ideas and, in this way, contribute to advancement of the theory.
4. In complex systems simple arguing may be misleading therefore models are developed to test theoretical predictions by explicitly calculating all the interactions in the system. Experiments, even those impossible to perform in the biological system, can be explored with the model.

3.2 Modeling approach

When modeling electrical activities of the brain, we first have to choose the level of neuronal organization at which we want to set a model. In practice, different factors may contribute to this choice. The level of detail necessary to investigate and bring information of the particular phenomena should be balanced with computational efficiency. Also, to determine parameter values and to validate modeling results, the level must be related to the nature of available real observations (e.g., micro- or macroelectrodes recordings). Roughly speaking, we may distinguish 4 orders of models of the electrical activity of brain systems, from micro- to the macroscopic levels. (i) In some models such as of hippocampal networks (Traub and Miles, 1991 [95]), each cell is realistically represented by multiple compartments for the soma, dendrites and axon, and each synaptic connection is simulated explicitly. It allows to elucidate the importance of different physiological details for the overall behavior of the network. This kind of realistic modeling requires large computing power. This is one of the reasons why the simplified versions of these models have been developed in which only one compartment is taken into account. (ii) These one-compartment models, however, lose the possibility to incorporate the morphology of the cells and the spatial distribution of ionic conductances. Nevertheless, such models may reveal the contribution of various ionic conductances to the behavior of either a single cell (McCormick and Huguenard, 1992 [64]; Wang, 1994 [103]) or a set of cells forming a network with different connectivity patterns (e.g., Destexhe et al., 1996a [26], Destexhe, 1998 [22]; Wang et al., 1995 [104]; Golomb et al., 1996 [30]; Lytton et al., 1997 [62], Rinzel et al., 1998 [83] and references therein). In the latter case we talk about a distributed model. In order to simulate the behavior of a large population of neurons, such highly detailed models can be cumbersome. (iii) In order to model large populations of interacting neurons at the macroscopic level another approach may be followed, i.e., lumped circuit models instead of distributed models. In lumped model one doesn't simulate single cells in a distributed network but rather takes a spatial average over populations that consist of neurons of a given type. In this way simplified network of interconnected populations is constructed and it is believed that it captures essential properties of the real system. Examples of lumped models are the models of Wilson and Cowan (1972) [108], Freeman (reviewed in Freeman, 1975 [27]); Lopes da Silva et al. (1974, 1976) [59],[61]; Zetterberg et al. (1978) [113]; van Rotterdam et al. (1980) [97]; Leung (1982) [51]; and Wright et al. (1994) [110]. (iv) In addition to lumped models, there are mathematical models that simulate dynamics of the EEG in global terms (e.g., Nunez 1981, 1995 [69], [70]; Wright

and Liley, 1995 [109], Wright).

In general, model building is a stepwise process. It starts with including the minimal principal features of the system in question. The subsequent features are added, as necessary, to replicate specific experimental results (Bower, 1995 [8]; Jeager, et al., 1997 [40]). Such approach was also followed in this thesis. Models presented in Chapters 5 and 6 belong to the class of lumped models. This is justified by the fact that focal ERD/surround ERS is a phenomenon that reflects the dynamic properties of neuronal populations at the macroscopic level. This modeling approach turned out to be not sufficient for simulating the mechanisms responsible for generation of SW seizures, because the latter depend critically on both the neuronal and network properties of the thalamocortical system. Therefore model presented in Chapter 7 is an extended version of the model presented in Chapter 6 and includes a key neuronal properties of the thalamic cells. It sets the model at the intermediate hierarchical scale between the single cell and population level. It is advantageous for the following reasons. (i) It allows to establish relation between model parameters and both cellular and synaptic (network) properties of the modeled system. (ii) It enables investigation of the system's dynamics, which is hardly accessible from models of distributed networks. (iii) It models local neurophysiological signals at the macroscopic scale and therefore allows to compare model's output with electric brain signals such as local field potentials or EEG. (iv) It also allows, under some assumptions, application of system analysis methods to quantify the system's behavior. And finally, (v) it is computationally efficient.

Simulations presented in this thesis were performed using the Simulink toolbox in MATLAB. Simulations were run using the ode3 (Bogacki - Shampine) integration method with a fixed time step of 2 or 4 ms duration. Model's behavior was not sensitive to the choice of the integration method. For one module model presented in Chapter 7, 10 seconds of simulated time took 12 seconds to run on the 400 MHz Pentium II PC, 64 MB RAM. All postprocessing analysis was done in MATLAB.

Chapter 4

Physiology

4.1 Thalamocortical network

Objective of this thesis is to provide understanding, by means of computer modeling, of the EEG changes related to voluntary movements and absence seizures. Therefore the model has to be based upon real anatomical and physiological data. The schematic diagram of somatosensory and motor system is depicted in Fig. 4.1. The stimulus to initiate and complete voluntary motor action is

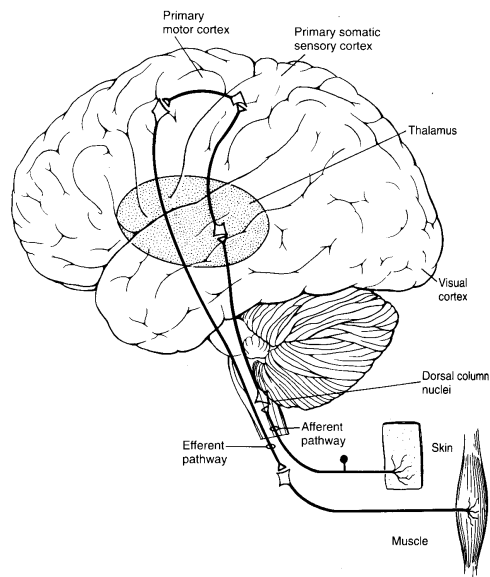


Figure 4.1: Schematic diagram of the somatosensory and motor pathways of the arm. Motor commands are generated in the primary motor cortex and are targeted to the muscles. Sensory information from muscles, skin and joints ascends to the relay in the thalamus and reaches primary sensory cortex. From Kandel et al. (1991) [42].

provided by the motivational (limbic) system, which acts on the motor system. The motor command goes through the brain stem to the motor neurons in the spinal cord and from there to the muscles. Sensory inputs from skin, muscles and joints ascend to the thalamus and are relayed to the somatic sensory areas. From there, somatosensory information is transmitted to the motor cortex and is used to modulate motor performance. The role of the thalamus is not restricted to relaying somatic sensory signals. Distinct sensory thalamic nuclei receive inputs about other sensory modalities (audition, vision) and relay them to local regions of the cerebral cortex (auditory, visual). Additionally the motor nuclei of the thalamus transmit information from the cerebellum and basal ganglia to the motor cortex. Furthermore, the thalamus consists not only of relay nuclei. The other functional group are diffuse-projection nuclei. An example of the nucleus, belonging to the latter group, is the thalamic reticular nucleus, which is critically involved in mediating rhythmic activities in thalamocortical network. The schematic diagram of connections between cells of the thalamic relay nucleus (i.e., TCR cells), cells of the thalamic reticular nucleus (i.e., RE cells) and cortical cells is shown in Fig. 4.2

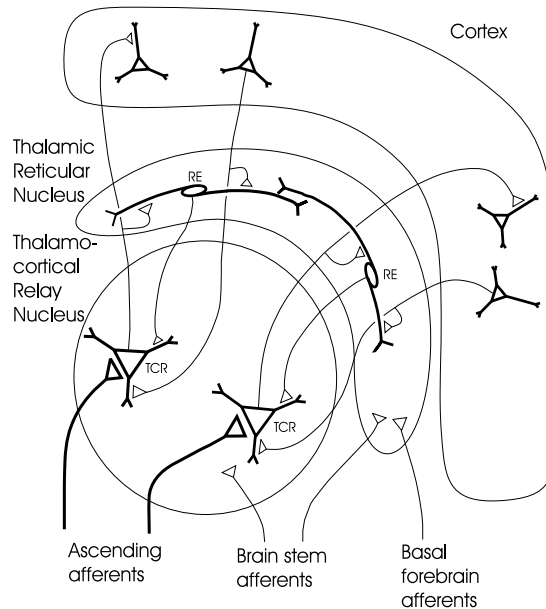


Figure 4.2: The schematic diagram of connections between main thalamic relay cells (TCR), cells of the reticular nucleus (RE) and cortex. Two main thalamic nuclei, each corresponding to single (sensory or motor) modality, are shown. Each specific thalamic nucleus receives input from ascending specific afferents and projects upon localized region of the cortex. The cortex sends recurrent connections to both thalamic relay and reticular nuclei. The thalamic relay cells send excitatory input to the reticular nucleus neurons. The RE cells are connected to each other by means of dendrodendritic synapses and send GABAergic inhibitory fibers to the TCR cells. The relay nuclei receive cholinergic modulatory input from the brain stem while the reticular nucleus also receives cholinergic input but from both the brain stem and basal forebrain.

As described above the thalamus is main relay station for the sensory signals on their way to the cortex. But it is also the first station at which sensory signal can be blocked when brain falls asleep or undergoes an absence seizure. The two functional modes (relay and non-relay) of the thalamus are associated with two distinct modes of action potential generation by the thalamic neurons: tonic firing (single spike) mode and burst firing (oscillatory) mode as shown in Fig. 4.3. The tonic firing mode is associated with the relay function of the thalamic cells because, in this state, the incoming sensory information may be transmitted accurately to the cortex. On the contrary, the burst mode is associated with synchronized oscillations in the thalamus during which the transmission of incoming sensory signals is depressed. These two modes of activity come from the properties of the specific ionic current, described in the next section.

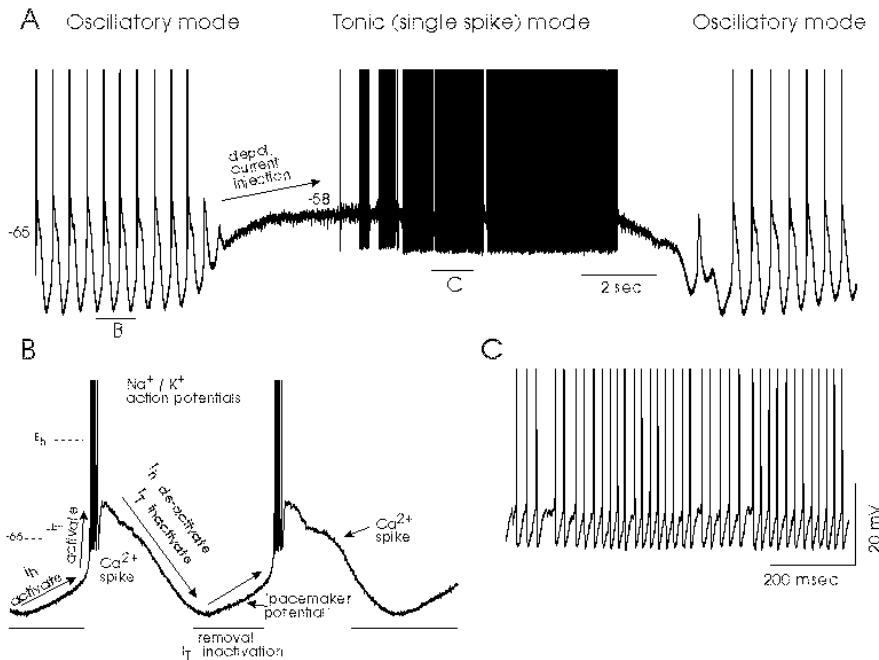


Figure 4.3: Two firing modes of the single thalamocortical relay neuron. (A) Burst firing is present at hyperpolarized levels, tonic firing at depolarized levels. (B) Expanded trace of membrane potential in oscillatory mode and the currents mediating this activity. (C) Expanded trace of membrane potential in tonic mode showing generation of single spikes. From McCormick and Pape (1990) [65]

4.2 Cellular mechanisms

The continuous intracellular recording in the upper panel of Fig. 4.3 shows that the firing pattern is controlled by the level of membrane potential. When a cell is relatively depolarized it generates a train of single spikes (action potentials). Hyperpolarized state promotes burst firing. Single spikes are mediated

by sodium and potassium currents while a burst consists of a calcium spike, sometimes called a low threshold spike (LTS), and 3 to 10 fast action potentials on the top of it (as shown in Fig. 4.3B). The LTS is generated by activation of a Ca^{2+} current, known as the low-threshold, or transient, (I_T) calcium current (Jahnsen and Llinás 1984 a,b [37], [38]). The I_T calcium current shows both activation and inactivation. Following Huguenard and McCormick (1992) [33], in the TCR cells activation occurs at membrane potentials positive to approximately -65 mV while inactivation becomes complete at membrane potentials positive to approximately -70 mV and is removed at hyperpolarized levels (negative to -70 mV). The kinetics of inactivation are slow while the activation is relatively fast. If a cell is depolarized from resting potential (around -70 mV), where the I_T current is almost completely inactivated, a cell will respond with the fast sodium-potassium spikes. If a cell is hyperpolarized first, the inactivation is removed and subsequent depolarization or even release from hyperpolarization is able to activate the I_T current which then slowly inactivates, generating a low threshold spike with a burst of fast action potentials.

4.3 Generation of thalamocortical rhythms

The low threshold Ca^{2+} spikes underlying burst firing in thalamic cells are essential for the rhythmogenesis of the activity in the alpha frequency range in the TCR-RE network. The thalamocortical relay (TCR) cells excite the reticular (RE) cells with glutamatergic AMPA synaptic transmission. The RE cells are inhibitory and hyperpolarize the TCR cells by means of GABA inhibition. This hyperpolarization is mediated mainly by the fast GABA_A receptors in the TCR cells, since GABA_B receptors have higher threshold for activation. The GABA_A receptor mediated hyperpolarization enables the TCR cells to fire rebound bursts which excite again the RE cells and the cycle repeats itself giving rise to rhythmic activity. The thalamic network, cycle of events, and resulting signals are shown in Fig. 4.4, upper panel. The frequency (7-14 Hz) of the rhythmic activity is largely determined by time courses of both excitatory and inhibitory postsynaptic potentials. The thalamic network scheme in Fig. 4.4 also depicts mutual inhibitory connection between the RE cells. The role of these connections is to control the discharges of those cells. This can be put in evidence by application of the bicuculine that blocks GABA_A receptors through which the RE-RE inhibition is mediated. It results in disinhibition of the RE cells and in an increase of discharges of those cells. Such prolonged discharges may activate GABA_B receptors in the TCR cells. GABA_B receptor mediated hyperpolarizations have longer duration and are efficient in the removal of the inactivation of the I_T current in the TCR cells resulting in larger bursts that excite the RE cells further. Also, the long duration of GABA_B postsynaptic potentials is responsible for slowing down the oscillations from 10 to 3 Hz. The bicuculine induced paroxysmal 3 Hz activity observed in the thalamic network *in vitro* resembles that generated *in vivo* in the interconnected thalamic and cortical networks during absence seizures. Further evidence for the critical role of the activation of GABA_B receptors in the thalamic relay nuclei comes from experimental animal studies. In animals with genetic absence epilepsy, thalamic injection of selective agonists of GABA_B receptors results in spike and wave discharges whereas administration of GABA_B receptor antagonists diminishes

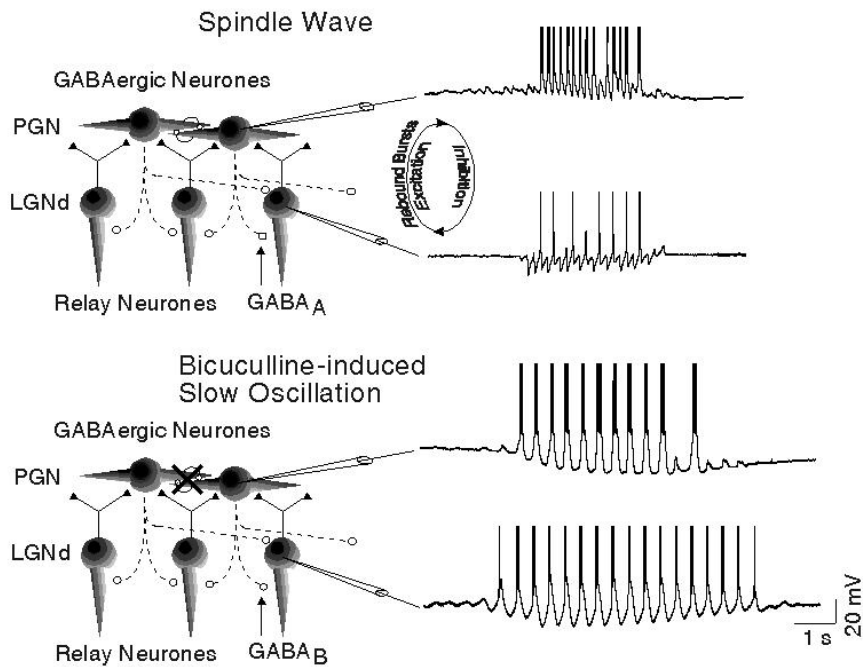


Figure 4.4: Generation of thalamic rhythms; Spindle waves at frequency around 10 Hz are generated through the interaction of GABAergic (RE) cells and relay (TCR) neurons, as shown in upper panel. The RE cells inhibit the TCR cells, which fire rebound bursts following GABA_A IPSPs. These rebound bursts excite the RE cells and the cycle repeats itself. Blocking GABA_A receptors (lower panel) results in disinhibition of the RE cells, which increase their discharges and activate GABA_B receptors in relay neurons. Consequently, network activity is transformed from 10 Hz to 3 Hz seizure-like activity. From Bal et al. (1995a) [4]

the occurrence of SW in a dose-dependent manner (Liu et al., 1992 [54]).

The thalamocortical projections transfer thalamic activity to the cortical cells while the corticothalamic feedback plays a major role in synchronization of thalamic oscillations.

Chapter 5

Alpha rhythm model

5.1 Distributed network vs. lumped circuit

The alpha rhythm model was developed as a possible explanation of the origin of the alpha rhythm in dog by Lopes da Silva and collaborators about 25 years ago. This model, as described in original publication (Lopes da Silva et al., 1974 [59]), consisted of two parts. The first part described the distributed network model where each neuron was modeled individually. This was in contrast to the second part describing the model of the lumped type, which means that it dealt with spatially localized populations of neurons rather than with individual cells. While the former approach helped to elucidate the relationship among activities of single cells, and between single cell activity and the whole populations's signals, the latter approach allowed to apply system analysis and in this way to analytically evaluate the influence of different neurophysiological parameters upon the statistical properties of the output rhythmic activity. This was a significant step forward and it may be a reason why this lumped alpha rhythm model became classic in a sense that it is repeatedly described in seminal works of the EEG literature (e.g., Niedermeyer and Lopes da Silva, 1999 [68]; Nunez, 1981 [69], 1995 [70]). The original population model of the alpha rhythm will be described in this chapter because models that we developed to account for the phenomena of interest in this thesis are extended versions of the above mentioned model and are based on the same concept.

5.2 Model description

The population alpha rhythm model is based on two interacting populations of neurons. They represent the populations of excitatory thalamocortical relay cells (TCR) and of inhibitory interneurons (IN) that are interconnected in the negative feedback fashion as shown in Fig. 5.1. Each population is described by statistical spatial average over the population. $V_e(t)$ is the average membrane potential in the excitatory population at time t and $V_i(t)$ of the inhibitory population. $E(t)$ is the proportion of excitatory cells (TCR), which become active (i.e., fire an action potential) per unit of time and $I(t)$ is the proportion of inhibitory cells (IN) firing per unit of time. $f_e(x)$ and $f_i(x)$ are static functions, which relate the average level of the membrane potential to the pulse density of

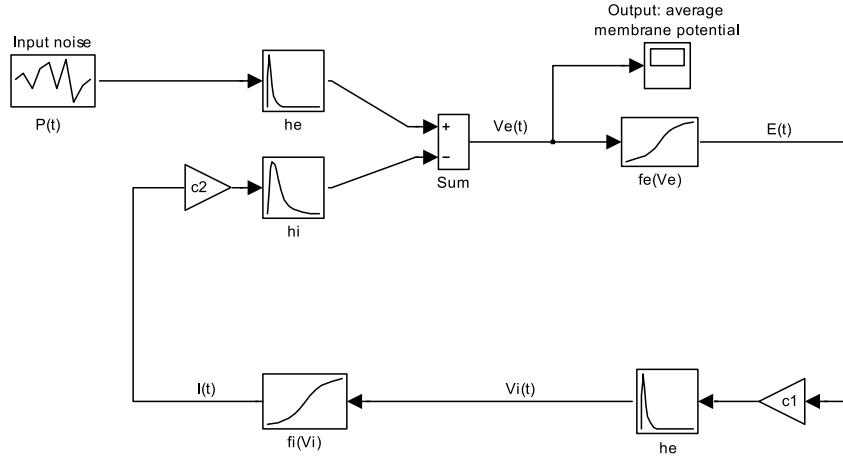


Figure 5.1: Block diagram of the alpha rhythm model. The TCR neurons are represented by impulse responses $h_e(t)$ and $h_i(t)$ simulating EPSP and IPSP, respectively and the sigmoidal function $f_e(V)$ relating the average membrane potential to the pulse density of the population. Similarly, the IN neurons are represented by the impulse response $h_e(t)$ and the sigmoidal function $f_i(V)$. The coupling constant c_1 represents the average number of IN cells to which one TCR cell projects and similarly c_2 represents the average number of TCR cells to which one IN cell projects. The TCR population receives excitatory external input $P(t)$.

the excitatory and inhibitory populations, respectively. They have a sigmoidal form that follows from the assumed Gaussian distribution of the firing threshold as shown in Fig. 5.2. The coupling constants c_1 and c_2 may be interpreted as

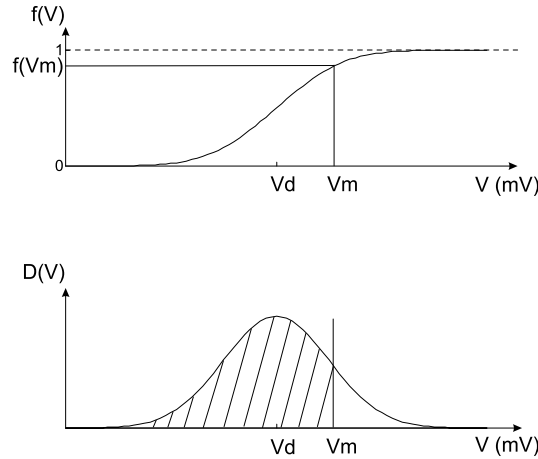


Figure 5.2: Sigmoidal population response function (upper plot) resulting from Gaussian distribution of individual firing thresholds (lower plot); For a given level of excitation in a population, V_m , the proportion of cells excited above a threshold is given by: $f(V_m) = \int_{-\infty}^{V_m} D(V')dV'$.

the average numbers of synaptic contacts that one output cell makes with cells in target population. $h_e(t)$ and $h_i(t)$ are the impulse responses for the excitatory and inhibitory synapses. They represent excitatory postsynaptic potentials (EPSP) and inhibitory postsynaptic potentials (IPSP), respectively. Input $P(t)$ represents excitatory input to the TCR population and is considered to be white Gaussian noise with a non-zero mean.

5.3 Linear system analysis

In this section derivation of the transfer function of the system is done as in the original paper (Lopes da Silva, 1974 [59]). It starts with equations relating firing densities, $E(t)$, $I(t)$ with corresponding average membrane potentials:

$$\begin{aligned} E(t) &= f_e(V_e(t)) \\ I(t) &= f_i(V_i(t)) \end{aligned} \quad (5.1)$$

The functions f_e and f_i are monotonously increasing and hence they have unique inverses that can be written:

$$\begin{aligned} V_e(t) &= f_e^{-1}(E(t)) \\ V_i(t) &= f_i^{-1}(I(t)) \end{aligned} \quad (5.2)$$

Function $f_e^{-1}(y)$ and $f_i^{-1}(y)$ may be expanded in the Taylor series around the mean values \bar{E} and \bar{I} , respectively:

$$\begin{aligned} f_e^{-1}(E(t)) &= a_{e0}(\bar{E}) + a_{e1}(E(t) - \bar{E}) + a_{e2}(E(t) - \bar{E})^2 + a_{e3}(E(t) - \bar{E})^3 + \dots \\ f_i^{-1}(I(t)) &= a_{i0}(\bar{I}) + a_{i1}(I(t) - \bar{I}) + a_{i2}(I(t) - \bar{I})^2 + a_{i3}(I(t) - \bar{I})^3 + \dots \end{aligned} \quad (5.3)$$

In the linear approximation only the two first terms are taken into account. It is convenient to introduce new variables that represent variations around the means (i.e., steady states) of stochastic processes $E(t)$, $I(t)$, $P(t)$, $V_e(t)$ and $V_i(t)$:

$$\begin{aligned} e(t) &= E(t) - \bar{E} \\ i(t) &= I(t) - \bar{I} \\ p(t) &= P(t) - \bar{P} \\ v_e(t) &= V_e(t) - \bar{V}_e \\ v_i(t) &= V_i(t) - \bar{V}_i \end{aligned} \quad (5.4)$$

After applying Laplace transforms the equations governing the operations indicated in the scheme in Fig. 5.1 are given by

$$p(s)h_e(s) - c_2i(s)h_i(s) = a_{e1}e(s) = v_e(s) \quad (5.5)$$

and

$$c_1h_e(s) = a_{i1}i(s) = v_i(s) \quad (5.6)$$

where $p(s)$, $e(s)$, $i(s)$, $h_e(s)$, $h_i(s)$, $v_e(s)$ and $v_i(s)$ are the Laplace transforms of $p(t)$, $e(t)$, $i(t)$, $h_e(t)$, $h_i(t)$, $v_e(t)$ and $v_i(t)$, respectively. Combining the expressions (5.5) and (5.6) we obtain the expression for $v_e(s)$:

$$v_e(s) = \frac{p(s)h_e(s)}{1 + \frac{c_1c_2h_i(s)h_e(s)}{a_{i1}a_{e1}}} \quad (5.7)$$

setting

$$\frac{1}{a_{i1}} = q_{i1} \text{ and } \frac{1}{a_{e1}} = q_{e1}$$

where q_{e1} represents the slope of the function f_e at the operating point \bar{V}_e and the same holds for q_{i1} . We get:

$$v_e(s) = \frac{p(s)h_e(s)}{1 + c_1c_2h_i(s)h_e(s)q_{i1}q_{e1}} \quad (5.8)$$

The impulse responses $h_e(t)$ and $h_i(t)$ approximating real postsynaptic potentials are given by the expressions:

$$h_e(t) = A[\exp(-a_1t) - \exp(-a_2t)] \quad (5.9)$$

$$h_i(t) = B[\exp(-b_1t) - \exp(-b_2t)] \quad (5.10)$$

with $a_2 > a_1$ and $b_2 > b_1$. The corresponding transfer functions are:

$$h_e(s) = \frac{A(a_2 - a_1)}{(a_1 + s)(a_2 + s)} \quad (5.11)$$

$$h_i(s) = \frac{B(b_2 - b_1)}{(b_1 + s)(b_2 + s)} \quad (5.12)$$

Including these expressions in (5.8) we get:

$$v_e(s) = \frac{Ap(s)(a_2 - a_1)(b_1 + s)(b_2 + s)}{(a_1 + s)(a_2 + s)(b_1 + s)(b_2 + s) + K} \quad (5.13)$$

where

$$K = c_1c_2q_{e1}q_{i1}(a_2 - a_1)(b_2 - b_1)AB \quad (5.14)$$

The coefficient K is characteristic of the model and is sometimes called a feedback gain factor. It is a linear combination of coupling constants c_1 and c_2 , the derivatives of the sigmoids in their working points q_{e1} and q_{i1} and the parameters of synaptic responses. The power spectrum of $V_e(t)$ may be obtained from eq. (5.13) by substituting s with $i\omega$ and using a constant for $p(s)$, since $P(t)$ is white noise. Fig. 5.3 shows the power spectrum of $V_e(t)$, calculated from eq. (5.13) for different values of K .

If the feedback coupling is weak (small K), there is not much interaction between the populations and the system is reduced to the transfer function $h_e(t)$ and the gain element $f_e(V)$. It results in a spectrum of a low-pass filter (the least peaked line in Fig. 5.3). When synaptic coupling ensures interaction between the populations, the feedback gain factor increases and the two poles of expression (5.13) become complex. The response of the system to a single pulse starts to oscillate, in a damped fashion. If the system is driven by white noise, instead of a single pulse, the response, $V_e(t)$, becomes a continuous signal, having a spectrum with a peak approximately at 10 Hz. The height of the peak increases with increasing value of K , while the width of the peak decreases. For K larger than the critical value $K_c = 3.74 \cdot 10^8 \text{ s}^{-4}$ the complex poles of expression (5.13) enter the right half of the s -plane. A bifurcation in the behavior takes place. A linearized version of the system becomes unstable, i.e., it starts oscillating with an ever growing amplitude, up to the limit of the

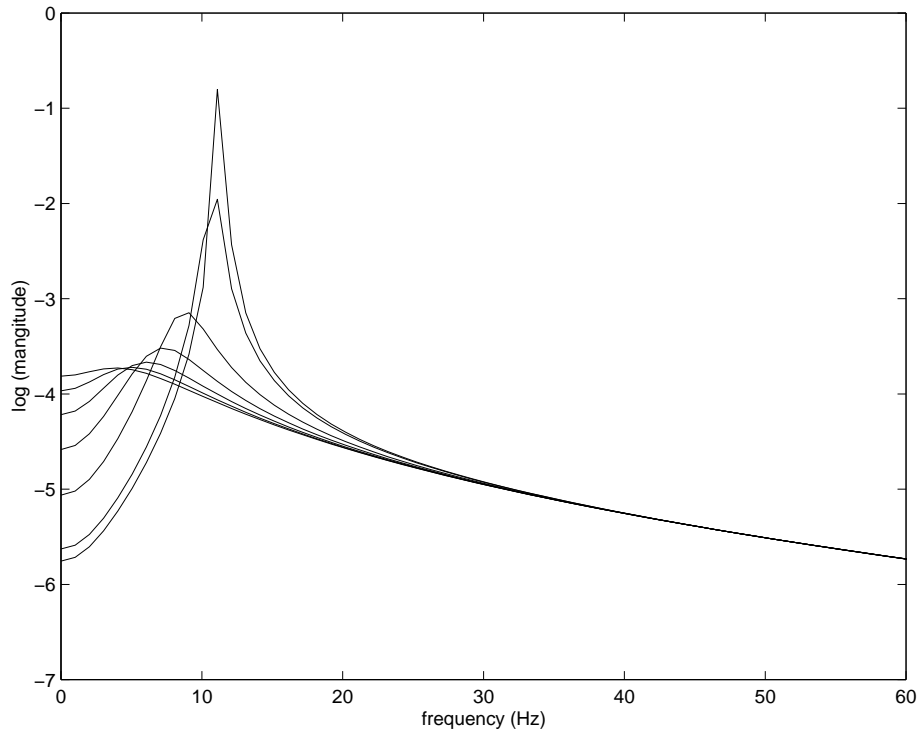


Figure 5.3: Power spectrum of the $V_e(t)$, displayed logarithmically as a function of frequency, for different values of the feedback factor K varied from $1 \cdot 10^7 \text{ s}^{-4}$ to $3.5 \cdot 10^8 \text{ s}^{-4}$. The spectrum has been calculated from eq. (5.13) for a flat input frequency spectrum $p(i\omega) = 1$. Other parameters used for this figure are: $A = 1.65 \text{ mV}$, $B = 32 \text{ mV}$, $a_1 = 55 \text{ s}^{-1}$, $a_2 = 605 \text{ s}^{-1}$, $b_1 = 27.5 \text{ s}^{-1}$, $b_2 = 55 \text{ s}^{-1}$.

computer (a stability analysis can be found in Appendix I of van Rotterdam et al., 1982 [97]).

The calculated power spectra are in good agreement with spectra derived from measured EEG signals. Additionally, the family of spectra of Fig. 5.3 approximates the development of the EEG as a function of age. Assuming that threshold parameters q_{e1} and q_{i1} should not change much and the synaptic time constants only slightly, it follows that the coupling constants c_1 and c_2 and post-synaptic potentials amplitudes A and B should increase during development. In this way system analysis of the alpha rhythm model provided a hypothesis that the evolution of the posterior EEG rhythm from the low dominant frequency to signal having a clear peak at around 10 Hz would depend upon an increase in interconnections and efficiency of synaptic contacts.

5.4 Nonlinear behavior

As stated above, the linearized version of the model produces an ever growing oscillation for K larger than the critical value $K_c = 3.74 \cdot 10^8 \text{ s}^{-4}$. This is, however, not the case when taking into account the nonlinear shape of the sigmoid what limits the amplitude of the signal. The nonlinear shape introduces different slopes, i.e., derivatives q_{e1} and q_{i1} , which means different gains during the operation. The oscillation obtained in this fashion, has a finite amplitude and it constitutes a limit cycle. Zetterberg et al. (1978) [113] showed that the frequency of these oscillations is determined solely by the time behavior of $h_e(t)$ and $h_i(t)$:

$$\omega^2 = \frac{(a_1 + a_2)b_1b_2 + (b_1 + b_2)a_1a_2}{a_1 + a_2 + b_1 + b_2} \quad (5.15)$$

For parameters we used, formula (5.15) yields $\omega = 11.3 \text{ Hz}$. The peak frequency of the linear model (Fig. 5.3) reaches the same value just before K reaches the critical value K_c . The transition in the dynamics of the model, i.e., from linear to nonlinear behavior (corresponding to a bifurcation from a point attractor to a limit cycle) is achieved by increasing K . K may be enlarged by changing the coupling constants c_1 or c_2 , or by increasing the mean value (i.e., the DC component) of the noise input to the model. We call the value of the input DC component, at which the transition happens, a bifurcation point. Interestingly, model prediction of the heterogeneous dynamical character of the alpha EEG rhythm was recently confirmed by experimental studies in humans (Lopes da Silva et al., 1997 [60]). Furthermore, we quantified a prevalence of nonlinearity in the human alpha rhythm by testing for nonlinearity 480 alpha epochs from sixty healthy subjects. Null hypothesis that signal is generated by linear stochastic process could be rejected in 1.25% while 98.75% of all epochs studied could not be distinguished from a linearly filtered noise (Stam et al., 1999 [89]).

5.5 Blurring of the bifurcation point due to dynamic noise

Lopes da Silva and colleagues (1974) [59] implemented the model in a form of executable computer program and Zetterberg et al. (1978) [113] constructed an

electronic circuit to investigate model's behavior. We used Simulink toolbox in MATLAB dedicated to simulations of dynamical systems. It allowed to vary parameters interactively, which helped us to investigate the model in more detail and to demonstrate its one additional feature. When the input $P(t)$ has zero variance the bifurcation described in the previous section is well defined. In that case we are dealing with one single bifurcation point. When $P(t)$ consists, apart from a DC offset, also of noise this is no longer the case. For such input the bifurcation point becomes blurred over a range of input values. We demonstrate this in Fig. 5.4, showing the bifurcation diagrams in case of DC input only (Fig. 5.4A) and DC plus noise (Fig. 5.4C).

Parts B and D of Fig. 5.4 show that, in case of a DC input, the signal changes qualitatively in dynamical properties when passing through the bifurcation point. It goes from a steady state to a regular limit cycle oscillation. When the input also contains noise the signals do, however, not differ in character, only the amplitude changes gradually around that point. As a consequence, it is no longer possible to denote a particular value for the offset of the input above which the transition in dynamics occurs. The range of input values over which the bifurcation point is blurred increases for increasing values of the variance of the noise. The blurring of the bifurcation point is well known among mathematicians (Crutchfield et al., 1982 [20]; Wiggins, 1990 [107]; Takens, 1996 [94]) and physicists (Horsthemke and Lefever, 1984 [32]; Longtin et al., 1990 [57]; Longtin, 1991 [56]) and definition of the bifurcation in the stochastic context has been proposed (Horsthemke and Lefever, 1984 [32]). On the other hand, to best of our knowledge such phenomenon has not been described in any model of neural circuits although bifurcations are a key feature of real neuronal networks which are, at the same time, never purely deterministic.

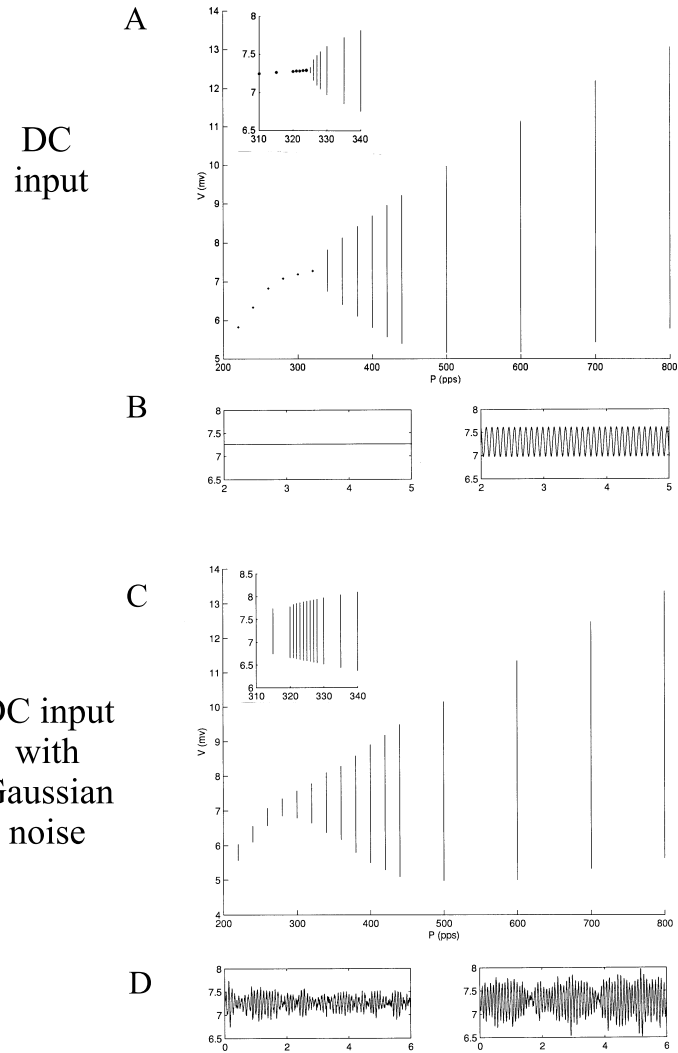


Figure 5.4: Hopf bifurcation in the model without (AB) and with (CD) noise present in the input. Big diagrams (A) and (C) show bifurcation diagrams with DC input level P as a control parameter on the X - axis and values of membrane potential V_e during 3 s of simulation on the Y - axis. Insets show the zooms at the vicinity of the bifurcation point ($P = 325$ pps). Time behavior of the system before and after the bifurcation is shown below each bifurcation diagram. In deterministic case (B), the system before the bifurcation ($P = 315$ pps) is in a steady state and after the bifurcation ($P = 330$ pps) exhibits limit cycle oscillations. In the presence of noise (D), both signals, before ($P = 315$ pps) and after the bifurcation ($P = 330$ pps), exhibit waxing and waning oscillations and there is no obvious qualitative change in dynamics from the time series point of view.

Chapter 6

Two modules - nonlinear feedback model of ERD/ERS

6.1 Formulation of the model

The model presented in this chapter is an extended version of the lumped model initially proposed by Lopes da Silva and collaborators (1974) [59]. The latter model, presented in a previous chapter, was based on two interacting populations of neurons forming a negative feedback loop. We showed that such a module produces rhythmic activity between 8 and 11 Hz when submitted to a random input. Here we present a version of the above mentioned model consisting of two of such modules, mutually interconnected by means of the synapses formed by a chain of reticular nucleus (RE) neurons according to Deschênes et al. (1985) [21], and also shown in Fig. 4.2 and 4.4. This turned out to be sufficient to simulate the spatial inhomogeneity of the rhythmic activity within the alpha frequency range in the thalamus. Such antagonistic behavior at the thalamic level is likely to produce focal ERD/surround ERS of alpha band rhythms at the cortical level. An even more extensive model consisting of five interconnected modules was also constructed in order to investigate interactions at longer distances. The block scheme of the model is shown in Fig 6.1. Notice the use of indices 1 and 2 for most of the variables belonging to the first and second module (the indices of the coupling constants c are an exception to this rule). Similarly as in the alpha rhythm model, each module of the present model consists of the following elements: the TCR population is characterized by two linear transfer functions $h_e(t)$, $h_i(t)$ and by the static nonlinearity $\lambda_e g_e(V)$ (here we adopt the notation of Zetterberg et al. (1978) [113]). The functions $h_e(t)$ and $h_i(t)$ represent the equivalent population depolarizing post-synaptic potential (PopDPSP) and the equivalent population hyperpolarizing post-synaptic potential (PopHPSP), respectively. Static nonlinearity $\lambda_e g_e(V)$ relates the algebraic sum of the postsynaptic potentials with the number of action potentials triggered per unit of time (the action potential density or $E(t)$) within the TCR population. The RE population is similarly characterized by $h_e(t)$, $h_i(t)$ and

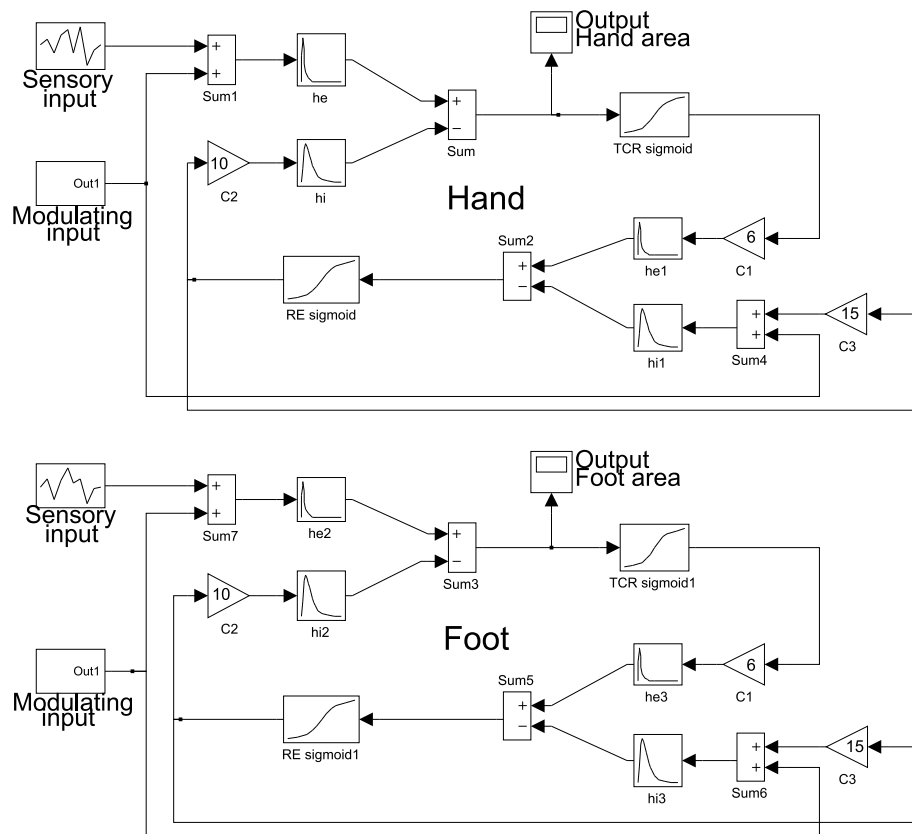


Figure 6.1: Block scheme of the two modules model; Each module is based on alpha rhythm model presented in a previous chapter. Additional modulating input represents cholinergic input from the brain stem. Each TCR population represents thalamic nucleus corresponding to single sensory or motor modality, e.g., hand or foot. Two modules are interconnected by means of mutual inhibitory connections between the RE cells.

$\lambda_i g_i(V)$ functions. Within each module, coupling constants c_1 and c_2 represent the number of connections that any RE cell receives, on the average, from the TCR cells and vice versa, respectively. (This definition is consistent with the definitions for divergence and convergence used by Traub and Miles (1991, pg. 58) [95].) The efficiency of each synaptic connection is expressed by the amplitude of the postsynaptic potentials, denoted as A and B in formula (6.4) and (6.5), respectively. Finally, the constant c_3 represents the number of reciprocal connections between the RE cells of two neighboring modules. Each module of the model has excitatory input to the TCR population. These inputs are denoted $P_1(t)$ and $P_2(t)$ in the first and second module, respectively. They represent the glutamatergic sensory input from the ascending thalamic afferents to the TCR cells in the thalamus (see also Fig. 4.2). The modulating input $M(t)$ represents cholinergic input originating, for example, from the brainstem mesencephalic cholinergic neurons and from the forebrain basilar nucleus. It is modeled as an excitatory input to the TCR cells and inhibitory input to the RE cells. This is justified taking into account that acetylcholine released by cholinergic pathways decreases a potassium conductance in the TCR cells and brings about depolarization of the TCR population (McCormick and Prince, 1987 [67]), while it increases the potassium conductance in the RE neurons and induces hyperpolarization of the RE population (McCormick and Prince, 1986 [66]). The gain c_4 reflects the different influence of cholinergic input on the TCR- and RE cells. In addition, other thalamic afferents arising from the midbrain consisting of monoaminergic fibers can also cause depolarization of the TCR cells (McCormick and Bal, 1997 [63]) but they were not simulated explicitly here. Attentional activity focussed on one single modality is simulated by enhancing the modulating input $M(t)$ to the corresponding module, which we will call the target module. The output of the model consists of two signals. The first signal is the average of the postsynaptic potentials of the TCR₁ cells. The second output signal is the equivalent signal from the other module. These output signals are denoted $V_{1e}(t)$ and $V_{2e}(t)$, respectively, and simulate what is generally considered to generate local field potentials. We assume that the dynamics of this activity induces similar dynamics at the cortical level. The latter is expressed in the scalp EEG recording (not modeled here).

6.2 Mathematical description of the model

Zetterberg et al. (1978) [113], taking into account the absolute refractory period of neurons (i.e., the period after generation of an action potential when a cell is inexcitable) derived the following expressions relating average membrane potential with average action potential density in a neuronal subset:

$$E(t) = \frac{\lambda_e f_e(V_e(t))}{1 + \lambda_e r_e f_e(V_e(t))} \equiv \lambda_e g_e(V_e(t)) \quad (6.1)$$

$$I(t) = \frac{\lambda_i f_i(V_i(t))}{1 + \lambda_i r_i f_i(V_i(t))} \equiv \lambda_i g_i(V_i(t)) \quad (6.2)$$

where variables $E(t)$ and $I(t)$ are defined as the proportion of excitatory and inhibitory cells firing per unit of time. Variables $V_e(t)$ and $V_i(t)$ are the average membrane potentials in the excitatory and inhibitory cells populations,

respectively. The constants λ_e and λ_i are maximal firing rates of cells in the two populations and r_e, r_i are absolute refractory periods of the cells in these populations. The function $f(V(t))$, in the two equations above was introduced by Wilson and Cowan (1972) [108]. The input of this function, $V(t)$, stands for the average level of excitation within the population while the output of $f(V(t))$ gives the proportion of cells in the population for which the input is so high that the level of firing threshold is reached or excelled (when they are refractory, however, they will not fire). The function $f(V(t))$ increases monotonically with $V(t)$ and approaches 0 or 1 as $V(t)$ approaches its lowest and highest value, respectively. The shape of the function $f(V(t))$ is related to the distribution of individual firing thresholds within a population. If the distribution has only one maximum (at a population threshold point), the function is assumed to have an S-shape, and, therefore, is called a sigmoid (see also Fig. 5.2). (It should be noted however that in addition to the thresholds spread in a population, in individual cells the relation between probability of response and stimulus intensity also has sigmoidal characteristic as was first shown by Verveen (1960 [99], 1961 [100])). Assuming that $f(V(t))$ is a sigmoid it follows that functions $g(V(t))$ in the equations (6.1) and (6.2) are also sigmoids but less steep than $f(V(t))$. Zetterberg et al. (1978) [113] used:

$$g(V) = \begin{cases} g_0 \exp[q(V - V_d)] & \text{if } V \leq V_d \\ g_0 \{2 - \exp[q(V_d - V)]\} & \text{if } V > V_d \end{cases} \quad (6.3)$$

The parameters chosen for the sigmoid were: $q = 1.5 \text{ mV}^{-1}$, $V_d = 7 \text{ mV}$, $\lambda g_0 = 25 \text{ s}^{-1}$. The physiological interpretation of these parameters is the following. The constant λg_0 , the value of the sigmoid at the inflexion point, specifies the mean firing rate of the population when the average membrane potential is at such a value that half of the population has reached firing threshold. λ is the maximal firing rate for any single cell within the population (not the same as the maximal firing rate of the whole population). Maximal firing rate of the population $2\lambda g_0 = 50 \text{ s}^{-1}$ is slightly less than the maximal firing rate of the single cells in the population. Wang (1994) [103] obtained, in a model of a thalamocortical relay neuron, a value for the firing rate of his cell in the same order of magnitude, namely 100 Hz, what is comparable with experimental data. The constant q determines the slope of the sigmoid. The slope is related to the variance of the thresholds of the cells. The value we choose, i.e., $q = 1.5 \text{ mV}^{-1}$, fits within the range of experimental results (Freeman, 1975 [27]). V_d is the mean firing threshold with respect to the level of the resting membrane potential. In the model of Wang (1994) [103], the resting membrane potential is -65.7 mV while the firing threshold is approximately -58 mV, thus $V_d = 7.7 \text{ mV}$. This is in agreement with the choice of the threshold we use in our model (7 mV).

The linear transfer functions, $h_e(t)$ and $h_i(t)$, are given by the following expressions (Lopes da Silva et al., 1974 [59]):

$$h_e(t) = A[\exp(-a_1 t) - \exp(-a_2 t)] \quad (6.4)$$

$$h_i(t) = B[\exp(-b_1 t) - \exp(-b_2 t)] \quad (6.5)$$

With the following parameters: $A = 1.6 \text{ mV}$, $B = 3.2 \text{ mV}$, $a_1 = 55 \text{ s}^{-1}$, $a_2 = 605 \text{ s}^{-1}$, $b_1 = 27.5 \text{ s}^{-1}$, $b_2 = 55 \text{ s}^{-1}$. With these values, the equivalent PopDPSP reaches its maximum around 5 ms and the equivalent PopHPSP has the peak at

around 25 ms. The amplitudes A and B are adjusted such that the maximum of the PopDPSP is 1.2 mV and the maximum of the PopHPSP is -0.8 mV. The postsynaptic potentials in our model are similar to the postsynaptic potentials in other models of the thalamical cells (Wang and Rinzel, 1992 [105], 1993 [106]; Wang et al., 1995 [104]).

Precise experimental estimates of the number of connections, the convergence factor, between TCR - RE, RE - TCR and RE - RE neurons are presently not available. In the present model we used $c_1 = 6$, $c_2 = 10$ and $c_3 = 15$. These values are in the same order of magnitude as the convergence factors used by Wang et al. (1995) [104] in his model of the thalamic network.

The $P_1(t)$ and $P_2(t)$ sensory inputs were modeled, each, as a random signal (Gaussian white noise) with a DC offset. The mean value of $P(t)$ input stands for the average number of pulses per second (pps) in the afferent fibers and the variance of the input for the variation in the incoming pulse intensity. In the present simulations we set the offset value of the input to 312 pps and the variance of the Gaussian noise to 169 pps². These values were set identical in both modules. We always used different seeds for the noise generators of the two (or more) modules in order to obtain independent inputs for each module. The modulating input $M(t)$ was modeled as a step function having value 8 pps during activation and 0 otherwise. The gain $c_4 = 10$ enhanced the influence of the modulation on the RE population.

6.3 Results

6.3.1 Two modules model

In order to investigate whether the interplay of two thalamocortical modules could generate the phenomenon of focal ERD/surround ERS of alpha band activity we implemented two interconnected modules with independent noise inputs. The two modules were made identical to each other and were mutually interconnected through the inhibitory RE cells. The two module system behaved similar to the alpha rhythm model, i.e., each module worked in a linear range and exhibited rhythmic activity at around 10 Hz. However, these alpha rhythm-like signals were less synchronized than signals from isolated modules. Attentional activity was simulated by applying the modulating input $M(t)$ to the target module (i.e., $M(t)$ was raised above zero). Both the target and the neighboring module changed their activity. These changes corresponded to a change of the positions of the operating points on the sigmoid of each of the population as demonstrated in Fig. 6.2. It can be seen that in the absence of $M(t)$ the positions of the operating points on the sigmoids of the corresponding cells of both modules are equivalent. However, in the presence of $M(t)$ the operating points of all four populations change, each in a different way. In the target module the operating points of the TCR and RE cells move further apart. The TCR₁ cells become almost saturated. This happened because, in the first place, the TCR₁ cells were excited by the raised input. The raised input, however, was also connected to the RE₁ cells where, in contrast, it caused inhibition (moving the operating point towards the asymptote at level zero). Second, the inhibition of the RE₁ cells, in turn, caused disinhibition of the TCR₁ cells, enhancing still more the upward movement of the operating point of the TCR₁ cells. Since the

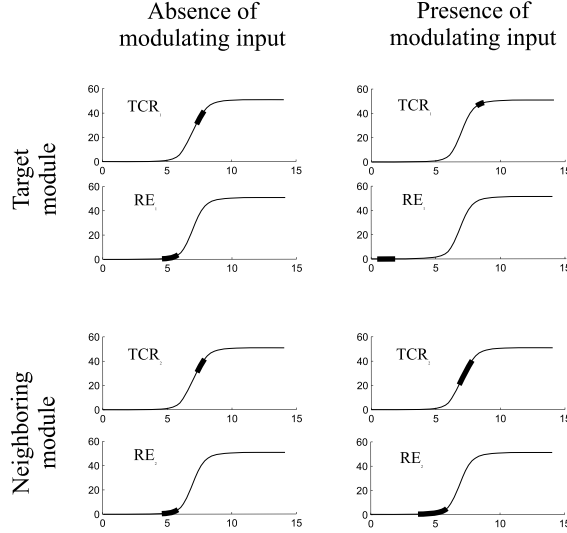


Figure 6.2: Positions of the operating points on the sigmoids of the four neuronal populations in the model. Left column: positions of the operating points in the absence of modulating input; right column: positions of the operating points in the presence of the modulating input. In each panel the sigmoid is plotted according to eq. (6.3). The labels denote populations where the range of operating points (thick lines) was measured. X - axis: average membrane potential with respect to the resting membrane potential (mV); Y - axis: firing density (pps).

operating points both moved to more flat parts of the sigmoids the feedback gain K_1 (being proportional to the derivatives of the sigmoids) dropped to a lower value. As may be inferred from Fig. 5.3, the reduction of the feedback gain, K , of a module results in desynchronization of the signal of that module. When the modulating input is removed (i.e., $M(t) = 0$), the signal returns to the original level of synchronization. These effects are illustrated in Fig. 6.3. It can also be seen that during the application of the modulating input $M(t)$ the signal $V_{1e}(t)$ shows an increase of the DC level. This change in signal offset reflects the depolarization of the TCR_1 cells mediated by cholinergic activation. The desynchronization of $V_{1e}(t)$ signal at the time of the modulation can also be put in evidence by way of the power spectrum shown in Fig. 6.4A. Application of the modulating input $M(t)$ to the target module had an opposite effect on the neighboring module. The effect of $M(t)$ on the neighboring module is an indirect effect, resulting from the reciprocal inhibitory connections between the two modules. The fact that the RE_1 cells of the target module are inhibited leads to disinhibition of the RE_2 cells of the second module. Consequently, the TCR_2 cells in this module become relatively more inhibited. In Fig. 6.2, these changes are expressed as movements of the operating points towards steeper parts of the sigmoids of these populations. This results in an increase of the value of K_2 in the neighboring module, reaching almost its critical value. This causes enhanced synchronization between third and sixth second as may be seen directly from the signal $V_{2e}(t)$ (Fig. 6.3, third panel) or from the changes in the

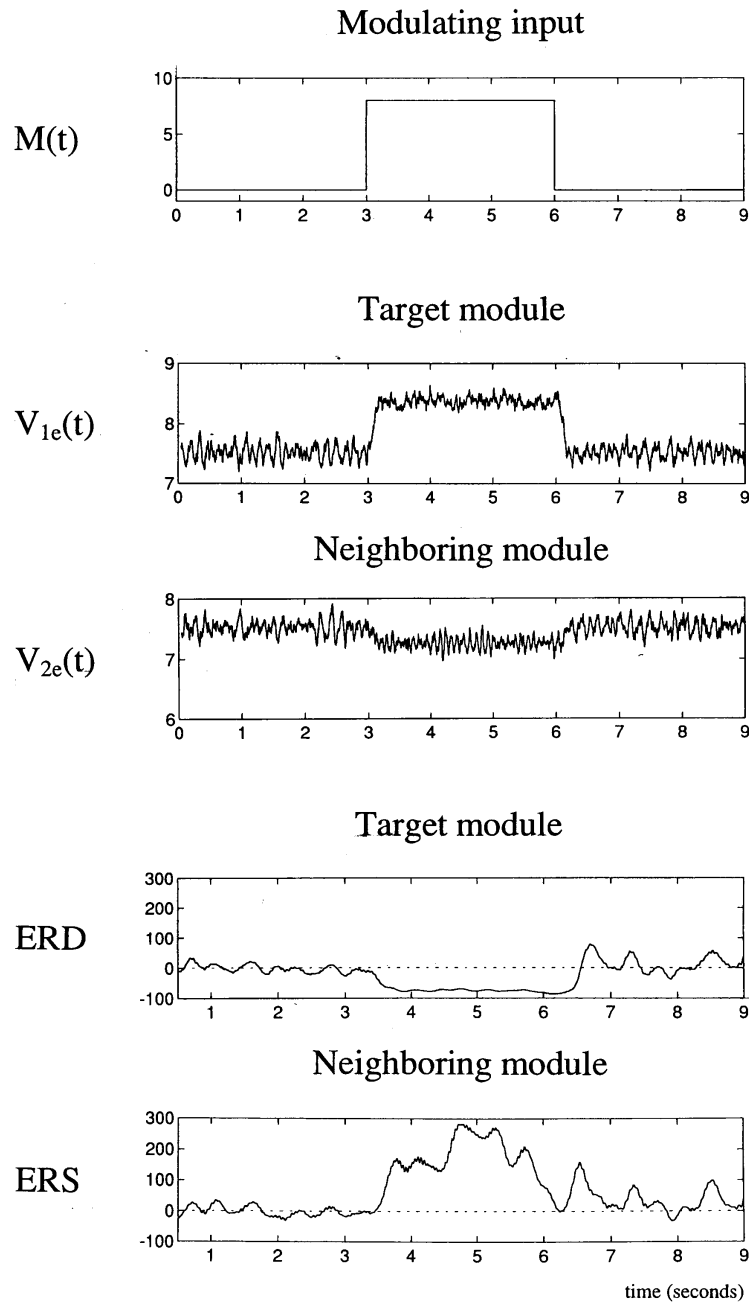


Figure 6.3: A single trial epoch of model output during modulating activity. The modulating input $M(t) = 8$ pps was applied between second three and six as shown in the first panel. Second panel: signal $V_{1e}(t)$ from the target module. Third panel: signal $V_{2e}(t)$ from the neighboring module. Fourth and fifth panel: time courses of the power change in alpha frequency range averaged over 12 trials from the target and neighboring modules, respectively.

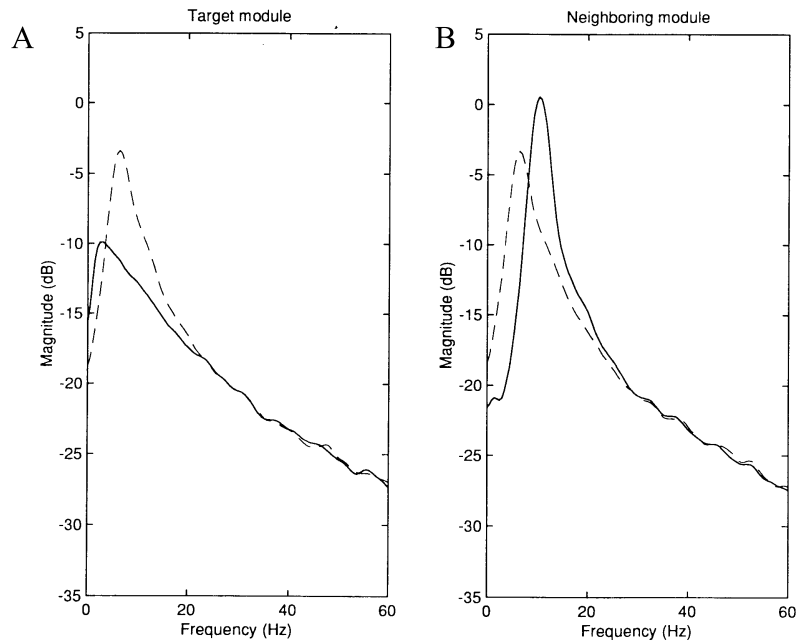


Figure 6.4: Power spectrum of signals from the target (A) and neighboring (B) module. Dotted lines represent spectra with absence of the modulating input, solid lines represent spectra with presence of the modulating input. (A) The power spectrum of the signal in the target module, during modulation applied to that module, exhibits lower and broader peak than in the reference situation, when the modulation was absent. (B) In contrast, the power spectrum of the signal in the neighboring module, during modulation applied to the target module, exhibits higher and narrower peak than the reference power spectrum.

spectrum in Fig. 6.4B.

It is interesting to note that the nonlinear shape of the function $g(V)$ in the model is essential for the change of the level of synchronization and desynchronization as a function of input. This implies that, although the generation of all signals may be accounted for by linear processes, the phenomena of ERS and ERD are essentially nonlinear.

6.3.2 Quantitative analysis

In order to emulate the ERD/ERS phenomena in a more realistic way we simulated twelve trials having a duration of nine seconds, and applied post-processing analysis as done in human recordings and described in section 2.1. We used the Signal Processing Toolbox of MATLAB for this purpose. For each trial we used different seeds for the noise generators of the two modules. Modulation was applied from the third to the sixth second, as shown in Fig 6.3 (top panel). Each trial was filtered between 8 and 12 Hz, using a linear-phase Remez FIR equiripple bandpass filter. Thereafter, each sample was squared and averaged over all trials. A quasi-instantaneous power was calculated using a sliding window of 200 ms (the samples within the window were averaged and the window was slid by one sample). A reference power (R) was computed as the mean power between the first and the third second. The relative power of each sample (A) was calculated according to the formula $100(A - R)/R[\%]$. Resulting signals are plotted in Fig 6.3 (two lowest panels). Positive values of these signals indicate ERS while negative values indicate ERD. A rebound in form of synchronization is present in both signals after termination of the $M(t)$ input. Such an ERS has also been observed experimentally in the beta (postmovement beta ERS (Pfurtscheller et al., 1996 [78], 1997b [79])) but also in the alpha frequency band (Pfurtscheller et al., 1996 [78], 1997b [79])). In our model this rebound phenomenon is the step response of the system that is frequency selective within alpha frequency range.

6.3.3 More modules

In order to test the spatial extent of the phenomenon of focal ERD/surround ERS we simulated a chain of five connected modules. In this case, each module (except the two at the extremes) was connected with its two neighbors. To take into account the influence of one module extra, we reduced the number of reciprocal connections between the RE populations, i.e., c_3 , by factor of two. Application of the modulating input $M(t)$ to the target module resulted in desynchronization of this module and enhanced synchronization of both neighboring modules. The disinhibition of the RE populations in these neighboring modules, in turn, caused enhanced inhibition of the RE cells to which they project. In this way a repeating pattern of desynchronization - synchronization in the chain of modules should arise. However, this does not appear to occur, as shown in Fig 6.5. Here we applied $M(t) = 8$ pps as input to the second module. Both neighboring modules, i.e., the first and the third exhibit ERS during modulation. The fourth module, however, does not show ERD but instead tends to show ERS. This may be explained as follows. The effect of the modulating signal on the DC level of the successive modules decreases as a function of distance such that the ERD/ERS fades away with distance from the target.

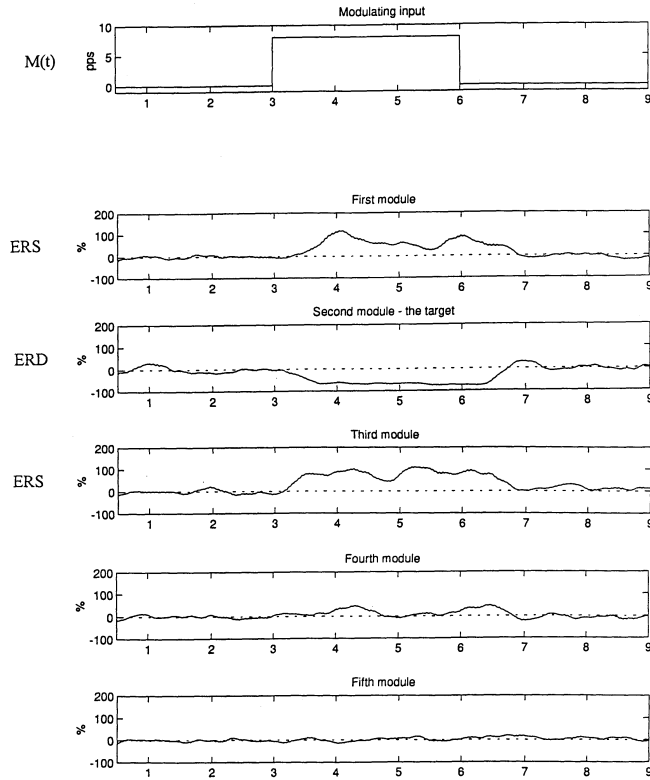


Figure 6.5: Time courses of the power change in the alpha frequency range averaged over 25 trials from five modules. The time course of the modulation $M(t)$ applied to the second module is shown at the top of the figure. Note the ERD in second module and ERS in the first and third module.

The change of the feedback gain K is negligible in the fourth module during modulation. In addition, the fourth module receives now highly synchronized input from the third module which works as a driving force. With the present choice of the model parameters, the effect of this synchronous 'driving' causes weak ERS in the fourth module. However, with another set of parameters (for example: offset of the sensory input $P(t) = 460$ pps, modulating input $M(t) = 10$ pps, $q = 0.34 \text{ mV}^{-1}$, $c_1 = 10$, $c_2 = 1$, used for all modules) all modules, except the fourth, showed the same ERS and ERD as in the previous simulations. The fourth module, however, instead of displaying ERS exhibited now weak ERD (data not shown). It is remarkable that experimental data are also ambiguous in this respect. In the situation of the right part of Fig 2.2 the foot corresponds to module two (the target module), the hand to module three and the tongue to module four. The map (bottom left part of Fig. 2.2) shows a very slight ERD for the tongue area during foot movement (corresponding with our 'non-standard' parameter setting), but clearly the opposite may also happen as shown in Fig. 6 of Pfurtscheller et al. (1997a) [77].

6.4 Discussion

The main result of the study is that a model consisting of a chain of modules of the TCR - RE neurons interconnected by mutual inhibitory synapses is capable of displaying dynamic changes in synchronization that reproduce the essential properties of focal ERD/surround ERS of the rhythms within the alpha frequency range, experimentally demonstrated by Pfurtscheller et al. (1992b [73], 1994 [76], 1997a [77], see also review [80]). Indeed, these authors reported antagonistic behavior in the alpha band activity in the neighboring cortical areas when different types of body movements were performed. In addition, synchronization of central mu rhythms was observed in relation with desynchronization of occipital alpha rhythms during visual processing (Pfurtscheller 1992b [73]; Koshino and Niedermeyer, 1975 [45]). In some biological systems mutual inhibition is a mechanism providing the basis for antagonistic behavior (e.g., lateral inhibition in the retina, competitive exclusion in ecology, Glass and Mackey, 1988 [29]). The model simulations presented here are consistent with the hypothesis that mutual interactions between inhibitory neurons may be responsible for this neurophysiological "flip-flop" switch. Our results are in agreement with the statement of Yao and Freeman (1990) [112] that mutual inhibition promotes spatial contrast. However, in our present studies the antagonistic behavior is at the level of the dynamics of a population (i.e., coherent firing in a population) rather than in a number of impulses per second. We found that the nonlinear shape of the sigmoid functions characterizing the TCR and RE neuronal populations in our model is essential for the change of the level of synchronization of the generated activity. This holds for the antagonistic behavior of interacting modules but it is even necessary for one module on its own. This cannot be accomplished in a linearized version of a single module if the coupling constants are not changed. The position of the operating point on the slope of the nonlinear sigmoid conditions the level of synchronization of the output. The behavior of the model is rather robust regarding the set of parameters that are used. The allowed variations of each parameter (while all others are kept constant), can be very large as shown in the Appendix in Suffczynski et al. (1999) [93]. However, many parameters are interrelated and changes of one parameter may be compensated by changes of another one. Accordingly, the range of allowed values for different parameters may even be larger than indicated in the Appendix. When the model operates in a linear range the ERS and ERD phenomena are not only manifested as a change in degree of synchronization of a signal, but also as a shift of peak frequency (Fig. 6.4). This prediction of our model was verified experimentally in a number of subjects. Another prediction of this study is that the blockade of mutual inhibitory connections between modules will result in enhancement of synchrony in all modules. We found this in our simulations (not shown). The latter coincides with the results of the model of Wang et al. (1995) and with experimental studies of Huntsman et al. (1999) [36].

In conclusion the present model study, that was inspired by neurophysiological observations, has led to a hypothesis concerning the mechanisms at the network level that may be responsible for the antagonistic behavior of the alpha band rhythms in neighboring cortical areas during performance of motor and sensory tasks.

Chapter 7

Model of normal and pathological brain thalamic oscillations

7.1 Integrating neuronal and network properties

Our simple model of the thalamic populations, presented in the previous chapter, was capable of reproducing experimental results of the dynamics of mu rhythms during preparation and execution of voluntary movements. That model suggested that the antagonistic behavior in the neighboring cortical areas was mediated at the network level by mutual inhibitory connections between reticular cells. However it did not identify the mechanisms at the cellular level that are essential for this phenomenon to occur. Furthermore the population model of ERD/ERS could not account for abnormal 3 Hz spike and wave oscillations that are associated with absence epileptic seizures. It was shown (Section 4.3) that both GABA synaptic transmission, mediated either by A or B receptors, the level of the membrane potential of the thalamic neuronal populations and low-threshold Ca^{2+} currents, play a role in the generation of alpha spindle oscillations and 3 Hz spike and wave activity. In order to obtain a better understanding of how these different factors condition the two main modes of activity in the thalamus, and the transition between both, we have developed the model further.

7.2 Model description

The model was extended by adding new features to the lumped models presented in the previous chapters. In the present model the transformation between mean membrane potential and firing density takes into account the low-threshold I_T calcium current that underlies burst firing in the thalamic cells. In addition, we included a slow GABA_B receptor mediated inhibition with nonlinear activation properties. We also added cortical input that controls and shapes the activity

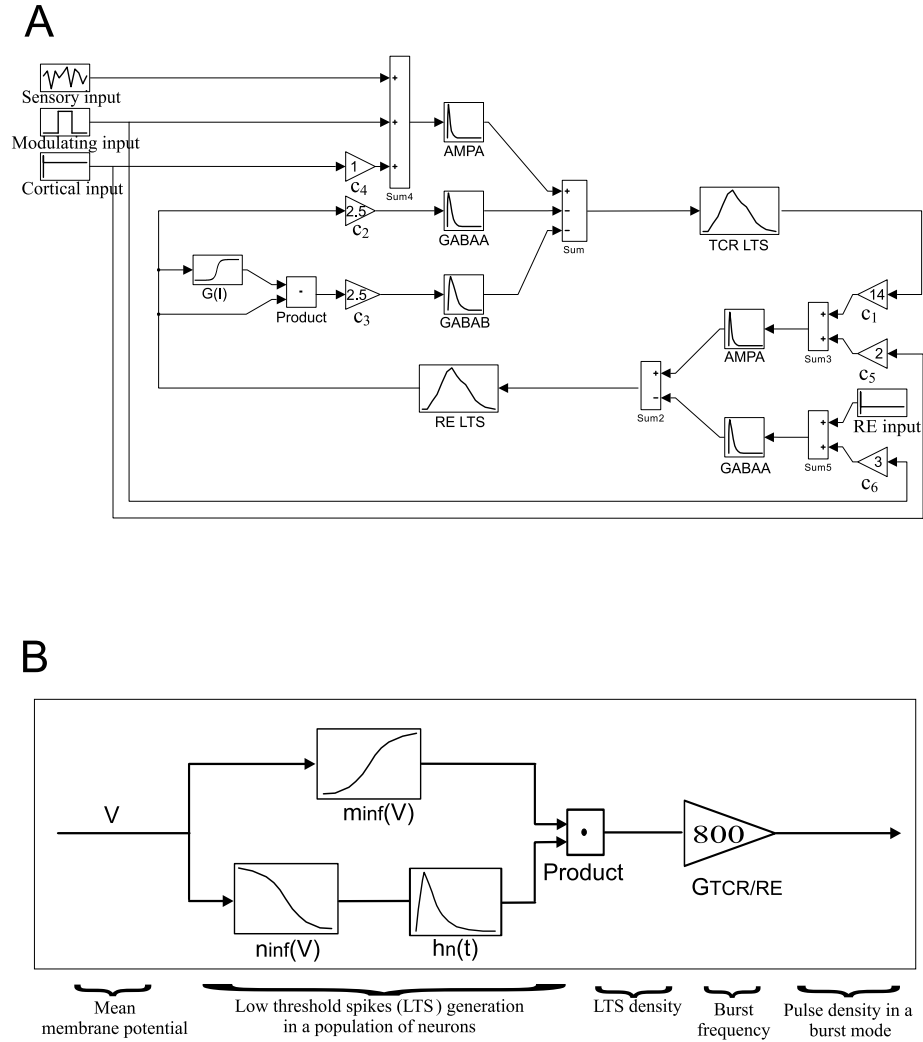


Figure 7.1: The schematic diagram of the model. (A) Single module consisting of two interconnected populations of TCR and RE neurons. The TCR population is described by impulse responses representing AMPA, GABA_A and GABA_B postsynaptic potentials and the transformation TCR LTS that represents bursts generating process. The function $G(I)$ represents the nonlinear activation properties of GABA_B receptors. The TCR population receives sensory, cortical and neuromodulatory inputs. Similarly, the RE population is described by impulse responses representing AMPA, GABA_A postsynaptic potentials and the transformation RE LTS that represents bursts generating process. The RE population receives neuromodulatory and external inhibitory inputs. Coupling constants c_1 – c_6 represent the average numbers of connections between different cell types. (B) Details of the blocks TCR LTS and RE LTS that relate mean membrane potential of the population to the firing density in a burst firing mode. Functions m_{inf} and n_{inf} describe the fractions of cells in which the I_T current is activated and inactivated, respectively. Impulse response function h_n represents the time delay of the inactivation process. The gain $G_{TCR/RE}$ represents the frequency of action potentials during single burst.

of the thalamic nuclei. Besides, we also considered extended version of the basic thalamic model with a cortical module included. The scheme of the one module of basic thalamic model is shown in Fig. 7.1A. Each element of the model is described successively.

Postsynaptic potentials. Postsynaptic potentials mediated by glutamatergic AMPA and GABAergic GABA_A and GABA_B receptors were simulated, as before, using a general form of the alpha function:

$$h(t) = \beta[\exp(-\alpha_1 t) - \exp(-\alpha_2 t)] \quad (7.1)$$

where β denotes amplitude and α_1, α_2 are the decay and rise time constants, respectively. In the notation below, for each type of postsynaptic potential, first parameter denotes its amplitude and the next two denote its decay and rise time constants, respectively. We used: $E_x = 6$ mV, $e_1 = 50$ s⁻¹, $e_2 = 130$ s⁻¹ for AMPA receptors; $A = 1$ mV, $a_1 = 30$ s⁻¹, $a_2 = 130$ s⁻¹ for GABA_A receptors and $B = 18$ mV, $b_1 = 8$ s⁻¹, $b_2 = 15$ s⁻¹ for GABA_B receptors. Parameters for AMPA and GABA_A postsynaptic potentials were obtained by fitting the alpha functions to the postsynaptic potentials generated in the TCR and RE cells reproduced according to the thalamic slice model of Golomb et al. (1996) [30]. The time course of the GABA_B IPSPs in our model, had time to peak at around 200 ms, in agreement with Kim et al. (1997) [44]. Additionally, following the observation (Kim et al., 1997 [44]) that high stimulus intensity is needed to activate GABA_B receptor in the thalamic cells, we assumed that the amplitude of the GABA_B postsynaptic potentials increases nonlinearly with the spiking rate of the RE population. This nonlinear relation was described by the sigmoidal function of the form:

$$G(I) = [1 + \exp(\frac{I - \theta_G}{\sigma_G})]^{-1} \quad (7.2)$$

where I denoted pulse density of the RE population, $\theta_G = 11$ pps was the assumed threshold for GABA_B receptor activation and $\sigma_G = -0.01$ pps determined the slope of the sigmoid. Values of θ_G and σ_G were set in a phenomenological way by assuming that during normal activity GABA_B receptors were not activated.

Low threshold spikes. In the models presented in the previous chapters the activity of a neural population was characterized by the proportion of cells that became active per unit of time or, in other words, by the average firing rate in a population. We also followed this approach here and described the activity of neural populations by a single variable that reflects the mean value of the underlying statistical process. Furthermore, we were interested in more realistic modeling of synchronized oscillatory activity of the thalamic populations that occurs at the hyperpolarized membrane potential levels of the thalamic cells. Under these conditions the thalamic neurons fire bursts of action potentials rather than tonic trains of spikes (Section 4.2). Therefore in the present model to characterize activity of a population we considered the spike density associated with burst firing. The procedure is as follows. First we compute the proportion of a population that fires low-threshold spikes (LTS). Next, the fraction of cells in a population firing LTS is multiplied by a firing rate of a single burst, which gives firing rate of a population associated with burst firing.

In a population, the relative number of cells that fire LTS at the time t is equal to the proportion of cells in which the I_T current is deinactivated and

which, at the same time, are depolarized above the threshold for LTS generation. We introduce new variables $n(t)$, $n_\infty(V)$ and $m_\infty(V)$. $n(t)$ denotes the relative number of cells in which the I_T current is deinactivated at time t . $n_\infty(V)$ and $m_\infty(V)$ denote the steady state functions of the mean membrane voltage of the population $V(t)$. These functions express the fractions of cells in which the I_T current is deinactivated and activated, respectively as a function of V . If we assume that activation of the I_T current is immediate at the appropriate value of the membrane potential V , the fraction of cells that fire LTS at time t is given by $m_\infty(V)n(t)$. If we assume that the effect of the change in mean membrane potential decays and rises exponentially with the rate constants n_1 and n_2 , respectively, then the expression for the $n(t)$ is given by:

$$h_n(t) * n_\infty(V(t))$$

where "*" denotes convolution,

$$h_n(t) = N[\exp(-n_1 t) - \exp(-n_2 t)]$$

and the constant N is normalization factor equal:

$$\frac{n_1 n_2}{n_2 - n_1}, \quad n_2 > n_1$$

Finally, assuming that each LTS triggers a burst of fast action potentials at, for example, the frequency of 800 Hz, the pulse density associated with burst firing of the TCR or RE population is

$$G_{TCR/RE} m_\infty(V(t)) n(t)$$

where the gain elements G_{TCR} and G_{RE} are set equal to 800 pps in both the TCR and RE populations. The scheme of the transformation between the mean membrane potential and the average firing rate in a burst mode is depicted in Fig. 7.1B. The activation and inactivation functions in both the TCR and RE populations have the same form:

$$f(x) = [1 + \exp(\frac{x - \theta_f}{\sigma_f})]^{-1} \quad (7.3)$$

with the following parameters: $\theta_n = -16$ mV $\sigma_n = 6$ mV, $\theta_m = 6$ mV $\sigma_m = -1.5$ mV, for the TCR population and $\theta_n = -6$ mV $\sigma_n = 6$ mV, $\theta_m = 16$ mV $\sigma_m = -1.5$ mV, for the RE population. Activation and inactivation thresholds are given with respect to the resting potentials: -65 mV in the TCR cells and -70 mV in the RE cells. Values of thresholds were based on the corresponding thresholds in single thalamic relay cells (Huguenard and McCormick, 1992 [33]) and reticular cells (Huguenard and Prince, 1992 [34]). The slope parameters of the network model, however, were modified with respect to the corresponding slope parameters of single thalamic cells due to the following reasons. First, we assume that the activation and inactivation thresholds of the I_T current in a group of cells have a Gaussian distribution around their mean values. The estimation of an average over a population corresponds to the operation of convoluting a given sigmoidal function, describing activation or inactivation of the I_T current in a single cell, with a Gaussian Kernel. This results in another

sigmoidal function that is less steep than the original one as we also verified numerically (not shown). Second, we do not simulate the LTS generation mechanism itself but rather the average LTS occurrence under certain conditions, e.g., the average rebound response of a population. Therefore we adjusted the slopes of the sigmoids within the physiological range to obtain the desired model behavior. The same reasoning applies to the choice of the rate constants for the $h_n(t)$ function describing the dynamics of inactivation. We chose $n_1 = 10 \text{ s}^{-1}$, $n_2 = 20 \text{ s}^{-1}$ for both the TCR and RE populations.

Connectivity. Coupling constants c_1 (TCR→RE), c_2 (RE→TCR), and c_3 (RE→TCR) represent the average number of synaptic contacts between different cell types. We chose $c_1 = 14$, $c_2 = 10$, $c_3 = 10$. These values are in the same order of magnitude as the number of connections between the TCR and RE cells in other models of the thalamic networks (Wang et al., 1995).

External inputs. The TCR population receives external excitatory input P that represents glutamatergic sensory inputs from the ascending afferents. This was modeled as a random signal (Gaussian white noise) with a DC component. We set the offset value of the input \bar{P} to 110 pps and the variance of the noise σ_P^2 to 4 pps². Both the TCR and RE populations receive excitatory input P_{Cx} that stands for glutamatergic corticothalamic input from the pyramidal cells in the layer VI of the cortex. It was modeled as a DC offset signal having the value 25 pps. The gains c_4 (Cx→TCR) and c_5 (Cx→RE) describe the influence of the cortical cells on the TCR and RE populations, respectively. The choice $c_4 = 1$, $c_5 = 2$ is motivated by the fact that the RE cells are more sensitive to corticothalamic input (Contreras et al., 1993 [13]), possibly due to a powerful T-current in dendrites (Destexhe et al., 1996b [25]). In the TCR neurons, the influence of cortical EPSPs decreases as the cortical synapses are distributed only on the distal dendrites of those cells (Liu et al., 1995 [53]). Additionally, the TCR and RE populations receive a modulating input M . As in the previous model, it represents mainly the cholinergic neuromodulatory input originating, from the brain-stem mesencephalic cholinergic neurons and from the forebrain basilar nucleus. The modulating input M was modeled as a step function having the value of 6 pps during cholinergic activation and 0 otherwise. The gain $c_6 = 12$ enhanced the influence of the modulation on the RE population. Finally, the RE population receives an inhibitory offset signal Q of 40 pps. It represents the inhibitory bias from the neighboring RE cells, since the latter are interconnected by mutual inhibitory synapses.

Model output. The output of the model is the sum of the postsynaptic potentials in the TCR population. This output signal is denoted $V(t)$ and have interpretation as in the previous models. It follows that the scalp EEG recordings are, in general, not explicitly modeled here. On the other hand in Fig. 7.8 in section 7.3.5 we present signal generated by the model and compare it with real EEG signals. For this purpose, we computed extracellular currents as derivatives of postsynaptic potentials of AMPA, GABA_A and GABA_B type. We added them and applied a low pass filter. The best correspondence between real EEG signals and simulated signal was achieved when AMPA currents generated in the RE population lagged by 50 ms GABA currents generated in the TCR population.

Extension of the model. In extended version of the model we included a cortical module representing a population of cortical pyramidal cells. The cortical module receives excitatory inputs from the TCR population and projects

to both the TCR and RE populations by means of corticothalamic projections as shown in Fig. 7.2. The cortical module is characterized by the time course of the postsynaptic potentials mediated by AMPA receptors and the sigmoid function that relates the mean membrane potential of the cortical population to the average firing density of fast Na^+/K^+ action potentials fired by pyramidal cells. The sigmoid function $S(V)$ was of the form of expression (7.3) with the threshold parameter $\theta_S = 7$ mV and slope parameter $\sigma_S = -5$ mV. We assumed that the maximal firing rate of the cortical population was 50 pps and the number of connections that one pyramidal cell receives, on average, from one TCR cell was set as $c_7 = 2$ (TCR→Cx). Taking into account that corticothalamic projections outnumber roughly ten times the thalamocortical ones (Sherman and Koch, 1986 [87]) we set the gains $c_4 = 10$ (Cx→TCR) and $c_5 = 20$ (Cx→RE).

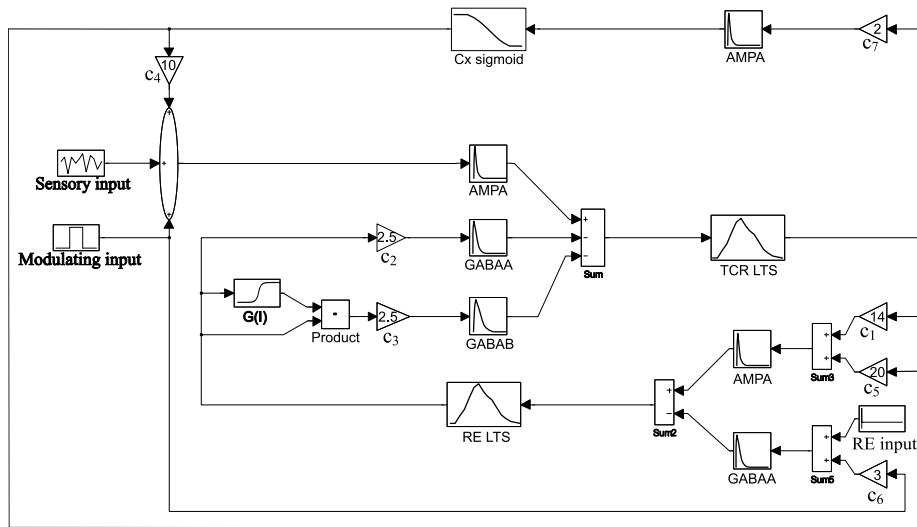


Figure 7.2: Extended version of the thalamic model with cortical module included. The cortical population receives excitatory glutamatergic input from the TCR population and provides recurrent glutamatergic input to both the TCR and RE populations. The function *Cx sigmoid* converts the mean membrane potential to the average number of action potentials generated by the cortical population.

Two modules. More extensive model consisting of two thalamic modules mutually interconnected by means of synapses formed by a chain of reticular nucleus neurons was also constructed in order to investigate the role that reciprocal inhibitory connections may exert regarding the network dynamics. The schematic diagram of the two modules model is shown in Fig. 7.3. The coupling constant c_8 (RE→RE) represents the number of reciprocal connections between the RE cells in neighboring modules. In the present model we chose $c_8 = 8$. In each module the parameters were identical except for the seeds of input noise generators. The difference in seeds of noise generators ensured independent inputs for each module.

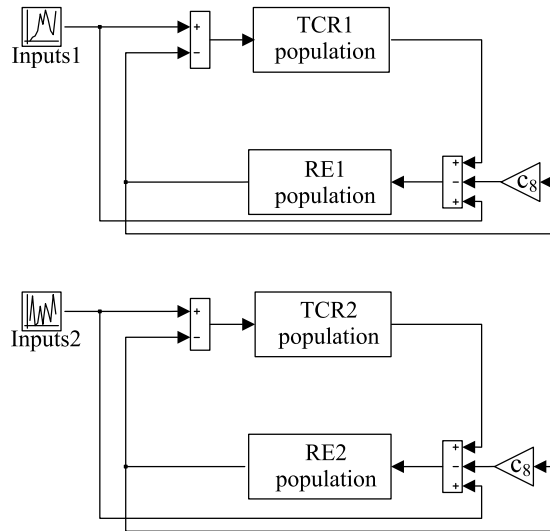


Figure 7.3: Schematic diagram of two modules model. Each TCR population represents specific thalamic relay nucleus corresponding to single sensory or motor modality.

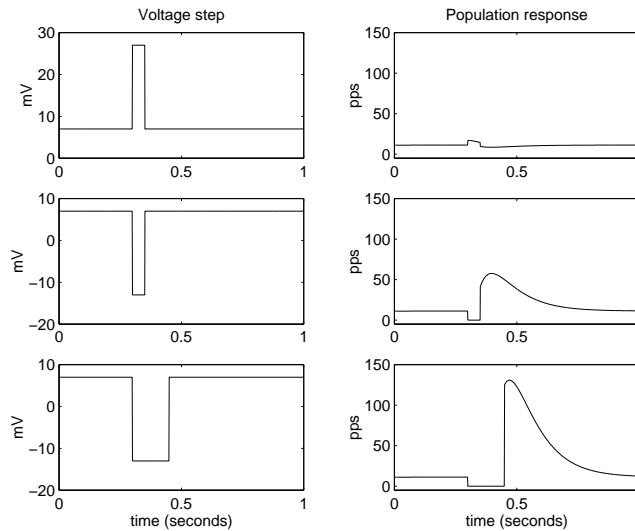


Figure 7.4: Simulation of responses of the TCR population to changes in mean membrane potential in that population. Depolarization from the resting level produces very weak response (top row). After release from hyperpolarization lasting 50 ms (which may correspond to $GABA_A$ IPSP) the TCR population generates rebound burst response (middle row). Longer hyperpolarization lasting 150 ms (which may correspond to $GABA_B$ IPSP) results in larger burst response (bottom row)

7.3 Results

7.3.1 Simulation of burst firing

With the functions described in the section *Low threshold spikes* we can reproduce essential properties of the burst firing in the thalamic populations. In Fig. 7.4 a population response to different voltage commands is shown. When a population is depolarized from rest no bursts are present. When a population is first hyperpolarized it produces rebound bursts after release from hyperpolarization. Also, a population response depends on the duration of hyperpolarization. Longer hyperpolarization results in larger burst response.

7.3.2 Activities in a single module

The single module of the model, such as shown in Fig. 7.1A may exhibit various qualitatively different types of behavior depending on the model parameters, the inputs and the initial conditions. The output signal may have the following forms: (i) desynchronized, i.e., random activity having a spectrum with approximately $1/f$ characteristic, (ii) waxing and waning spindle-like oscillations having a spectrum with a peak at approximately 10 Hz, (iii) high amplitude seizure-like paroxysmal oscillations at a frequency around 3 Hz. These different types of the model output and the corresponding power spectra are shown in Fig. 7.5.

7.3.3 Desynchronized activity and 10 Hz oscillations

The desynchronized activity is generated when the modulating cholinergic input is present. Removal of the cholinergic activation, i.e., setting M to 0, shifts the mean membrane potential in the TCR population to more hyperpolarized levels at which rebound low threshold spikes can be elicited in a response to IPSPs of the RE population origin. In this way the network is entrained into cyclical interaction between the TCR and RE populations. Similarly as in previous models, the dominant alpha frequency (at around 10 Hz) in the present model, is largely determined by the time courses of both excitatory and inhibitory postsynaptic potentials and to a lesser degree by other factors like the characteristics of the LTS spikes, synaptic coupling constants and sensory input level. For example, a 50% decrease in the rise rate of the $GABA_A$ mediated IPSPs results in a decrease of 30% of the model output frequency, while a 50% decrease in the rise rate of the LTS inactivation results in the frequency change of only 6%. Depending on parameters the underlying dynamics of the alpha oscillations may be linear or nonlinear as it was also observed in human alpha rhythm by Lopes da Silva et al.(1997) [60] and by us (Stam et al., 1999 [89]). In the model, this may be seen in simulations where the noise component was removed from the input signal (not shown). When the model operates in a linear range, its behavior in linear approximation is given by a linear transfer function. The stability analysis and the derivation of the linear transfer function of the system are given in the Appendix.

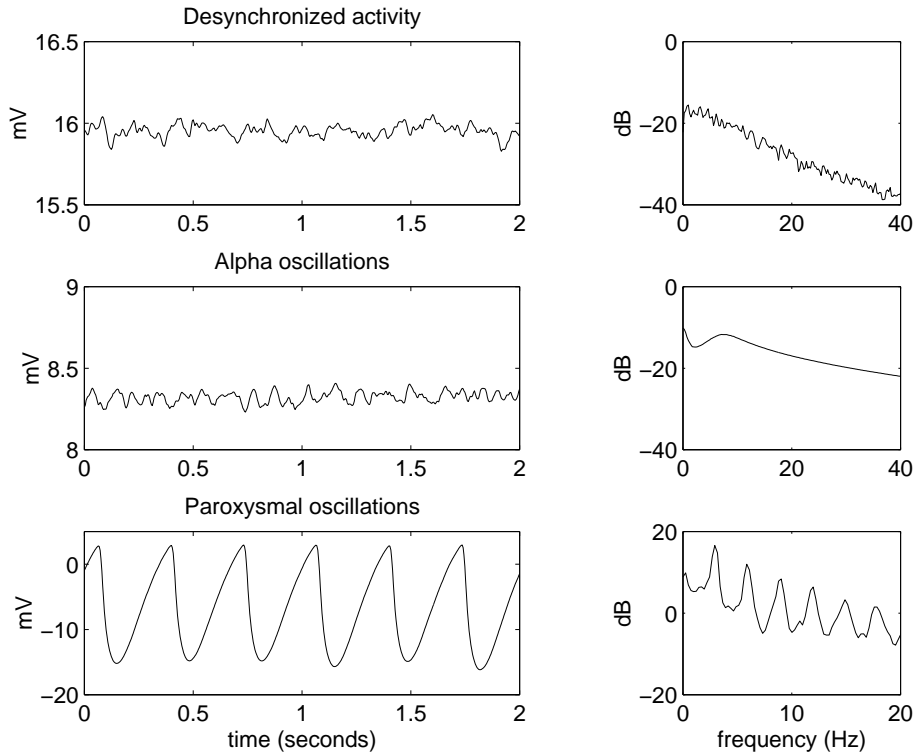


Figure 7.5: Three types of model output (i.e., mean membrane potential in the TCR population) and the corresponding power spectra. From top to bottom: desynchronized activity, alpha oscillations and paroxysmal oscillations.

7.3.4 Transition from 10 to 3 Hz oscillations induced by cortical input

During desynchronized and alpha activity the threshold for the activation of $GABA_B$ receptors is not reached. Under appropriate conditions, e.g., by increasing the corticothalamic input, it is possible to trigger $GABA_B$ receptor mediated IPSPs, which results in the sudden transition of the model's behavior from normal alpha rhythmic 10 Hz activity to paroxysmal 3 Hz high amplitude oscillations. The bifurcation diagram, summarizing the model's qualitative behavior corresponding to different values of the sensory and cortical inputs, is shown in Fig. 7.6

In all simulations performed to obtain these bifurcation diagrams, the noise component was removed from the sensory input. This was done because in the presence of noise the bifurcation points become blurred (i.e., it is difficult to pinpoint a value of the control parameter at which the transition happens) in contrast with the deterministic case, as shown in section 5.5 and described in the literature (e.g., Horsthemke and Lefever, 1984 [32]). When the noise component is removed from the input, the output signal $V(t)$ corresponding to alpha rhythmic activity becomes a constant signal while the output corresponding to the paroxysmal 3 Hz oscillations becomes a perfectly periodic oscillation. In

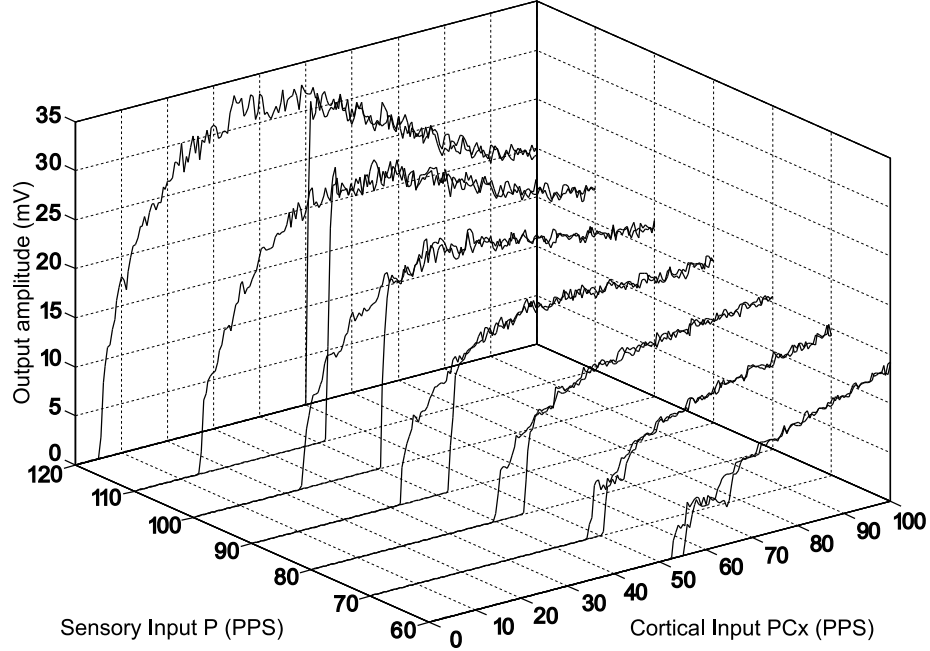


Figure 7.6: A two-parameter bifurcation diagram of the model. The noise component was removed from the sensory input and its DC level (in pps on the X - axis) was varied in steps of 10 pps in a range 60 - 120 pps. For each fixed value of sensory input the cortical input (in pps on the Y - axis) was increased from 0 to 100 pps and subsequently decreased back to 0 pps. The output amplitude (in mV on the Z - axis) was the difference between the maximal and minimal value of the mean membrane potential in the TCR population within a short time interval.

the bifurcation diagrams presented in this section, the output amplitude does not represent the mean membrane potential $V(t)$ itself, rather the difference between its maximal and minimal value within a short time interval (1 second). Therefore, the zero output amplitude represents constant output signal $V(t)$ corresponding to the normal (small amplitude 10 Hz) oscillations, while nonzero output amplitude represents oscillating $V(t)$ corresponding to the paroxysmal (high amplitude 3 Hz) oscillations. The transition between these two states occurs when the corticothalamic input P_{Cx} is increased beyond the bifurcation point at P_{Cx}^{th} , which we call the seizure threshold. Also, as the corticothalamic input is subsequently decreased there is a jump from large amplitude oscillations back to normal activity but this may take place at a value of P_{Cx}^* which is less than P_{Cx}^{th} . Thus for $P_{Cx}^* < P_{Cx} < P_{Cx}^{th}$, there are two stable attractors, an equilibrium point corresponding to normal activity and a limit cycle corresponding to paroxysmal oscillations. This may be seen in Fig. 7.7A, which shows the bifurcation diagram for the model with the reference set of parameters. For a fixed value of $P_{Cx} = 25$ pps there are two stable dynamics (a vertical line plotted at this P_{Cx} value crosses the curve in the diagram at two points) corresponding to normal and paroxysmal type of output $V(t)$ showed in Fig. 7.5 in the middle and lower panels, respectively.

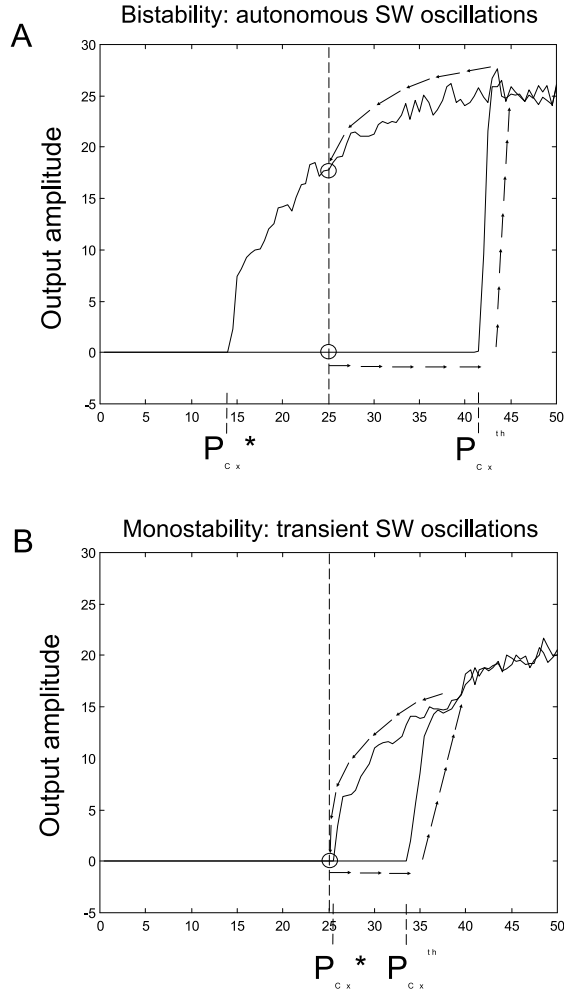


Figure 7.7: Bifurcation diagrams of the system with cortical input P_{Cx} as a control parameter on the X - axis (pps) and the output amplitude on the Y - axis (mV). Bifurcation curves were plotted with ramp P_{Cx} increasing from 0 to 50 pps and decreasing down to 0 pps. Values P_{Cx}^* and P_{Cx}^{th} specify domain of bistability. Vertical dotted lines are plotted at the reference value of $P_{Cx} = 25$ pps. Crossings of these lines with the bifurcation curves represent stable states, marked with open circles. Arrows represent the 'route' from normal to paroxysmal state when P_{Cx} is increased above P_{Cx}^{th} and decreased back to reference value (25 pps). (A) For reference set of parameters two stable attractors coexist. As P_{Cx} increases above P_{Cx}^{th} the system jumps suddenly to the upper branch of the bifurcation curve and stays there after subsequent decrease of P_{Cx} . It results in autonomous SW oscillations. (B) For parameters specified in the section *Spontaneous transitions* there is only one stable attractor corresponding to normal state. An increase of P_{Cx} above P_{Cx}^{th} results in sudden jump to upper branch of the bifurcation curve but as P_{Cx} decreases back to original value, the system eventually reaches normal state. It results in transient SW oscillations.

7.3.5 Spontaneous transitions.

From Fig. 7.7A it appears that in order to terminate the limit cycle 3 Hz oscillations the parameters of the networks should be changed, e.g., cortical input should be reduced (below P_{Cx}^*). However for another set of model parameters ($\bar{P} = 90$ pps, $\sigma_P^2 = 25$ pps², $B = 22$ mV, $G_{RE} = 1200$, other parameters have their reference values) the model is in a state where spontaneous transitions occur between normal and paroxysmal oscillations as shown in Fig. 7.8. In the upper panel one minute of a simulation is shown with the occurrence of two spontaneous seizure episodes. Both the on-going activity and a seizure episode are shown in an extended time scale in the two other panels. In these simulations we summed postsynaptic currents (i.e., derivatives of postsynaptic potentials) of both excitatory and inhibitory populations and applied low pass filtering to obtain more EEG-like signals. For comparison, normal and epileptic activity in real EEG signals are also shown in Fig. 7.8 in two lowest panels. The bifurcation diagram for the model with the parameters specified above is shown in Fig. 7.7B. For this parameter setting, the reference value of $P_{Cx} = 25$ pps is smaller than P_{Cx}^* , which means that there is only one stable attractor (a vertical line plotted at $P_{Cx} = 25$ pps crosses the curve in the diagram at one point) corresponding to the normal type of output. The system excited by transient suprathreshold stimulus (i.e., greater than P_{Cx}^{th}) tends towards the equilibrium state (at $P_{Cx} = 25$ pps) as time progresses. However, on its way to equilibrium, the system follows the upper branch of the bifurcation curve corresponding to paroxysmal activity, which gives rise to transient SW episodes. From the bifurcation plot on Fig. 7.7B it follows that spontaneous transitions to SW activity could be induced by fluctuating cortical input. However in this model, for simplicity, we may assume that P_{Cx} does not fluctuate and that the only source of noise in the model is the sensory input P . As shown in the upper panel in Fig. 7.8, these fluctuations in sensory input are effective in inducing transitions from normal alpha to abnormal SW oscillations. Except the triggering function the influence of noise is also reflected both on the shape of the signals and on the duration of the paroxysmal episodes.

7.3.6 Analysis of the seizure threshold.

We analysed the dependence of the seizure threshold on a number of model parameters. Due to the complexity of interactions in the model, a change of one parameter may influence the dependency of the seizure threshold on other parameters. Therefore we performed a parameter analysis for two sets of parameters, one with a strong and the other with a reduced mean value of sensory input \bar{P} (from 110 pps to 80 pps). These two conditions were chosen because we assume that the former represents the natural *in vivo* conditions, while the latter may simulate the *in vitro* situation of isolated tissue slabs. We performed these analyses because some of the experimental data available were obtained *in vitro*, but we are interested primarily in understanding the system's behavior in the intact animal, and both conditions can differ regarding the values of a number of parameters. Each parameter was varied in a range of $\pm 100\%$ around its reference value while all other parameters were kept constant. Results of the analysis are summarized in Fig. 7.9A–F and are described below.

A An increase in cholinergic input ('squares') and both a decrease and an in-

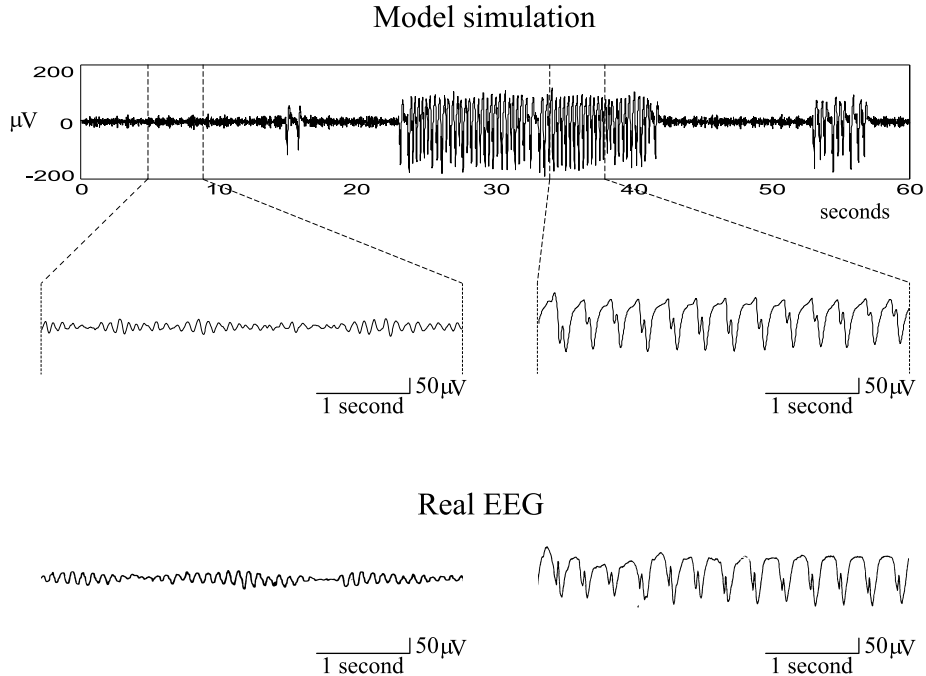


Figure 7.8: Upper panel: one minute of a simulation with the occurrence of two spontaneous seizure episodes. Middle panel: alpha activity and a seizure episode in an extended time scale. Signals in the upper and middle panels are summed postsynaptic currents of both excitatory and inhibitory populations. Lower panel: alpha and SW activity in real EEG signals.

crease of the sensory input ('circles') results in an increase of the seizure threshold. In the model the SW threshold dependence on the inputs comes from their influence on the ability to fire burst responses by the TCR and RE cells. This ability is mediated by the mean membrane potential levels in both populations. An increase in cholinergic activation shifts the membrane potential of the TCR population to a more depolarized level while that of the RE population is shifted to a more hyperpolarized level. This makes the I_T current unable to be deinactivated in the TCR population and to be activated in the RE population. Similarly an increase or a decrease of the sensory input level, away from the reference level, shifts the membrane potential in the TCR population to more depolarized or hyperpolarized levels, respectively, at which the ability to generate rebound LTS bursts is reduced. This may also explain why the reference value of sensory input corresponds to the lowest threshold. It corresponds to the fact that for this reference setting the burst firing underlying synchronized oscillations in the TCR-RE network is facilitated and the model produces alpha rhythmic activity with a clear peak in the power spectrum (Fig. 7.5). This means that when the network is tuned to 10 Hz oscillations it is most prone to transitions to seizure-like 3 Hz oscillations, because for both types of oscillations the mechanism of burst firing in thalamic neurons is essential.

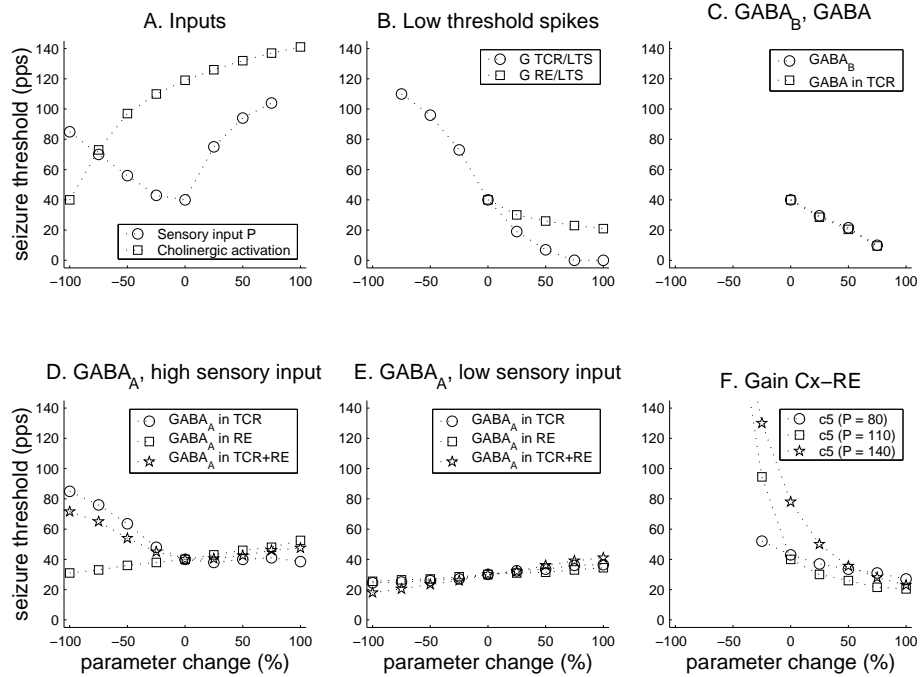


Figure 7.9: Dependence of the seizure threshold on model parameters. On each (A–F) diagram parameter change in a range of $\pm 100\%$ around its reference value, in steps of 25% , is shown on the X - axis and the seizure threshold (intensity of cortical input necessary to induce a seizure) is shown on the Y - axis (pps). Model parameters are specified in the legends inside each diagram. not be induced by any value of cortical stimulation when varied further.

- B** An increase in the gain element G of LTS in the TCR ('circles') and RE ('squares') populations, i.e., of the the gains G_{TCR} and G_{RE} , respectively, lowered seizure threshold. A decrease of the gains of LTS in both TCR and RE populations had the opposite effect. This is understandable since in the model larger burst discharges in TCR cells produces larger responses in RE population. In turn, increased RE burst firing is effective in triggering $GABA_B$ postsynaptic responses, which underlie SW oscillations.
- C** An enhancement of $GABA_B$ inhibition ('circles'), i.e., an increase of the amplitude and a decrease of the threshold for $GABA_B$ IPSPs resulted in lowered SW threshold. A reduction of $GABA_B$ inhibition had opposite effect. It follows directly from the fact that $GABA_B$ postsynaptic responses underlie SW oscillations in the model. The influence of overall GABA inhibition on the TCR population ('squares') is determined mainly by the threshold for $GABA_B$ IPSPs. This is why the effects of manipulating the overall GABA inhibition in the TCR population are related to that of changing $GABA_B$ inhibition alone.
- D** A reduction in the strength of mutual inhibitory connections between the RE cells ('squares'), reflected in the input Q , lowered seizure threshold

while an enhancement of Q increased the seizure threshold. This effect is attributable to the fact that a decrease of Q releases the membrane potential in the RE population from a too strong hyperpolarized level and, thus increases the ability of the RE cells to generate bursts that, in turn, can activate GABA_B receptors in the TCR cells. A reduction of GABA_A IPSPs in the TCR population ('circles') increased seizure threshold in the case of high level of sensory input. This is because the high level of sensory input together with reduced GABA_A inhibition led to a change of the membrane potential in the TCR population towards more depolarized levels and thus to a reduction of the ability of the TCR cells to generate rebound burst responses. The effect of reducing GABA_A IPSPs in both the TCR and RE populations ('stars') at the same time, is similar to the effect obtained when the change is restricted to the TCR cells, i.e., it is dominated by the seizure threshold dependence on the GABA_A inhibition of the TCR population ('circles').

- E** For the case with a low sensory input we also had to reduce the threshold for GABA_B activation θ_G (from 11 pps to 7 pps). The latter change was necessary to enable the transition to 3 Hz oscillations. Under these '*in vitro*' conditions the general relations between seizure threshold and model parameters remained unaltered except for the dependence on GABA_A inhibition. A reduction in GABA_A strength in either the TCR ('circles'), the RE neurons ('squares') or in both ('stars') resulted in a decrease of the seizure threshold. This difference from the situation in (D) is due to the fact that the TCR cells in the condition of low input were more deeply hyperpolarized. Under these conditions the reduction of GABA_A inhibition in these cells enabled them to reach the appropriate membrane potential (i.e., less hyperpolarized) that is favourable for burst responses.
- F** A relatively small (less than 50% of the reference value) reduction of c_5 (Cx→RE) for high ('stars'), intermediate ('squares') and low ('circles') levels of sensory input made cortical input P_{Cx} ineffective in inducing the transition to the seizure mode.

7.3.7 Periodic sensory stimulation.

We investigated under which conditions the primary sensory input could affect the occurrence of paroxysmal activity. This is interesting because it is known that some forms of 3 Hz absence seizures can be elicited by intermittent visual stimulation, particularly by flickering light. We simulated the effect of such periodic visual stimulation by adding a periodic square-wave signal to the sensory input P . The amplitude of the square wave was 2 pps and its frequency was varied in the range 0 - 25 Hz. For each frequency, $n = 5$ trials were performed and the average delay to the onset of the paroxysmal response was calculated. The average delay to seizure onset was the shortest for the stimulation at the frequency around 10 Hz (Fig. 7.10), which is the resonant frequency of the modeled neuronal circuit.

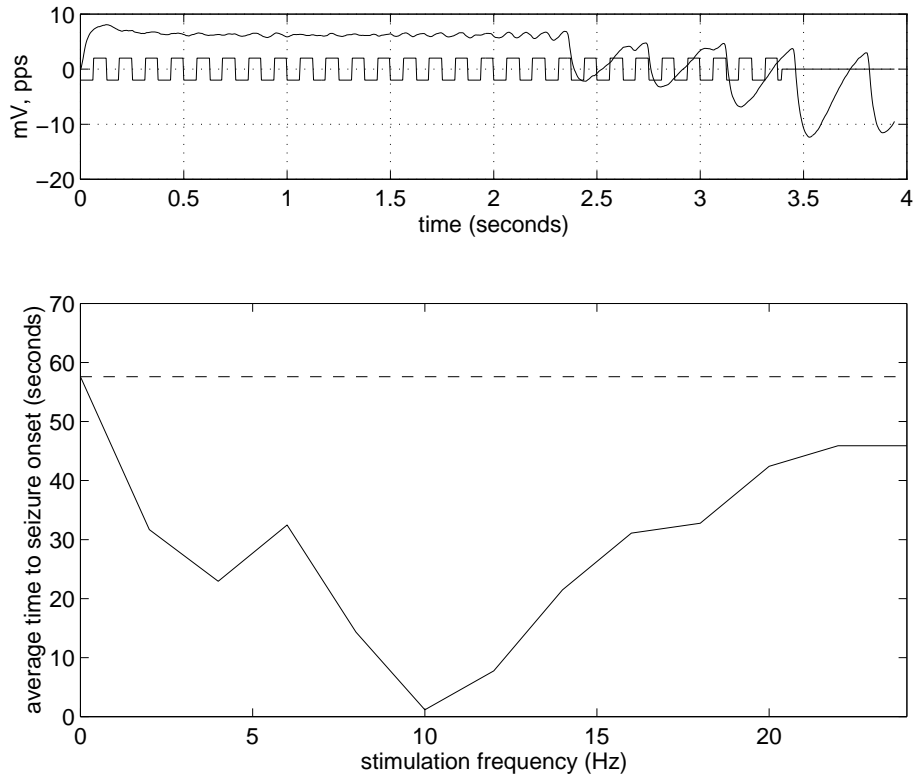


Figure 7.10: Upper panel: periodic stimulus (square wave) at frequency 8 Hz triggers paroxysmal response that outlasts the stimulus. Lower plot: dependence of the average delay to the paroxysmal response on stimulation frequency. At zero frequency which corresponds to the absence of the stimulation, the average delay to seizure onset is about 60 seconds (horizontal broken line). Paroxysmal responses are induced most efficiently by the stimulation at the frequency around 10 Hz, which is a dominant alpha frequency of the model. X - axis (Hz); Y - axis (seconds).

7.3.8 Counter-stimulation.

In bistable systems where a limit cycle coexists with a steady state, a perturbation delivered to the limit cycle may annihilate the oscillation (Glass and Mackey, 1980). An example of this phenomenon is shown in Fig. 7.11, where a limit cycle, corresponding to 3 Hz paroxysmal oscillations, is annihilated by a single sensory pulse. The triggering pulse was delivered to the corticothalamic input at time 1.5 seconds from the beginning of the simulation; it had 5 ms duration and amplitude 200 pps (with respect to reference P_{Cx} of 25 pps). The counter stimulation pulse was of 83 pps magnitude and 12.5 ms duration. It was applied to the sensory input, at time 2.075 seconds. The counter-stimulation was very sensitive to both the cycle phase (< 1 ms) and pulse magnitude (< 1 pps). Also, for a fixed set of pulses parameters, paroxysmal oscillations could be annihilated only for some but not for all realizations of noise input.

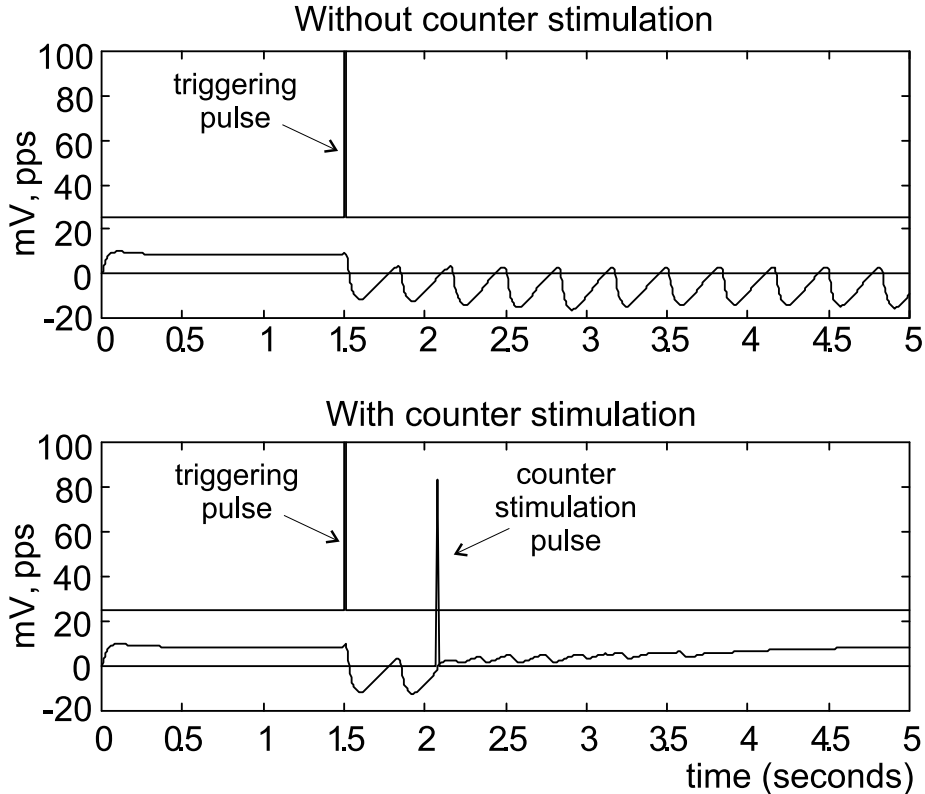


Figure 7.11: The counter stimulation phenomenon. The three signals in the upper and lower panel are: the output signal (i.e., mean membrane potential in the TCR population), the cortical input consisting of DC offset of 25 pps and triggering pulse delivered at time 1.5 second, the additional sensory input. In the upper panel paroxysmal oscillations triggered by cortical input never stop. In the lower panel the counter stimulation sensory pulse delivered at time around 2.1 seconds annihilates paroxysmal oscillations.

7.3.9 Role of the cortex.

The role of the cortex was investigated by including a cortical module. The qualitative behavior of the model was preserved but some quantitative features were altered. Alpha oscillations became more synchronized (i.e., the peak in the power spectrum was more pronounced) and their frequency slightly increased. The paroxysmal oscillations also exhibited a larger peak in the power spectrum but the frequency was slightly slowed down from 3 to 2.5 Hz. We also investigated whether the intra-thalamic TCR–RE connections are necessary for the generation of the normal and paroxysmal activity. To investigate this we opened the intra-thalamic loop by blocking the AMPA connections between the TCR and RE populations, i.e., setting $c_1 = 0$. Under such conditions oscillations in alpha frequency range disappeared and were replaced by desynchronized activity but the network was still bistable and could be switched to large amplitude paroxysmal oscillations. These paroxysmal oscillations were slower (around 2

Hz) and had larger amplitude than paroxysmal oscillations generated when the intra-thalamic TCR-RE loop was present.

7.3.10 Antagonistic behavior of two modules.

An extended model was implemented in order to confirm the results obtained in the previous chapter, namely that the phenomenon of focal ERD/surround ERS of alpha activity may be generated by the interplay of thalamic modules where cross-talk is provided by the reciprocal inhibitory connections between reticular nucleus cells. Under normal conditions, i.e., with cholinergic activation removed each module generated rhythmic activity at around 10 Hz. Attentional activity focussed on certain sensory or motor modality was simulated by applying the modulating input M to the first module called the target module. Similarly as described in section 6.3 both the target and the neighboring module changed their activity. The rhythmic 10 Hz component disappeared in the target module while it was enhanced in the neighboring module. Here we also emulated the ERD/ERS phenomena in a more realistic way by simulating 12 trials having a duration of 12 seconds, and applying post-processing analysis as done in human recordings and described in section 2.1. For each trial we used different seeds for the noise generators of the two modules. Results of the analysis are shown in Fig 7.12. Modulation was applied from the fourth to the eight second, as shown at the top of the figure. During modulation the target module exhibited ERD, the neighboring module - ERS. Also, weak rebound in synchronization is present in both signals after termination of the M input. This effect is more pronounced in the neighboring population and results from the rebound bursts generated by the TCR population after release from hyperpolarization.

7.3.11 Paroxysmal activity in two modules model.

Using two modules model we also investigated the role of the inter-RE connections on the process of spreading of paroxysmal activity. The latter was induced by cortical stimulation that consisted of either gradually increasing the DC level or of a single pulse. It was applied to either only one module or to both modules simultaneously. In general, the intensity of stimulation that was necessary to induce paroxysmal oscillations in the network was larger than when only one module was stimulated. In the case that one module only was stimulated the other module exhibited, after a delay of about two seconds, high amplitude paroxysmal oscillations that were out of phase with the oscillations in the module that was stimulated. When two modules were simultaneously stimulated paroxysmal oscillations emerged in both modules. They were initially in phase but after about two seconds they became out of phase and both increased in amplitude. In all types of stimulation protocol the intensity of stimulation necessary to induce the transition to paroxysmal activity increased linearly with the strength of mutual inhibitory connections between the RE cells c_8 (RE→RE).

7.4 Discussion

We constructed a model of interconnected TCR, RE and cortical populations with parameters directly related to synaptic and cellular properties in order

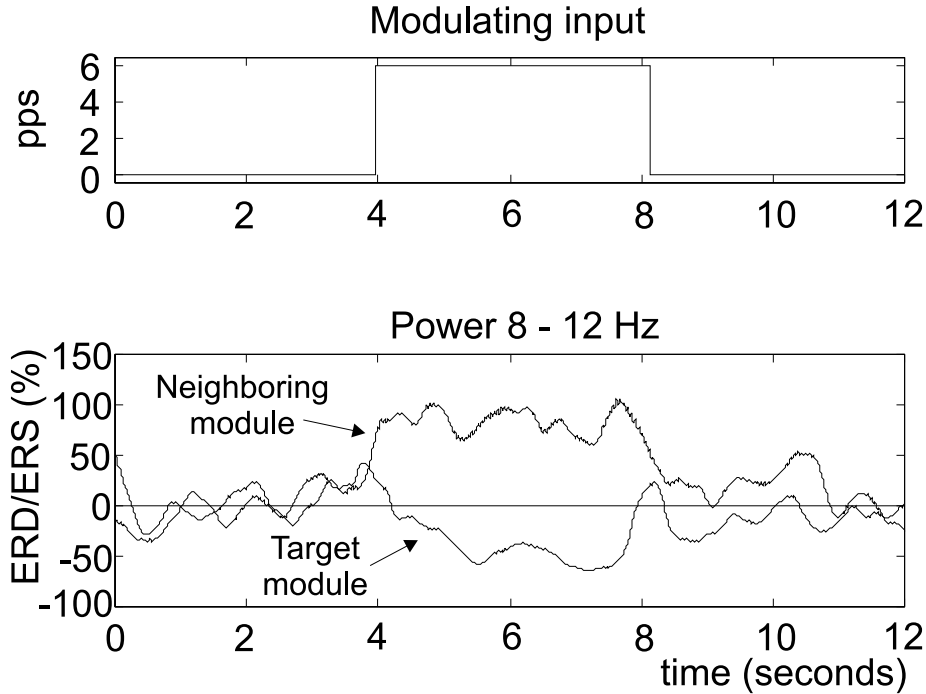


Figure 7.12: Upper panel: the modulating input M of 6 pps is applied between second four and eight. Lower panel: time courses of the power change in alpha frequency range averaged over 12 trials from the target and neighboring modules. Positive values of these signals indicate ERS while negative values indicate ERD.

to investigate the mechanisms of generation of synchronized oscillations in a thalamocortical neuronal network. This type of model study allowed to bring the novel hypotheses of the dynamics of the neuronal networks involved in the generation of SW oscillations associated with absence seizures and event-related de/synchronization of cortical alpha band rhythms. In particular, the present study suggests that absence seizures may represent transients that emerge in a network with bistability properties and that antagonistic changes in synchronization of alpha band rhythms in neighboring cortical areas may be mediated at the thalamic level by mutual inhibitory connections between reticular nucleus cells. Each modeled phenomenon will be discussed successively.

Start and termination of the absence seizures. Paroxysmal oscillations may be induced in the model in a number of ways, e.g., by an increase in corticothalamic input P_{Cx} . Depending on model parameters, the paroxysmal oscillations may be either autonomous or transient, i.e., they either continue after subsequent decrease of P_{Cx} or they transiently decay and terminate suddenly by themselves. Autonomy of the paroxysmal oscillations is associated with bistability present in the system. Namely, for the same parameter set, two stable states coexist, one corresponding to epileptic, second corresponding to nonepileptic behavior. Under such conditions paroxysmal oscillations, once initiated, continue until either critical, terminating stimulus is delivered or parameters of the

network are changed. Transient paroxysmal oscillations emerge when a network operates in the regime close to paroxysmal state but in which only the state corresponding to normal behavior is stable. We performed simulations with both increasing and decreasing P_{Cx} in order to sort out qualitative properties of the onset and termination of paroxysmal oscillations and, in this way, to identify the borders of the 'epileptic' region in the P_{Cx} control parameter space. On the bifurcation plots in Fig. 7.7, the value of P_{Cx} , at which the system operates (25 pps) is marked by a vertical broken line. It is either within the epileptic region, i.e., between P_{Cx}^* and P_{Cx}^{th} , as in Fig. 7.7A, or outside this region as in Fig. 7.7B. The former case corresponds to the autonomous paroxysmal oscillations while the latter corresponds to the transient SW oscillations. It is interesting to compare the duration of high amplitude 3 Hz oscillations in a model with the typical duration of absences. They range from 2 to 3 seconds to 1 or 2 minutes but their usual duration is 5–10 seconds (Penry et al., 1975 [72]). There are also rare cases of very prolonged absence-like stages that may last for hours or even days (Niedermeyer and Lopes da Silva, 1999 [68]). They are termed 'petit mal status' and are associated with almost constant generalized synchronous 3 Hz spike and wave activity. There is thus experimental support for the heterogeneous dynamical character of the paroxysmal 3 Hz oscillations. Additionally, the transient character of the SW episodes could also explain their spontaneous cessation. In our simulations, transient 3 Hz oscillations die out by themselves (Fig. 7.8) and do not require specific neuronal processes responsible for their termination like, e.g., progressive and persistent activation of the mixed ionic "sag" current as hypothesized by Bal and McCormick (1996) [2].

If random fluctuations in a bistable network are responsible for the sudden onset of the absence seizures, it seems reasonable to assume that occurrence of those seizures cannot be predicted as fluctuations are unpredictable by definition. This conclusion is consistent with clinical observations as expressed by Lennox & Lennox (1960) [49]: 'If warning occurs, the diagnosis of petit mal may be questioned'. On the other hand it is in contrast with the report of Rogowski et al. (1981) [84], who reported on the prediction of absence attacks by several seconds.

Limit cycle oscillations, which coexist with normal steady state, may be annihilated by a brief stimulus of critical size delivered at a critical phase of a cycle (Glass and Mackey, 1980 [29]). This remarkable theoretical prediction is supported by our simulations where non-transient seizures corresponding to the limit cycle oscillations are terminated by a single, well timed pulse (Fig. 7.11). *In vitro* or/and *in vivo* application of these results may be feasible. The model may help to select parameters of the effective counter stimulation pulse.

We also simulated an effect of periodic sensory stimulation that may represent, for example, intermittent photic stimulation. Paroxysmal responses were induced most efficiently by the stimulation at the frequency around 10 Hz, which is dominant alpha frequency of the model. The most effective triggering frequencies reported in the literature (Niedermeyer and Lopes da Silva, 1999 [68]) are slightly higher (15-20 Hz) suggesting that the resonant properties of the thalamic networks cannot be considered as a sole explanation for the influence of sensory input frequency on abnormal EEG response. Possibly, frequency-dependent facilitation of corticothalamic EPSPs (Lindström and Wróbel, 1990 [52]; von Krosigk et al., 1999 [102]) and frequency-dependent depression of thalamic reticular IPSPs (von Krosigk et al., 1999 [102]) may play

a role here.

Seizure threshold. In the model many factors influence the seizure threshold. The latter is measured by the intensity of the cortical input P_{Cx} , at which the transition from normal to paroxysmal activity occurs. Our results are consistent with a number of experimental results on SW epilepsy. Many experiments on absence epilepsy are done on animal model of genetic absence epilepsy, e.g., the genetic absence epilepsy rat from Strasbourg (GAERS). Administration of GABA_A or GABA_B agonist to the thalamic relay nuclei induces absence seizures in epileptic rats, whereas GABA_A agonists in the RE nuclei and GABA_B antagonists in the TCR nuclei decrease these seizures (Liu et al., 1992 [54]). These results together with those from experiments of von Krosigk et al. (1993) [101] and Bal et al. (1995a,b) [4],[3] in which GABA_A antagonists block the spindle oscillations and induce 2-4 Hz paroxysmal oscillations, suggest an enhanced GABA_B receptor activation and decreased intra-RE inhibitory strength to underlie absence pathology. These results are consistent with analysis of a seizure threshold in our model. An increase in GABA_B inhibition (Fig. 7.9C) and a decrease in intra-RE mutual GABA_A inhibition (Fig. 7.9ED) results in lowering seizure threshold while a decrease of GABA_B in the model results in an increase of the threshold (Fig. 7.9C). Two differences have been found between brains of epileptic GAERS rats and brains of non-epileptic control strain. The first one is an elevation in T-channel conductivity in the RE cells (Tsakiridou et al., 1995 [96]). The other difference is a higher GABA concentration in the TCR nuclei (Richards et al., 1995 [82]). Increase of each of these parameters in our model resulted in lowering seizure threshold. Modeling results presented here are also consistent with the actions of antiepileptic drugs. The most selective antiabsence drug ethosuximide is believed to exert its antiepileptic effect by antagonizing the burst firing in the TCR neurons either by decrease of the I_T current (Coulter et al., 1989, 1990, 1991, [16],[17],[18]) or, as more recent study suggests, by acting on the noninactivating Na^+ current and Ca^{2+} -activated K^+ current (Leresche et al., 1998 [50]). In our model, reduction in the amplitudes of LTS generated in the TCR or RE population as measured by gain G_{TCR} or G_{RE} , respectively, results in an increase of the seizure threshold (Fig. 7.9B). The effect of clonazepam is network related. This antiabsence drug is believed to suppress GABA_B mediated inhibition in the TCR nuclei through enhancement of recurrent inhibitory connections within reticular nucleus (Huguenard and Prince, 1994 [35]). In the model, increase of inhibitory strength between the RE cells raises the threshold for seizures (Fig. 7.9DE)

Our results are also consistent with clinical observations that absence seizures most often develop from sleep patterns (Kellaway, 1985 [43]). We showed (Fig. 7.9A) that decrease of cholinergic activation, which underlies the transition from the waking state to sleep or decrease in sensory input would both facilitate SW generation. The latter result may be associated with the fact that SW discharges in GAERS rats occurred primarily when attention and activity were reduced (Snead et al., 1999 [88]). Additionally, strong dependence of the seizure threshold on the level of sensory and cholinergic inputs is consistent with the observations that strong, unexpected stimulation interrupted SW discharges in rats (Snead et al., 1999 [88]) and humans (Schwab, 1974 [85]). In our model the ability of the cholinergic activation and sensory input to promote or suppress SW oscillations is mediated by their influence on the mean membrane potential levels in both the TCR and RE populations. These membrane poten-

tials are critical regarding the ability of these cells to fire LTS underlying burst responses.

Role of the cortex. Role of the cortex in absence seizures is a critical issue. In our model, strong corticothalamic discharge may initiate the SW oscillations. However the necessary condition is that the corticothalamic EPSPs are larger in the RE than in the TCR cells. As shown in Fig. 7.9F, a decrease in c_5 (Cx→RE), while c_4 (Cx→TCR) is kept constant, drastically raises the seizure threshold. Dominance of cortical EPSPs in the RE cells as compared with TCR cells is supported by experimental evidences (Contreras et al., 1993 [13]; Destexhe et al., 1996b [25]; Liu et al., 1995 [53]). Except for the fact that phasic corticothalamic input may trigger paroxysmal oscillations in the TCR–RE loop, P_{Cx} is also considered in our simulations as a critical control parameter defining the operating point of the thalamic neuronal network. As may be seen in Fig. 7.6, 7.7, an increase in P_{Cx} brings the network closer to the region where "intact" intrathalamic loop may generate pathological activity. On the other hand, in simulations where cortical module was included, both normal and paroxysmal oscillations had larger amplitudes. In terms of the model, it may be interpreted as an increase in synchrony of firing in neuronal populations. These results support the conclusions from other experimental (Steriade et al., 1994 [91]; Contreras et al., 1996, 1997a,b [13],[14],[15]; Destexhe et al., 1999 [24]) and modeling (Destexhe et al., 1998, 1999 [23],[24]) studies of powerful role for the cortex in triggering and synchronizing thalamic oscillations.

Comparison with other models of SW activity. Our model resembles similarities and differences with other computational models of SW seizure. In the model of Lytton et al. (1997) [62] only spike and wave activity was investigated. With single parameter sets, two modes of the RE–TCR interaction were observed but both modes corresponded to epileptic activity. In a first one both cells oscillated mutually with a frequency 2–4 Hz and in the other one the TCR cells were quiescent and the RE cells showed intrinsic repetitive bursts. Cortical stimulation could trigger the transition between the two modes. In our model, the quiescent mode of the TCR neurons was not observed as we did not consider cells in the RE population to be intrinsic oscillators. On the other hand, the seizure activity generated in the RE–TCR interaction mode is consistent with our simulations and suggests that intrathalamic loop may serve as peacemaker of SW oscillations. More detailed model of Destexhe (1998) [22] is capable to reproduce various types of behavior depending on the parameters. It exhibits spindle activity, SW seizures and waxing and waning 3 Hz oscillations that were observed experimentally as distinct from SW (Steriade and Contreras, 1998 [90]; Castro-Alamancos, 1999 [10]). Similarly as in the model of Lytton et al., (1997) [62], in our study we don't distinguish between these two types of oscillations as we don't model the exact wavefronts of the local field potentials generated in the neocortex. On the other hand, in our model, paroxysmal oscillations could be of either intrathalamic or corticothalamic origin. These two distinct mechanisms could correspond to two distinct patterns of 3 Hz oscillations observed both experimentally and in the model of Destexhe. In the latter model, the transition from spindle oscillations to absence type of activity was achieved by reduction in intracortical GABA_A inhibition and cortex was actively involved in the generation of the SW pattern. Bistability in that system was not reported.

Model prediction. Our model predicts bistability in both intrathalamic and

corticothalamic neuronal networks. However bistability is present only under some conditions, i.e., parameter and input settings, that may be difficult to accomplish *in vivo* or *in vitro*. E.g., from Fig. 7.6 it follows that domain of bistability increases with increasing sensory input, a condition that may not be easily reproduced in slice preparation. Besides, as sensory input increases, the threshold for seizure also increases (Fig. 7.9A) which may again decrease the chance to observe this phenomenon experimentally.

Two modules. The two modules model confirmed the main results of the model presented in the previous chapter. Namely, that two thalamic modules interconnected by mutual inhibitory synapses are capable of displaying dynamic changes in synchronization that reproduce the essential properties of focal ERD/surround ERS of the rhythms within the alpha frequency range. A hypothesis linking simulated neural mechanism to its functional role is presented in the next chapter.

Chapter 8

General discussion and conclusions

8.1 Discussion

8.1.1 Questions for modeler

The main purpose of this modeling study was to provide insight into brain oscillations observed in thalamocortical neuronal network. The models presented here were able to reproduce experimentally observed phenomena related to mental (focusing attention) or motor (voluntary movement) actions and to absence type of epileptic seizures. The question arises whether such theoretical studies are relevant. In other words, do the models presented here advance our understanding of the neural mechanisms responsible for generation of normal and pathological rhythms in question? Besides, do they contribute to the understanding of functional role of normal rhythms or suggest improvements of therapy or diagnosis of brain dysfunction associated with pathological rhythms? Perhaps the first question that should be addressed is how can we prove that mechanisms suggested by our models are likely to play a role in a real brain?

8.1.2 Answers

Model confidence

Despite the fact that models presented here are based on anatomical and physiological data and are consistent with many experiments *in vivo* and *in vitro*, they are also greatly simplified representations of real brain structures being modeled. We assumed that some level of understanding of a neural system may be possible without consideration of all detailed features of that system. On the other hand, it is not possible to prove that the particular model is correct. To increase confidence in a model, its unanticipated properties - model predictions should be first confirmed experimentally. All models presented here generated testable predictions, which were presented in discussions in the previous chapters (Sec. 6.4, 7.4). Therefore, at present, concepts and ideas given below are hypotheses that need further experimental evidence.

Focal ERD/surround ERS

Models of focal ERD/ surround ERS phenomenon tested the hypothesis that mutual inhibition at the thalamic level may be responsible for antagonistic behavior of alpha band rhythms observed in the EEG at the cortical level. In the nonlinear feedback model (Chapter 6) the general relation between excitation level and response characterizing the TCR and RE neuronal populations was essential for the change of the level of synchronization of the generated activity. In the model with cellular properties included (Chapter 7) the mean membrane potential level in the TCR and RE populations was critical regarding the ability of these cells to fire LTS underlying burst responses associated with synchronized oscillations. In this way we identified essential cellular and network properties responsible for focal ERD/surround ERS phenomenon. The question remained what functional properties may underlie the enhancement and the decrease of the alpha band rhythms over the different cortical areas. The hypothesis that alpha band activity in the human EEG may reflect the resting or 'idling' state of the underlying cortex was first put forward by Adrian and Matthews (1934) [1]. We should emphasize that thalamic neurons may present two modes of activity: a burst like mode that is characteristic of EEG synchronized sleep and a relay mode by which these neurons transfer sensory information (section 4.1). Lopes da Silva (1991) [58] noted that the fact that during the burst mode, when spindles are present, the mean membrane potential of the TCR cells is shifted in the hyperpolarized direction may explain why in this mode the thalamic population closes a gate to incoming sensory information. This would be the neurophysiological substrate for the resting state mentioned above. The occurrence of an oscillatory state entraining a population of neurons within a network would be an efficient mechanism for setting the mean level of the membrane potential of these neurons to a level such that the network may enter a closed gate state for a desired period of time; breaking the oscillation would bring the network back to the open gate or relay state. We should note that these considerations apply, strictly speaking, to the oscillations that are characteristic of spindles occurring during sleep. Although the situation in awake subject is different we may assume that the oscillations characteristic of sleep and those occurring in the awake conditions, such as alpha and mu rhythms share the same basic mechanisms albeit they may differ quantitatively regarding some parameters, such as frequency and duration of the burst of rhythmic activity. The experimental evidence for the existence of mu rhythm in the thalamic nuclei was provided by Bouyer et al. (1983) [7]. Kuhlman (1978) [46] regarded mu rhythms characteristic for the resting state of the cortical sensorimotor areas. Following this concept, when movement is planned and performed local event-related desynchronization reflects activation of the corresponding cortical area (Pfurtscheller et al., 1994 [76]). A conclusion of our model study is that the desynchronization-synchronization pattern over specific cortical areas reflects a neurophysiological mechanism that subserves the focusing of attention on one specific motor sub-system or sensory system. The effect of the focus of attention is accentuated by active inhibition of surrounding cortical areas not directly involved in the performance of the specific motor or sensory task.

Finally, the neurophysiological mechanism that was simulated in the present study appears to be akin to the selection process that has been proposed as the

basis of visual attention, and has been called "searchlight" (Posner, 1980 [81]; Crick, 1984 [19]; Jules, 1984 [41]). The reticular nucleus with its lateral inhibitory properties has been considered as a possible substrate for this process of selective attention (Sherman and Koch, 1986 [87]; LaBerge and Brown, 1989 [47]). This hypothesis was tested on a network simulation of thalamic circuit including the pulvinar and the reticular nuclei (LaBerge et al., 1992 [48]). These studies showed that obtaining a relative enhancement of the input at a target location with respect to its surround would depend on the participation of the lateral inhibitory connectivity of the thalamic nuclei and of corticothalamic feedback. It is interesting to underline the similarity between the idea behind this model and our present hypothesis. However, we should also note that the processes being simulated in the study of LaBerge et al. (1992) [48] and in present study are completely different since those authors deal with abstract amounts of activation of abstract units while in our model we simulate actual neuropsychological signals and changes in their rhythmicity.

Absence seizures

The model presented in Chapter 7 provides hypothesis concerning mechanisms of spontaneous generation of 3 Hz SW oscillations associated with absence epileptic seizures. It suggests that absence attacks are critically dependent on activation of GABA_B receptor mediated inhibition in the TCR cells and identified corticothalamic feedback as essential factor in triggering and synchronizing both normal and pathological thalamic oscillations. The question which can still be addressed is whether identifications of neuronal and network mechanisms in a computer model of epileptic seizures may, by any means, contribute to improvement of epilepsy treatment in clinical practice. It seems that positive answer to this important question may be given. One of advantages of the model is the ability to investigate the system behavior during selective change of certain system parameters to simulate, for example, complex pharmacological effects (Jansen, 1996 [39]). Indeed, parameters of our model, which were identified as factors that raised seizure threshold (sec 7.3.6), are already targets of antiepileptic drugs. Another benefit from the modeling study of this type is the insight into the dynamical properties of a system. In a much simpler organ - a heart, understanding system's dynamics enabled to develop pacing methods that prevent abnormal heart rhythms (Garfinkel et al., 1992 [28]; Christini and Collins, 1996 [11]). Similarly, identification of the dynamics of a neuronal network involved in seizure generation may lead to improvement of the existing methods ([31], Velasco, 1995 [98]) of seizure suppression by electrical stimulation through electrodes implanted in the brain. Our model of thalamocortical networks suggests that absence seizures of longer duration may represent a bifurcation from a state corresponding to a point attractor to a state corresponding to a limit cycle. We showed that the latter may be annihilated by appropriate stimulus. Our study also indicated that counter stimulation effect was extremely sensitive to both the time of delivery and amplitude of the perturbation, what may be critical obstacle in application of this method to real neural system with spatiotemporal complexity and randomness. Still, model results may be relevant for experimentalist attempting application of a counter stimulation in practice. Quantitative neural models may not only contribute to design and test new methods of seizure suppression. Insight into system's dynamics may also help

to assess theoretically seizure predictability. The latter may depend on the type of bifurcation associated with the transition from normal to pathological state. E.g., EEG recordings of spontaneous absence seizures (Fig. 2.3) and output produced by our model (Fig. 7.8) suggest that transitions from normal background activity to SW oscillations may correspond to hard excitation (subcritical Hopf bifurcation) as the latter is associated with the onset of oscillations of large amplitude. However, the nature of bifurcation associated with particular transition is hardly accessible from signals generated by a system. Instead, it may be derived from the set of differential equations describing the system in which the bifurcation takes place. Bifurcation analysis of our model as well as other developments may be done in future. Therefore the discussion is concluded with possible future continuation of the present study.

8.1.3 Future directions

As was observed by Pfurtscheller (summarized in Pfurtscheller (1999) [74] and [80]), hand or foot movements resulted not only in changes in power in the alpha frequency range but changes in the beta and gamma frequencies of the EEG were also apparent. Also, Bekisz and Wróbel (1993) [5] and Wróbel et al. (1994) [111] have shown that the oscillations in the beta range recorded from the visual cortex and visual part of the thalamus of the cat increased in amplitude and frequency during situations requiring visual attention. Our models were not developed to account for these phenomena. On the other hand, these interesting experimental findings may be closely related to the processes simulated here. Therefore, we hope that our models could be extended to simulate other rhythmic activities of the brain, in particular in beta and gamma range. Such extended models could help to elucidate which cellular and network features are critical for oscillatory properties of neuronal populations. They could also provide additional insight into functional role of oscillations in different frequency bands in processing of neural information.

Apart from extensions of the model's structure, it could be beneficial to analyse its behavior in more detail. The questions concerning types and domains of attraction of normal and pathological attractors may be answered by bifurcation analysis of the set of differential equations describing the model. Knowledge of topology of the system's phase space may help to establish the set of conditions under which transition, e.g., from normal to pathological attractor happens. In turn, it may determine the potential for predicting seizure occurrence and for annihilating the pathological rhythm. Bifurcation analysis of our model presented in Chapter 7 may provide range of parameters for a perturbation terminating SW oscillations. Subsequently, results obtained *in computo* could be tested in *vitro* and *in vivo*.

8.2 Conclusions

Main conclusions of this thesis are listed below.

With respect to phenomenon of focal ERD/surround ERS:

- A model consisting of a chain of modules of the TCR-RE neurons is capable of displaying experimentally demonstrated dynamical changes in synchronization of alpha band rhythms.

- Antagonistic behavior in the alpha band activity in the neighboring cortical areas may result from the cross-talk between thalamic modules, which is provided by mutually inhibitory reticular nucleus neurons.
- Enhanced alpha band activity reflects resting state of the underlying cortex. Alpha blocking reflects activation of the corresponding cortical area. Therefore, desynchronization-synchronization pattern over specific cortical areas may reflect a neurophysiological mechanism that serves to focus attention on one specific motor subsystem or sensory system.

With respect to SW seizures:

- Activation of $GABA_B$ receptors in the thalamic relay nuclei and bursts mediated by the I_T current are essential for paroxysmal activity in thalamocortical network.
- Increased corticothalamic input or abnormal values of certain parameters, e.g., amplitudes of the I_T currents in the thalamic relay and reticular nucleus neurons may bring the thalamic network close to the threshold for epileptic behavior. Under such conditions bifurcation to abnormal oscillation may be induced even by very weak stimulus.
- Depending on network parameters and on inputs, epileptic oscillations may be transient or autonomous. The former case may correspond to absence seizures, the latter to absence status condition.
- Spontaneous absence seizures may be unpredictable.
- Autonomous paroxysmal oscillations may be annihilated by well-timed stimulus.

Appendix

In the appendix linear analysis of the model presented in Chapter 7 is given. The model depicted in Fig. 7.1 is described by the set of integral equations of the following form:

$$\begin{aligned}
V_e(t) &= \int_{-\infty}^t [P(\tau) + M(\tau) + c_4 P_{Cx}(\tau)] h_e(t - \tau) d\tau - \\
&\quad - \int_{-\infty}^t I(\tau) [c_2 h_{ia}(t - \tau) + c_3 G(I(\tau)) h_{ib}(t - \tau)] d\tau \\
V_i(t) &= \int_{-\infty}^t (c_1 E(\tau) + c_5 P_{Cx}(\tau)) h_e(t - \tau) d\tau - \\
&\quad - \int_{-\infty}^t [Q(\tau) + c_6 M(\tau)] h_{ia}(t - \tau) d\tau \\
E(t) &= G_{TCR} m_{\infty}^{TCR}(V_e(t)) \int_{-\infty}^t n_{\infty}^{TCR}(V_{\tau}(t)) h_n(t - \tau) d\tau \\
I(t) &= G_{RE} m_{\infty}^{RE}(V_i(t)) \int_{-\infty}^t n_{\infty}^{RE}(V_i(\tau)) h_n(t - \tau) d\tau
\end{aligned} \tag{A.1}$$

where V_e , V_i are the average membrane potentials and E , I are the pulse rates in the TCR and RE populations, respectively. G is activation function of GABA_B receptors. h_e , h_{ia} and h_{ib} are AMPA, GABA_A and GABA_B postsynaptic potentials, respectively. Coupling constants $c_1 - c_6$ represent the average number of synaptic contacts between different cell types. Constants G_{TCR} and G_{RE} represent maximal frequency of action potentials in a single burst. m_{∞} and n_{∞} are steady state activation and inactivation functions of the I_T current in respective populations and h_n describes time course of the inactivation of the I_T current in the population of cells. P , P_{Cx} and Q are external inputs from ascending afferents, the cortex and neighboring reticular nucleus cells, respectively. M represents cholinergic modulating input.

Steady state solutions of the above equations are found by assuming variables to be constant and inputs - stationary:

$$\begin{aligned}
\bar{V}_e &= (\bar{P} + \bar{M} + c_4 \bar{P}_{Cx}) H_e - \bar{I} [c_2 H_{ia} + c_3 G(\bar{I}) H_{ib}] \\
\bar{V}_i &= (c_1 \bar{E} + c_5 \bar{P}_{Cx}) H_e - (\bar{Q} + c_6 \bar{M}) H_{ia} \\
\bar{E} &= G_{TCR} m_{\infty}^{TCR}(\bar{V}_e) n_{\infty}^{TCR}(\bar{V}_e) H_n \\
\bar{I} &= G_{RE} m_{\infty}^{RE}(\bar{V}_i) n_{\infty}^{RE}(\bar{V}_i) H_n
\end{aligned} \tag{A.2}$$

where

$$H_r = \int_{-\infty}^t h_r(t - \tau) d\tau, \quad r = \{e, ia, ib, n\} \tag{A.3}$$

Further we investigate the linearized stability conditions for the solutions of eq. (A.2) and (A.3). We assume that the inputs $P(t)$, $P_{Cx}(t)$, $Q(t)$ and $M(t)$ fluctuate around a stationary level with so small variation that nonlinearities may be linearized around the operating points. We write:

$$\begin{aligned}
P(t) &= \bar{P} + p(t), P_{Cx}(t) = \bar{P}_{Cx} + p_{Cx}(t), Q(t) = \bar{Q} + q(t), M(t) = \bar{M} + m(t), \\
V_e(t) &= \bar{V}_e + v_e(t), V_i(t) = \bar{V}_i + v_i(t), E(t) = \bar{E} + e(t), I(t) = \bar{I} + i(t)
\end{aligned} \tag{A.4}$$

In this paper we have only studied the stability points with $\bar{M} = 0$ and consider only the variations of the input $P(t)$, thus $p_{Cx}(t) = q(t) = m(t) = 0$. After expanding nonlinearities $G(I), m_{\infty}^{TCR}(V_e), n_{\infty}^{TCR}(V_e), m_{\infty}^{RE}(V_i), n_{\infty}^{RE}(V_i)$ in Taylor series around equilibrium values, taking only linear terms and subtracting steady states (A.2) from the equations (A.1), we obtain:

$$\begin{aligned}
v_e(t) &= \int_{-\infty}^t p(\tau) h_e(t - \tau) d\tau - \\
&\quad - \int_{-\infty}^t i(\tau) [c_2 h_{ia}(t - \tau) + c_3 G(\bar{I}) h_{ib}(t - \tau) + c_3 \bar{I} d_G h_{ib}(t - \tau)] d\tau \\
v_i(t) &= \int_{-\infty}^t c_1 e(\tau) h_e(t - \tau) d\tau \\
e(t) &= G_{TCR} [m_{\infty}^{TCR}(\bar{V}_e) d_{n_{\infty}^{TCR}} \int_{-\infty}^t v_e(\tau) h_n(t - \tau) d\tau + \\
&\quad + d_{m_{\infty}^{TCR}} v_e(t) n_{\infty}^{TCR}(\bar{V}_e) \int_{-\infty}^t h_n(t - \tau) d\tau] \\
i(t) &= G_{RE} [m_{\infty}^{RE}(\bar{V}_i) d_{n_{\infty}^{RE}} \int_{-\infty}^t v_i(\tau) h_n(t - \tau) d\tau + \\
&\quad + d_{m_{\infty}^{RE}} v_i(t) n_{\infty}^{RE}(\bar{V}_i) \int_{-\infty}^t h_n(t - \tau) d\tau]
\end{aligned} \tag{A.5}$$

where $d_r, r = \{G, m_{\infty}^{TCR}, n_{\infty}^{TCR}, m_{\infty}^{RE}, n_{\infty}^{RE}\}$ are derivatives of the nonlinearities at the steady states:

$$\begin{aligned}
d_G &= \frac{dG(\bar{I})}{dI} \\
d_{m_{\infty}^{TCR}} &= \frac{dm_{\infty}^{TCR}(\bar{V}_e)}{dV_e} \\
d_{n_{\infty}^{TCR}} &= \frac{dn_{\infty}^{TCR}(\bar{V}_e)}{dV_e} \\
d_{m_{\infty}^{RE}} &= \frac{dm_{\infty}^{RE}(\bar{V}_i)}{dV_i} \\
d_{n_{\infty}^{RE}} &= \frac{dn_{\infty}^{RE}(\bar{V}_i)}{dV_i}
\end{aligned} \tag{A.6}$$

We assume solutions of the eq. (A.5) and (A.6) in the form:

$$\begin{bmatrix} v_e(t) \\ v_i(t) \\ e(t) \\ i(t) \end{bmatrix} = \begin{bmatrix} D_1 \\ D_2 \\ D_3 \\ D_4 \end{bmatrix} e^{\lambda t} \tag{A.7}$$

Substituting (A.7) to (A.5) and performing integrations we obtain:

$$\begin{bmatrix} D_1 \\ D_2 \\ D_3 \\ D_4 \end{bmatrix} = \begin{bmatrix} 0 & 0 & 0 & -K_1 \\ 0 & 0 & K_2 & 0 \\ K_3 & 0 & 0 & 0 \\ 0 & K_4 & 0 & 0 \end{bmatrix} \begin{bmatrix} D_1 \\ D_2 \\ D_3 \\ D_4 \end{bmatrix} \tag{A.8}$$

where

$$\begin{aligned}
K_1 &= c_2 A \frac{(a_2 - a_1)}{(\lambda + a_1)(\lambda + a_2)} + (G(\bar{I}) + \bar{I}d_G)c_3 B \frac{(b_2 - b_1)}{(\lambda + b_1)(\lambda + b_2)} \\
K_2 &= c_1 E x \frac{(e_2 - e_1)}{(\lambda + e_1)(\lambda + e_2)} \\
K_3 &= G_{TCR}[m_\infty^{TCR}(\bar{V}_e)d_{n_\infty^{TCR}}N \frac{(n_2 - n_1)}{(\lambda + n_1)(\lambda + n_2)} + d_{m_\infty^{TCR}}n_\infty^{TCR}H_n] \\
K_4 &= G_{RE}[m_\infty^{RE}(\bar{V}_i)d_{n_\infty^{RE}}N \frac{(n_2 - n_1)}{(\lambda + n_1)(\lambda + n_2)} + d_{m_\infty^{RE}}n_\infty^{RE}H_n]
\end{aligned} \tag{A.9}$$

We can rewrite eq. (A.8) as:

$$\vec{D} = \hat{K}\vec{D} \tag{A.10}$$

where \hat{K} denotes 4×4 matrix. The values of the exponential solutions are given by solutions of the equation

$$\det(\hat{K} - \hat{I}) = 0 \tag{A.11}$$

where \hat{I} is identity 4×4 matrix. Eq. (A.11) yields:

$$K_1 K_2 K_3 K_4 + 1 = 0 \tag{A.12}$$

which can be solved for λ . If all λ are negative than the steady point is locally stable.

When the system is in a stable condition, the linear approximation of its behavior, can be described by a transfer function. Transfer function of the system may be found by taking the Laplace transform of the linearized eq. (A.5) and (A.6):

$$\begin{aligned}
v_e(s) &= p(s)h_e(s) - i(s)[c_2 h_{ia}(s) + c_3(G(\bar{I}) + \bar{I}d_G)h_{ib}(s)] \\
v_i(s) &= c_1 e(s)h_e(s) \\
e(s) &= G_{TCR}v_e(s)[m_\infty^{TCR}d_{n_\infty^{TCR}}h_n(s) + d_{m_\infty^{TCR}}n_\infty^{TCR}H_n] \\
i(s) &= G_{RE}v_i(s)[m_\infty^{RE}d_{n_\infty^{RE}}h_n(s) + d_{m_\infty^{RE}}n_\infty^{RE}H_n]
\end{aligned} \tag{A.13}$$

where $h_e(s)$, $h_{ia}(s)$, $h_{ib}(s)$ and $h_n(s)$ are Laplace transforms of the respective alpha functions. Using:

$$\begin{aligned}
M_1(s) &= c_2 h_{ia}(s) + c_3(G(\bar{I}) + \bar{I}d_G)h_{ib}(s) \\
M_2(s) &= c_1 h_e(s) \\
M_3(s) &= G_{TCR}[m_\infty^{TCR}d_{n_\infty^{TCR}}h_n(s) + d_{m_\infty^{TCR}}n_\infty^{TCR}H_n] \\
M_4(s) &= G_{RE}[m_\infty^{RE}d_{n_\infty^{RE}}h_n(s) + d_{m_\infty^{RE}}n_\infty^{RE}H_n]
\end{aligned} \tag{A.14}$$

we can rewrite (A.13) in the matrix form:

$$\begin{bmatrix} 1 & 0 & 0 & M_1 \\ 0 & 1 & -M_2 & 0 \\ -M_3 & 0 & 1 & 0 \\ 0 & -M_4 & 0 & 1 \end{bmatrix} \begin{bmatrix} v_e(s) \\ v_i(s) \\ e(s) \\ i(s) \end{bmatrix} = h_e(s) \begin{bmatrix} p(s) \\ 0 \\ 0 \\ 0 \end{bmatrix} \tag{A.15}$$

The transfer matrix of the system is given by:

$$h_e(s) \begin{bmatrix} 1 & 0 & 0 & M_1 \\ 0 & 1 & -M_2 & 0 \\ -M_3 & 0 & 1 & 0 \\ 0 & -M_4 & 0 & 1 \end{bmatrix}^{-1} = \frac{h_e(s)}{1 + M_1 M_2 M_3 M_4} \begin{bmatrix} 1 & -M_1 M_4 & -M_1 M_2 M_4 & -M_1 \\ M_2 M_3 & 1 & M_2 & -M_1 M_2 M_3 \\ M_3 & M_1 M_3 M_4 & 1 & -M_1 M_3 \\ M_2 M_3 M_4 & M_4 & M_2 M_4 & 1 \end{bmatrix} \quad (\text{A.16})$$

Power spectrum of the output signal $v_e(t)$ may be obtained from eq. (A.16) by substituting s by $i\omega$ and assuming that $p(i\omega)$ is a constant since the spectrum of the input noise is flat. We get:

$$v_e(i\omega) = \frac{h_e(i\omega)}{1 + M_1(i\omega)M_2(i\omega)M_3(i\omega)M_4(i\omega)} \quad (\text{A.17})$$

For the parameters we have chosen for our model the spectrum of the $v_e(t)$ computed according to eq. (A.17) has a peak at 8 Hz and agrees with the spectrum of the simulated signal as shown in Fig. A.1.

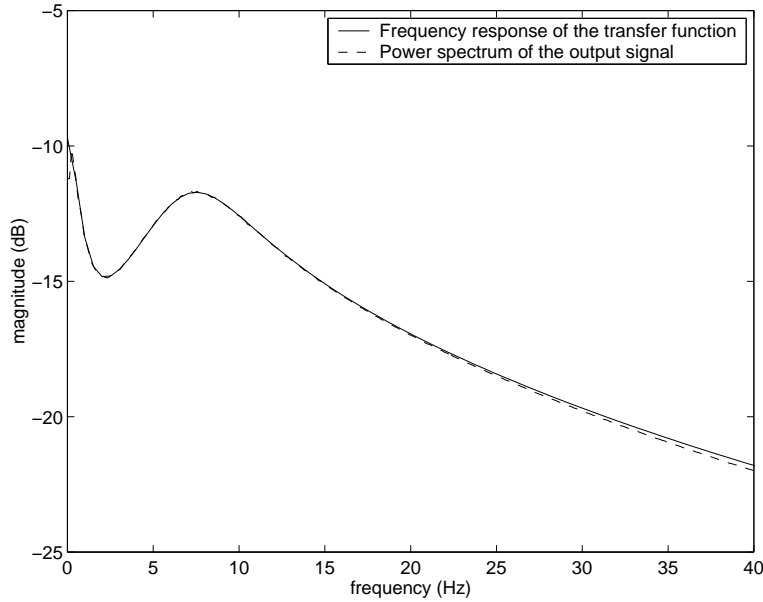


Figure A.1: Comparison between the power spectrum of the simulated output signal and the frequency response of the linear transfer function of the model. Input noise signal (P) and output signal (V) of duration 80 seconds were generated and their power spectra were computed. Dotted line plots the output spectrum divided by the input spectrum. Solid line represents the power spectrum output signal computed from eq. (A.17) using Symbolic Toolbox in Matlab.

Bibliography

- [1] E.D. Adrian and B.H. Matthews. The Berger rhythm: potential changes from the occipital lobes in man. *Brain*, 57:355–385, 1934.
- [2] T. Bal and D.A. McCormick. What stops synchronized thalamocortical oscillations? *Neuron*, 17:297–308, 1996.
- [3] T. Bal, N. von Krosigk, and D.A. McCormick. Role of the ferret perigeniculate nucleus in the generation of synchronized oscillations in vitro. *J. Physiol.*, 483(3):665–683, 1995.
- [4] T. Bal, N. von Krosigk, and D.A. McCormick. Synaptic and membrane mechanisms underlying synchronized oscillations in the ferret LGNd in vitro. *J. Physiol.*, 483(3):641–663, 1995.
- [5] M. Bekisz and A. Wróbel. 20 Hz rhythm of activity in visual system of perceiving cat. *Acta Neurobiol. Exp.*, 53:175–182, 1993.
- [6] H. Berger. Über das elektroencephalogramm des menschen. *Arch. Psychiatry*, 87:527–570, 1929.
- [7] J.J. Bouyer, C. Tilquin, and A. Rougeul. Thalamic rhythms in cat during quiet wakefulness and immobility. *Electroenceph. clin. Neurophysiol.*, 55:180–187, 1983.
- [8] J.M. Bower. *An Introduction to Neural and Electronic Networks*, chapter Reverse engineering the nervous system: An in vivo, in vitro, and in computo approach to understanding the mammalian olfactory system, pages 3–28. Academic Press, New York, 2 edition, 1995.
- [9] Theodore H. Bullock and Jerzy Z. Achimowicz. *Oscillatory Event-Related Brain Dynamics*, chapter A Comparative Survey of Event Related Brain Oscillations. Plenum Press, New York, 1994.
- [10] M.A. Castro-Alamancos. Neocortical synchronized oscillations induced by thalamic disinhibition in vivo. *J. Neurosci.*, 19(RC27):1–7, 1999.
- [11] D.J. Christini and J.J. Collins. Using chaos control and tracking to suppress a pathological nonchaotic rhythm in a cardiac model. *Phys. Rev. E.*, 53:R49–R52, 1996.
- [12] P.S. Churchland and T.J. Sejnowski. Prospectives of cognitive neuroscience. *Science*, 242:741–745, 1988.

- [13] D. Contreras, R. Curró Dossi, and M. Steriade. Electrophysiological properties of cat reticular thalamic neurones in vivo. *J. Physiol.*, 470:273–294, 1993.
- [14] D. Contreras, A. Destexhe, T.J. Sejnowski, and M. Steriade. Spatiotemporal patterns of spindle oscillations in cortex and thalamus. *J. Neurosci.*, 17:1179–1196, 1997.
- [15] D. Contreras, A. Destexhe, and M. Steriade. Spindle oscillations during cortical spreading depression in naturally sleeping cats. *Neuroscience*, 77:933–936, 1997.
- [16] D.A. Coulter, J.R. Huguenard, and D.A. Prince. Characterization of ethosuximide reduction of low-threshold calcium current in thalamic neurons. *Ann. Neurol.*, 25:582–593, 1989.
- [17] D.A. Coulter, J.R. Huguenard, and D.A. Prince. Differential effects of petit mal anticonvulsants and convulsants on thalamic neurons: calcium current reduction. *Br. J. Pharmacol.*, 100:800–806, 1990.
- [18] D.A. Coulter, J.R. Huguenard, and D.A. Prince. Mechanisms of block of thalamic "T"-type Ca^{2+} channels by petit mal anticonvulsants. *Exp. Brain Res.*, 20:201–204, 1991.
- [19] F. Crick. The function of the thalamic reticular complex: the searchlight hypothesis. *Proc. Natl. Acad. Sci. USA*, 81:4586–4590, 1984.
- [20] J.P. Crutchfield, J.D. Farmer, and B.A. Huberman. Fluctuations and simple chaotic dynamics. *Physics Rep.*, 92:45–82, 1982.
- [21] M. Deschênes, A. Madariga-Domich, and M. Steriade. Dendrodendritic synapses in the cat reticularis thalami nucleus: a structural basis for thalamic spindle synchronization. *Brain Res.*, 334:165–168, 1985.
- [22] A. Destexhe. Spike-and-wave oscillations based on the properties of GABA_B receptors. *J. Neurosci.*, 18(21):9099–9111, 1998.
- [23] A. Destexhe, D. Contreras, and M. Steriade. Mechanisms underlying the synchronizing action of corticothalamic feedback through inhibition of thalamic relay cell. *J. Neurophysiol.*, 79(2):999–1016, 1998.
- [24] A. Destexhe, D. Contreras, and M. Steriade. Cortically induced coherence of a thalamic-generated oscillation. *Neuroscience*, 92(2):427–443, 1999.
- [25] A. Destexhe, D. Contreras, M. Steriade, T.J. Sejnowski, and J.R. Huguenard. In vitro, in vivo, and computational analysis of dendritic calcium currents in thalamic reticular neurons. *J. Neurosci.*, 16:169–185, 1996.
- [26] A. Destexhe, D.A. McCormick, and T.J. Sejnowski. Ionic mechanisms underlying synchronized oscillations and propagating waves in a model of ferret thalamic slices. *J. Neurophysiol.*, 76:2049–2070, 1996.
- [27] Walter J. Freeman. *Mass Action in the Nervous System*. Academic Press, New York, 1975.

- [28] A. Garfinkel, M.L. Spano, W.L. Ditto, and J.N. Weiss. Controlling cardiac chaos. *Science*, 257:1230–125, 1992.
- [29] L. Glass and Mackey M.C. *From Clocks to Chaos. The Rhythms of Life*. Princeton University Press, Princeton, NJ, 1988.
- [30] D. Golomb, X.-J. Wang, and J. Rinzel. Propagation of spindle waves in a thalamic slice model. *J. Neurophysiol.*, 75:750–769, 1996.
- [31] The Vagus Nerve Stimulation Study Group. A randomized controlled trial of chronic vagus nerve stimulation for treatment of medically intractable seizures. *Neurology*, 45:224–230, 1995.
- [32] W. Horsthemke and R. Lefever. *Noise induced transitions: Theory and Applications in Physics, Chemistry and Biology*, volume 15 of *Springer series in Synergetics*. Springer, Berlin, 1984.
- [33] J.R. Huguenard and D.A. McCormick. Simulation of the currents involved in rhythmic oscillations in thalamic relay neurons. *J. Neurophysiol.*, 68(4):1373–1383, 1992.
- [34] J.R. Huguenard and D.A. Prince. A novel T-type current underlies prolonged Ca^{2+} - dependent burst firing in GABAergic neurons of rat thalamic reticular nucleus. *J. Neurosci.*, 12:3804–3817, 1992.
- [35] J.R. Huguenard and D.A. Prince. Clonazepam suppresses GABA_B mediated inhibition in thalamic relay neurons through effect in nucleus reticularis. *J. Neurophysiol.*, 71:2576–2581, 1994.
- [36] M.M. Huntsman, D.M. Porcello, G.E. Homanics, T.M. DeLorey, and J.R. Huguenard. Reciprocal inhibitory connections and network synchrony in the mammalian thalamus. *Science*, 283:541–543, 1999.
- [37] H. Jahnsen and R. Llinás. Electrophysiological properties of guinea-pig thalamic neurons, an in vitro study. *J. Physiol.*, 349:205–226, 1984.
- [38] H. Jahnsen and R. Llinás. Ionic basis for the electroresponsiveness and oscillatory properties of guinea-pig thalamic neurons in vitro. *J. Physiol.*, 349:227–247, 1984.
- [39] B.H. Jansen. *Frontier Science in EEG: Continuous Waveform Analysis*, chapter Nonlinear dynamics and quantitative EEG analysis, pages 39–56. Elsevier Science B.V., 1996.
- [40] D. Jeager, E. De Schutter, and J.M. Bower. The role of synaptic and voltage-gated currents in the control of Purkinje cell spiking: A modeling study. *J. Neurosci.*, 17:91–106, 1997.
- [41] B. Jules. *Dynamic Aspects of Neocortical Function*, chapter Toward an axiomatic theory of preattentive vision, pages 585–610. Wiley, 1984.
- [42] E.R. Kandel, J.H. Schwartz, and T.M. Jessel. *Principles of Neural Science*. Appleton and Lange, Norwalk, CT, 1991.
- [43] P. Kellaway. Sleep and epilepsy. *Epilepsia*, 26:S15–S30, 1985.

- [44] U. Kim, M.V. Sanchez-Vives, and D.A. McCormick. Functional dynamics of GABAergic inhibition in the thalamus. *Science*, 278:130–134, 1997.
- [45] Y. Koshino and E. Niedermeyer. Enhancement of rolandic mu-rhythm by pattern vision. *Electroenceph. clin. Neurophysiol.*, 38:535–538, 1975.
- [46] W.N. Kuhlman. Functional topography of the human mu rhythm. *Electroenceph. clin. Neurophysiol.*, 44:83–93, 1978.
- [47] D. LaBerge and V. Brown. Theory of attentional operations in shape identification. *Psychol. Rev.*, 96:101–124, 1989.
- [48] D. LaBerge, M. Carter, and V. Brown. A network simulation of thalamic circuit operations in selective attention. *Neural Comp.*, 4:318–331, 1992.
- [49] W.G. Lennox and M.A. Lennox. *Epilepsy and related disorders*, volume 1. Little, Brown & Co., 1960.
- [50] N. Leresche, H.R. Parri, G. Erdmeli, A. Guyon, J.P. Turner, S.R. Williams, E. Asproдини, and V. Crunelli. On the action of the anti-absence drug ethosuximide in the rat and cat thalamus. *J. Neurosci.*, 18(3):4842–4853, 1998.
- [51] L.W.S. Leung. Nonlinear feedback model of neuronal populations in hippocampal CA1 region. *J. Neurophysiol.*, 47(5):845–868, 1982.
- [52] S. Lindström and A. Wróbel. Frequency dependent corticofugal excitation of principal cells in the cat’s dorsal lateral geniculate nucleus. *Exp. Brain Res.*, 79:313–318, 1990.
- [53] X.B. Liu, C.N. Honda, and E.G. Jones. Distribution of four types of synapse on physiologically identified relay neurons in the ventral posterior thalamic nucleus of the cat. *J. Comp. Neurol.*, 352:69–91, 1995.
- [54] Z. Liu, M. Vergnes, A. Depaulis, and C. Marescaux. Involvement of intrathalamic GABA_B neurotransmission in the control of absence seizures in the rat. *Neuroscience*, 48:87–93, 1992.
- [55] Pierre Loiseau. *Epileptic syndromes in infancy, childhood and adolescence*, chapter Childhood absence epilepsy, pages 135–150. John Libbey & Company Ltd., 2nd edition, 1992.
- [56] A. Longtin. Noise induced transition at a Hopf bifurcation in a first order differential equations. *Phys. Rev. A*, 44, 1991.
- [57] A. Longtin, J.G. Milton, J.E. Bos, and M.C. Mackey. Noise and critical behavior of the pupil reflex at oscillation onset. *Phys. Rev. A*, 41, 1990.
- [58] F.H. Lopes da Silva. Neural mechanisms underlying brain waves: from neural membranes to networks. *Electroenceph. clin. Neurophysiol.*, 79:81–93, 1991.
- [59] F.H. Lopes da Silva, A. Hoeks, A. Smits, and L.H. Zetterberg. Model of brain rhythmic activity: The alpha-rhythm of the thalamus. *Kybernetik*, 15:23–37, 1974.

- [60] F.H. Lopes da Silva, J.P. Pijn, D. Velis, and P.C.G. Nijssen. Alpha rhythms: noise, dynamics and models. *Int. J. Psychophysiol.*, 26:237–249, 1997.
- [61] F.H. Lopes da Silva, A. van Rotterdam, P. Barts, E. van Heusden, and W. Burr. Models of neuronal populations: The basic mechanisms of rhythmicity. *Progress of Brain Research*, 45:281–308, 1976.
- [62] W.W. Lytton, D. Contreras, A. Destexhe, and M. Steriade. Dynamic interactions determine partial thalamic quiescence in a computer network model of spike-and-wave seizures. *J. Neurophysiol.*, 77:1676–1696, 1997.
- [63] D.A. McCormick and T. Bal. Sleep and arousal: thalamocortical mechanisms. *Annu. Rev. Neurosci.*, 20:185–215, 1997.
- [64] D.A. McCormick and J.R. Huguenard. A model of electrophysiological properties of thalamocortical relay neuron. *J. Neurophysiol.*, 68(4):1384–1400, 1992.
- [65] D.A. McCormick and H.C. Pape. Properties of a hyperpolarization-activated cation current and its role in rhythmic oscillation in thalamic relay neurones. *J. Physiol.*, 431:291–318, 1990.
- [66] D.A. McCormick and D.A. Prince. Acetylcholine induces burst firing in thalamic reticular neurones by activating a potassium conductance. *Nature*, 319:402–405, 1986.
- [67] D.A. McCormick and D.A. Prince. Actions of acetylcholine in the guinea-pig and cat medial and lateral geniculate nuclei in vitro. *J. Physiol. (Lond.)*, 392:147–165, 1987.
- [68] Ernst Niedermeyer and Fernando H. Lopes da Silva. *Electroencephalography: Basic Principles, Clinical Applications, and Related Fields*. Williams and Wilkins, Baltimore, 4 edition, 1999.
- [69] Paul L. Nunez. *Electric Fields of the Brain*. Oxford University Press, New York, 1981.
- [70] Paul L. Nunez. *Neocortical Dynamics and Human EEG rhythms*. Oxford University Press, New York, 1995.
- [71] W. Penfield and H. Jasper. *Epilepsy and the Functional Anatomy of the Human Brain*. Little, Brown, 1954.
- [72] J.K. Penry, R.J. Porter, and F.E. Dreifuss. Simultaneous recording of absence seizures with video tape and electroencephalography. A study of 374 seizures in 48 patients. *Brain*, 98:427–440, 1975.
- [73] G. Pfurtscheller. Event-related synchronization (ERS) an electrophysiological correlate of cortical areas at rest. *Electroenceph. clin. Neurophysiol.*, 83:62–69, 1992.
- [74] G. Pfurtscheller. *Electroencephalography: Basic Principles, Clinical Applications, and Related Fields*, chapter EEG Event-related Desynchronization (ERD) and Event-related Synchronization (ERS), pages 958–967. Williams and Wilkins, Baltimore, 4 edition, 1999.

- [75] G. Pfurtscheller and A. Aranibar. Evaluation of event-related desynchronization (ERD) preceding and following voluntary selfpaced movements. *Electroenceph. clin. Neurophysiol.*, 46:138–146, 1979.
- [76] G. Pfurtscheller and C. Neuper. Event-related synchronization of mu rhythm in the EEG over the cortical hand area in man. *Neurosci. Lett.*, 174:93–96, 1994.
- [77] G. Pfurtscheller, C. Neuper, C. Andrew, and G. Edlinger. Foot and hand area mu rhythms. *Int. J. Psychophysiol.*, 26:121–135, 1997.
- [78] G. Pfurtscheller, A. Stančák Jr., and G. Edlinger. Post-movement beta synchronization. A correlate of an idling motor area? *Electroenceph. clin. Neurophysiol.*, 98:281–293, 1996.
- [79] G. Pfurtscheller, A. Stančák Jr., and G. Edlinger. On the existence of different types of central beta rhythms below 30 Hz. *Electroenceph. clin. Neurophysiol.*, 102:316–325, 1997.
- [80] Gert Pfurtscheller and Fernando H. Lopes da Silva, editors. *Event-related desynchronization. Handbook of Electroencephalography and Clinical Neurophysiology, Revised Series*, volume 6. Elsevier Science B.V., 1999.
- [81] M.I. Posner. Orienting of attention: the VIIth Sir Frederic Barlett Lecture. *Q. J. Exp. Psychol.*, 32(3–25), 1980.
- [82] D.A. Richards, T. Lemos, P.S. Whitton, and N.G. Bowery. Extracellular GABA in the ventrolateral thalamus of rats exhibiting spontaneous absence epilepsy: a microdialysis study. *J. Neurochem.*, 65:1674–1680, 1995.
- [83] J. Rinzel, D. Terman, X.-J. Wang, and B. Ermentrout. Propagating activity patterns in large-scale inhibitory neuronal networks. *Science*, 279:1351–1355, 1998.
- [84] Z. Rogowski, I. Gath, and E. Bental. On the prediction of epileptic seizures. *Biol. Cybern.*, 42:9–15, 1981.
- [85] R.S. Schwab. Reaction time in petit mal epilepsy. *Ass. Res. Ment. Dis. Proc.*, 26:339–341, 1974.
- [86] Gordon M. Shepherd. *Neurobiology*. Oxford University Press, New York, 1994.
- [87] S.M. Sherman and C. Koch. The control of retinogeniculate transmission in the mammalian lateral geniculate nucleus. *Exp. Brain. Res.*, 63:1–20, 1986.
- [88] C.O. Snead, A. Depaulis, M. Vergnes, and Ch. Marescaux. *Jasper’s Basic Mechanisms of the Epilepsies*, volume 79 of *Advances in Neurology*, chapter Absence Epilepsy: Advances in Experimental and Animal Models, pages 253–279. Lippincott Williams & Wilkins, 3 edition, 1999.

- [89] C.J. Stam, J.M.P. Pijn, P. Suffczynski, and F.H. Lopes da Silva. Dynamics of the human alpha rhythm: evidence for nonlinearity? *Clin. Neurophysiol.*, 110:1801–1813, 1999.
- [90] M. Steriade and D. Contreras. Spike-wave complexes and fast components of cortically generated seizures. I. Role of neocortex and thalamus. *J. Neurophysiol.*, 80:1439–1455, 1998.
- [91] M. Steriade, D. Contreras, and F. Amzica. Synchronized sleep oscillations and their paroxysmal developments. *Trends Neurosci.*, 17:199–208, 1994.
- [92] M.P. Stryker. Is grandmother an oscillation? *Nature*, 338:297–298, 1989.
- [93] P. Suffczynski, J.P.M. Pijn, G. Pfurtscheller, and F.H. Lopes da Silva. *Event-Related Desynchronization Handbook of Electroencephalography and Clinical Neurophysiology*, volume 6 of *Revised Series*, chapter Event-related dynamics of alpha band rhythms: a neuronal network model of focal ERD/surround ERS, pages 67–85. Elsevier Science B.V., 1999.
- [94] F. Takens. The effect of small noise on systems with chaotic dynamics. In S.J. van Strien and S.M. Vduyn Lunel, editors, *Stochastic and Spatial Structures of Dynamical Systems*, volume 4, pages 3–15. Verhandelingen Afd. Natuurkunde, KNAW, 1996.
- [95] R.D. Traub and R. Miles. *Neuronal Networks of the Hippocampus*. Cambridge University Press, New York, 1991.
- [96] E. Tsakiridou, L. Bertollini, M. De Curtis, G. Avanzini, and H.C. Pape. Selective increase in T-type calcium conductance of reticular thalamic neurons in a rat model of absence epilepsy. *J. Neurosci.*, 15(4):3110–3117, 1995.
- [97] A. van Rotterdam, F.H. Lopes da Silva, J. van den Ende, M.A. Viergever, and A.J. Hermans. A model of the spatial temporal characteristics of the alpha rhythm. *Bull. Math.Biol.*, 44(2):238–305, 1982.
- [98] F. Velasco, M. Velasco, A. Velasco, F. Jimenez, I. Marquez, and M. Rise. Electrical stimulation of the centromedian thalamic nucleus in control of seizures: long-term studies. *Epilepsia*, 36:63–71, 1995.
- [99] A.A. Verveen. On the fluctuation of threshold of the nerve fibre. In D.B. Tower and J.P. Schade, editors, *Structure and function of the cerebral cortex. Proc. 2nd Int. Meeting Neurobiologists*, Amsterdam, 1959. Elsevier.
- [100] A.A. Verveen. *Fluctuation in Excitability*. PhD thesis, University of Amsterdam, 1961.
- [101] M. von Krosigk, T. Bal, and D.A. McCormick. Cellular mechanisms of a synchronized oscillation in the thalamus. *Science*, 261:361–364, 1993.
- [102] M. von Krosigk, J.E. Monckton, P.B. Reiner, and D.A. McCormick. Dynamic properties of corticothalamic excitatory postsynaptic potentials and thalamic reticular inhibitory postsynaptic potentials in thalamocortical neurons of the guinea-pig dorsal lateral geniculate nucleus. *Neuroscience*, 91(1):7–20, 1999.

- [103] X.-J. Wang. Multiple dynamical modes of thalamic relay neurones : rhythmic bursting and intermittent phase locking. *Neuroscience*, 59(1):21–31, 1994.
- [104] X.-J. Wang, D. Golomb, and J. Rinzel. Emergent spindle oscillations and intermittent burst firing in a thalamic model: specific neuronal parameters. *Proc. Natl. Acad. Sci. USA*, 92:5577–5581, 1995.
- [105] X.-J. Wang and J. Rinzel. Alternating and synchronous rhythms in reciprocally inhibitory model neurons. *Neural Comp.*, 4:84–97, 1992.
- [106] X.-J. Wang and J. Rinzel. Spindle rhythmicity in the reticularis thalami nucleus: synchronization among mutually inhibitory neurons. *Neuroscience*, 53:899–904, 1993.
- [107] S. Wiggins. *Introduction to Applied Nonlinear Dynamical Systems and Chaos*. Springer-Verlag, New York, 1990.
- [108] H.R. Wilson and J.D. Cowan. Excitatory and inhibitory interactions in localized populations of model neurons. *Biophys. J.*, 12:1–24, 1972.
- [109] J.J. Wright and D.T.J. Liley. Simulation of electrocortical waves. *Biol. Cybern.*, 72:347–356, 1995.
- [110] J.J. Wright, A.A. Sergejew, and D.T.J. Liley. Computer simulation of the electrocortical activity at millimetric scale. *Electroenceph. clin. Neurophysiol.*, 90:365–375, 1994.
- [111] A. Wróbel, M. Bekisz, and W. Waleszczyk. *Oscillatory Event-Related Brain Dynamics*, chapter 20 Hz Bursts of Activity in the Cortico-thalamic Pathway During Attentive Perception, pages 311–324. Plenum Press, New York, 1994.
- [112] Y. Yao and J.W. Freeman. Model of biological pattern recognition with spatially chaotic dynamics. *Neural Networks*, 3:153–170, 1990.
- [113] L.H. Zetterberg, L. Kristiansson, and K. Mossberg. Performance of the model for a local neuron population. *Biol. Cybern.*, 31:15–26, 1978.

List of author's papers

- [1] P. Suffczynski, J.P.M. Pijn, G. Pfurtscheller, and F.H. Lopes da Silva. *Event-Related Desynchronization Handbook of Electroencephalography and Clinical Neurophysiology*, volume 6 of *Revised Series*, chapter Event related dynamics of alpha band rhythms: a neuronal network model of focal ERD/surround ERS, pages 67–85. Elsevier Science B.V., 1999.
- [2] P. Suffczynski, J.P.M. Pijn, G. Pfurtscheller, and F.H. Lopes da Silva. Attentional mechanism based on the dynamics of cortical alpha rhythms investigated with a neuronal network model. *Abstracts Fluctuations in Biological Systems*, Sigtuna, Sweden, 1999.
- [3] C.J. Stam, J.P.M. Pijn, P. Suffczynski, and F.H. Lopes da Silva. Dynamics of the human alpha rhythm: evidence for non-linearity? *Clin. Neurophysiol.*, 110:1801–1813, 1999.
- [4] J. Parra, H.K.M. Meeren, S. Kalitzin, P. Suffczynski, J.C. de Munck, D.G.A. Kasteleijn-Nolst Trenite, F.H. Lopes da Silva. Magnetic source imaging in fixation-off sensitivity: relationship with alpha rhythm. *J. Clin. Neurophysiol.*, 17(2):212–223, 2000.
- [5] P. Suffczynski, S. Kalitzin, F.H. Lopes da Silva. A lumped model of thalamocortical oscillations. *Abstracts Computational Neuroscience Meeting*, Brugge, Belgium, 2000.
- [6] J. Zygierewicz, K.J. Blinowska, P. Suffczynski. A model of sleep spindle generation. *Abstracts Computational Neuroscience Meeting*, Brugge, Belgium, 2000.